Soil Water Characteristics in Winter - origin and impact of low soil water pressure measurements

Master's Thesis Geo 511

April 30th, 2014

Lea Reusser
s08-731-846
lea.reusser@gmx.ch

Supervisor: **Dr. Peter Lehmann**

ETH Zürich, Environmental Systems Science, Soil and Terrestrial Environmental Physics
Universitätstrasse 16, 8092 Zürich
peter.lehmann@env.ethz.ch

Faculty representation: **Prof. Dr. Markus Egli**

University of Zurich, Department of Geography
Head of Geochronology, Physical Geography Division
Winterthurerstrasse 190, 8057 Zürich

Department of Geography, University of Zurich

Preface

Soil compaction is a relevant topic in physical soil protection. In the past decades, heavier machinery in agriculture, forestry and building have led to stronger pressure exerted on soil. However, a soil can only bear a pressure that is smaller or equal to its internal strength. Wet soils are therefore prone to be compacted by heavy vehicles. Only recently, the Cantonal Soil Protection authorities as well as research centres such as Agroscope or the WSL have started to take measures against soil compaction. Among these measures are stations recording soil water pressure as a proxy for soil stability. To successfully prevent soil compaction, it is important to understand the soil water pressure measurements and to be sure that they reliably estimate the current situation.

In this thesis, the focus will be on the soil water pressure values of these sites recorded during wintertime. Most sites appear to measure very low absolute soil water pressure values from November to March, meaning that the soil is close to saturation. I looked at how these values came about and what they mean for the implementation in soil protection. To be able to answer these questions, a series of field and lab experiments have been carried out.

Abstract

Recently, many Cantons in Switzerland have set up monitoring networks measuring soil water pressure automatically to estimate the vulnerability of soils to compaction. Several threshold values are used to guide the traffic on bare soil in building industry, agriculture and forestry. The first threshold value has been set at 60 hPa (equal to ≈ 60 cm head or 6 cbar; absolute value), below which no traffic on bare soil and no excavation are allowed. The newly available winter data lets the Soil Protection authorities of the Cantons face a challenge for implementation, because 90% of the measurements recorded between October and March of the available dataseries (years 2011 to 2014) datarow lie below 60 hPa. Up to now, it remains unclear whether these low winter measurements truly represent the prevailing conditions. The aim of this study is accordingly to reveal (i) whether the T8 tensiometers (UMS, 2008) used by the Cantons provide reliable measurements, (ii) how these soil water pressure measurements are influenced by temperature, (iii) whether these low measurements are caused by atmospheric conditions or rather by the hydraulic conductivity of the soil, (iv) what role hysteresis, macropores and spatial heterogeneity play and (v) what hydromechanical properties these low soil water pressure measurements represent.
To exclude sensor-specific artifacts, additional tensiometers from a different brand as well as water content sensors (TDR and 10HS of Decagon) have been installed at the Stüsslingen site in the Canton of Solothurn (Regosol, loamy texture), which forms part of the "Bodenmessnetz Nordwestschweiz" (BMN; www.bodenmessnetz.ch). Furthermore, the reaction of the T8 sensor to temperature change has been tested in a closed system in the lab. Data recorded at the BMN sites in the Canton of Solothurn (SO) has been analysed to estimate the influence of single variables such as temperature and relative humidity on the soil water pressure measurements. The hydraulic conductivity of the Stüsslingen loam was measured in the lab and a reconstruction of soil water dynamics has been obtained with the help of the van Genuchten-Mualem (1980; 1976) model for three soils. SWRC for undisturbed soil samples were measured in the lab for the Stüsslingen loam as well as the Aetigkofen sandy loam for both drying and wetting branch. Also, penetration resistance was regularly measured at the Stüsslingen site with the help of a cone penetrometer.

For both tensiometers and water content sensors, the additionally installed sensors showed differing absolute values, but very similar reaction to precipitation when compared to the measurements of the permanent sensors of the BMN (soil water pressure: T8, water content: Stevens Hydra Probe). The variation of the water content measurements, differing around 10 Vol. % between all the sensors, could be attributed to spatial heterogeneity. Therefore, no significant difference between the low-cost 10HS and Hydra Probe sensors and the more expensive TDR probes could be detected. The additionally installed tensiometers showed a deviation from the T8 tensiometers of about 15 hPa, which is not much more than the local variability recorded within a few meters distance. Although soil water pressure is physically expected to decline with increasing temperature if other factors are excluded, the measurements of a T8 in a climate chamber have been found to increase with a slope of 0.21 hPa/°C for temperatures from 0 to 12°C at constant water content. This temperature dependency, although not completely negligible, is not able to explain the low soil water pressure measurements observed in winter. Furthermore, several analyses including data already recorded in the field could not identify a strong dependence of the T8 measurements on temperature. The obtained soil water pressure values at the BMN sites are thus assumed to be correct.
The issue of the cause of these low soil water pressure measurements could not be fully answered. While evapotranspiration explains the daily soil water pressure change better than only temperature or relative humidity, no distinct relationship of the mentioned variables with daily soil water pressure measurements themselves could be observed. The hydraulic conductivity of the Stüsslingen loam yielded a much larger value when measured in the lab (78.35 cm/d) than expected from its texture (14.19 cm/d) as predicted by the Rosetta database (Schaap et al., 2001). According

to this measurement and the results of the water balance reconstruction, hydraulic conductivity is not considered to limit the drainage of the soils studied in wintertime.

When looking at the field SWRC of four soils (texture: sandy loam, loam), a typical annual pattern could be made out with higher water contents recorded at a given soil water pressure in spring and early summer than in autumn. The variability of the water content measurements in the field at a given soil water pressure is thus to some extent believed to be due to hysteresis of the soil water characteristics. For the Stüsslingen loam, a hysteresis loop of similar shape as the field SWRC could be reproduced in the lab. For the Aetigkofen sandy loam, at least part of the variability observed in the field could be explained with the lab drainage and wetting curve. The presence of macropores, as found in the lab SWRC, contributes to a quick drainage after a precipitation event and may have had an influence on the relatively high hydraulic conductivity measured in the lab. Spatial heterogeneity has shown to be of uttermost importance when estimating soil water dynamics at the Stüsslingen site.

Even within the narrow range of soil water pressure measurements recorded on penetration measurement days, the penetration resistance shows a rise with increasing soil water pressure for both 20 and 35 cm depth. Its relationship with the water content is, as expected, inversely proportional. A distinct trend remains difficult to establish because of the narrow range of water content measurements available.

The present study shows that both water content and soil water pressure measurements indicate persistently wet soil conditions at the BMN sites from November to March. This means for the implementation that, for most of the soils, crossing over their surface is not recommended during the time mentioned. However, the correlation found between soil water pressure and penetration resistance even below the first threshold at 60 hPa may have consequences with respect to the threshold choice. The results have also proven that spatial heterogeneity as well as hysteresis effects make the unique description of soil stability at a site rather difficult. However, further study is needed to fully understand the dynamics of soil water pressure and its relation to soil stability.

Table of Contents

List of Figures

List of Tables

List of Abbreviations

AG	Canton of Aargau
BAFU	Bundesamt für Umwelt, Federal Office for the Environment
BL	Canton of Baselland
BMN	Bodenmessnetz Nordwestschweiz, soil monitoring network
EMI	Electromagnetic Induction
ER	Electrical Resistivity
ESA	European Space Agency
ET	Evapotranspiration
FaBo	Fachstelle Bodenschutz (Canton of Zurich), Soil Protection authority
FC	Field capacity
FDR	Frequency Domain Reflectometry
FS BS	Fachstelle Bodenschutz (Canton of Solothurn), Soil Protection authority
GPR	Ground Penetrating Radar
h	Soil water pressure
K(h)	Unsaturated Hydraulic Conductivity (dependent on soil water pressure)
Ksat	Saturated Hydraulic Conductivity
LU	Canton of Lucerne
P	Precipitation
PTF	Pedotransfer function
PWP	Permanent wilting point
RH	Relative humidity
SO	Canton of Solothurn
SMOS	Soil Moisture and Ocean Salinity
SWC	Soil Water Characteristics
SWRC	Soil Water Retention Curve
TDR	Time Domain Reflectometry
TG	Canton of Thurgau
UR	Canton of Uri
VBBo	Verordnung über Belastungen des Bodens, ordinance relating to impacts on the soil
WSL	Institut für Wald, Schnee und Landschaft
ZH	Canton of Zurich
θ	Water content

1   Introduction

Soil as a non-, or at least not quickly renewable resource is competed for by various actors representing different interests. Especially in countries with a high population density, such as Switzerland, an economical use of soil is essential, since the growing population density is competing against the agricultural lands providing our livelihood. In Switzerland, natural soils are protected from physical, chemical and biological harms by law. The „Umweltschutzgesetz" (Federal Act on the Protection of the Environment, USG, SR 814.01) says in Art. 33, Abs. 2 with regard to physical soil protection (non-formal interpretation), that soil may only be physically stressed as long as its fertility can be sustainably guaranteed and that the Swiss Federal Council may enact regulations or guidelines concerning measures against physical stresses such erosion or compaction.

Since this law is quite general, the VBBo (Ordinance relating to impacts on the soil, SR 814.12) has been released in 1998. Its Art. 1 characterises the goal of the ordinance (non-formal interpretation) as follows: For the long-term sustainment of soil fertility, this ordinance manages: a. the observation, supervision and judgement of the situation regarding chemical contamination, biological condition and physical stresses of soils; b. the measures to avoid sustainable soil compaction as well as soil erosion; [...].

The overall goals of these laws are thus the protection and maintenance of soil fertility. The term „soil fertility" means more than just the ability to produce crops: As described in Art. 2, Abs. 1 a and b of the VBBo (1998), a fertile soil is also characterised by a locally typical, diverse soil fauna as well as structure and its ability of decomposition. Soil fertility can be endangered by many factors such as chemical pollution, soil compaction or erosion. Relevant for this thesis is predominantly soil compaction, which is one of the major topics in physical soil protection.

1.1   Soil Compaction

Compaction is one aspect of soil deformation, because the deformation of soil can be separated into a part of compaction and a part of shearing. Compaction reduces the relative amount of pores compared to the rigid soil particles, because the air-filled pores can be compacted more easily than the soil particles. Usually, the volume is reduced if a soil is compacted. Shearing forces do not change the void volume, but change their arrangement and promote their discontinuity (Scheffer and Schachtschabel, 2002, see Fig. 1). Soil compaction in a classical sense as mostly dealt with in the literature, thus, just involves compaction, but in fact shearing forces executed by tires of agricultural and forestal vehicles play an important role, too (Scheffer and Schachtschabel, 2002). Although the correct term therefore would be „soil deformation", the more often used term „soil compaction" will be made use of in this thesis.
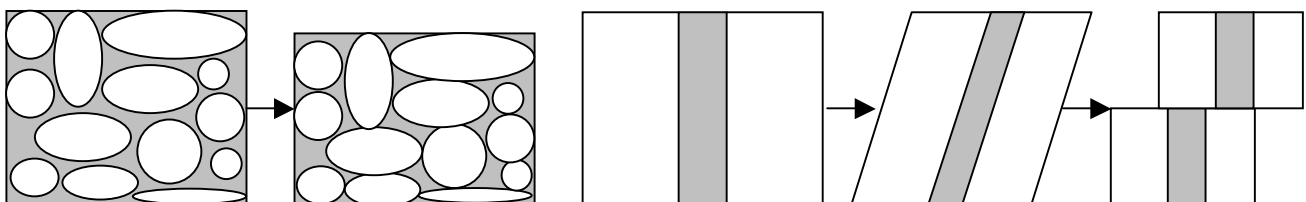
Fig. 1: *Processes of soil deformation: Compaction (left) leading to a reduction of pore volume and shearing (right) causing pore discontinuity (modified after Scheffer and Schachtschabel, 2002).*

Soil compaction occurs mainly due to heavy machinery driving on unconsolidated soils under unfavourable conditions, namely when soils are wet. This is often a discussion in the building industry, but soils are also prone to be compacted by agricultural and forest management (Goutal et al., 2013).

1.1.1   Soil Stability

A soil's sensibility to deformation caused by heavy loads on the soil surface can be estimated with the concept of precompression stress. The precompression stress is also looked at as the actual soil stability because it determines the maximum amount of pressure a soil can bear without being plastically deformed and thus without negative consequences (see 2.5 for details on precompression stress). The precompression stress of a soil depends on timely invariable factors: The higher the soil organic matter content, the coarser the texture at the same bulk density, the stronger aggregated, the higher the salinity of the liquid soil phase and the less swellable the clay minerals, the more load can a soil bear (Scheffer and Schachtschabel, 2002). Horn and Fleige (2003) used these properties to model the stability of a soil. However, probably the most important factor influencing soil stability is time-variable: the water saturation (Scheffer and Schachtschabel, 2002; see also 2.5). The wetter a soil is, the weaker are its capillary forces and thus the lesser its stability. The webbased prediction model Terranimo (Stettler et al., 2012; Lassen et al., 2012) for example uses the texture (clay content) and matric potential as a predictor of soil stability. Terranimo is one of the models for soil stability that is based on the assumption that the pressure applied onto a soil should not be bigger than its stability (determined by soil specific properties as well as saturation state).

1.1.2   Consequences of Soil Compaction

Soil compaction of the topsoil (approximately 0-30 cm, to where the soil is ploughed) can be moderated by ploughing in agriculture (Arvidsson and Håkansson, 1996). Nevertheless, it takes several years for a topsoil to recover, as shown by Alakukku (1996) and Weisskopf et al. (2010). Compactions in the subsoil, however, are regarded as irreversible, because they cannot recover within a reasonable timespan (Etana and Håkansson, 1994; Arvidsson, 2001).

The consequences of a compacted soil are manifold and will be described shortly here. A good overview can be read in Van der Ploeg et al. (2006). Consequences of soil compaction can be:

- Reduction of the pore volume (through reduction in size or number) (Dexter and Richard, 2009; Berisso et al., 2013) and thus weaker soil aeration as well as inhibition of water percolation (Van der Ploeg et al., 2006). This is the start of a positive feedback loop: The stronger the compaction, the less water can percolate into the soil and be retained by the soil, the wetter thus the site. As mentioned before, the wetter a soil the higher its risk to be compacted.
- Diminishment of plant root growth due to denser soil as well as possible waterlogging. This leads to a reduction of crop yields in agricultural fields (Van der Ploeg et al., 2006).
- Missing possibility for rainwater to percolate, leading to stronger erosion due to overland flow on hillslopes (Van der Ploeg et al., 2006).
- Indirect effects, such as emission of nitrous oxide (greenhouse gas) due to waterlogging, less groundwater formation because less water percolates through the soil and increase in fuel use caused by hindered soil working (Van der Ploeg et al., 2006).

1.1.3   Measures taken against Soil Compaction

Attempts to avoid soil compaction involve actions on both sides of the balance between soil stability and pressure exerted onto it. The simplest way to avoid negative consequences is the omission of passing over unconsolidated wet soil (Håkansson, 2005). However, especially on building sites, time is money. Therefore, work on bare soil may be carried out even though conditions are unfavourable. If there is no choice but to drive, the machining should be performed as gentle as possible by reducing the pressure exerted on the soil. A simple and effective way is thus to reduce the weight of the vehicle, for example by driving with only half-filled tank. In the building industry, most machines drive on caterpillars, which lead to a better distribution of the heavy load on the soil. In agricultural and forest management, a pressure reduction can be achieved either by augmenting the contact area of the wheels (broad tires and low tire pressure) or by

choosing an alternative management (for example On-Land ploughing in agriculture where a farmer does not drive in the plough marks, but on the consolidated land beside it; see Geischeder and Demmel, 2006 for details). Soil stability can be favoured sustainably by agronomic precaution measures, such as a wise choice of crop rotation leaving enough time between harvest and sowing or the method of intertillage for soil stabilisation (Moitzi and Boxberger, 2007). In the field of agriculture, there are many ongoing research projects in the field of agriculture that deal with soil compaction and its prevention.

In Switzerland, the problem of soil compaction has been detected in the 1950s and first impacts on soil fertility have been recorded after the construction of the gas transit pipe in the 1970s. Nevertheless, many years have passed before action has been taken (Buchter and Häusler, 2009). The first help to implement the relatively new laws concerning physical soil protection has been published in 1993, its second edition in 1997 (guideline for the construction of pipelines; Bundesamt für Energiewirtschaft, 1997). These guidelines include a so-called „Nomogramm" which helps to decide whether driving on a soil is allowed or not (see Fig. 2). It has been developped for the building industry by U. Vökt in 1993 based on his experiences from the agricultural field. The start of physical soil protection implementation took thus place in the building industry, where tensiometers measuring soil water pressure have been applied. In the nomogram, soil stability is therefore deduced from soil water pressure measurements, which determine the force with which water is bound to the soil. Absolute soil water pressure values are low when close to saturation and rise the more a soil dries making it more stable (see also 2.1). The pressure exerted on a soil is approximated by the total weight of the machine and its contact stress (weight per area). With these two parameters, the minimal soil water pressure necessary for passing over a soil without harming it can be calculated for machinery with caterpillars (see Fig. 2).
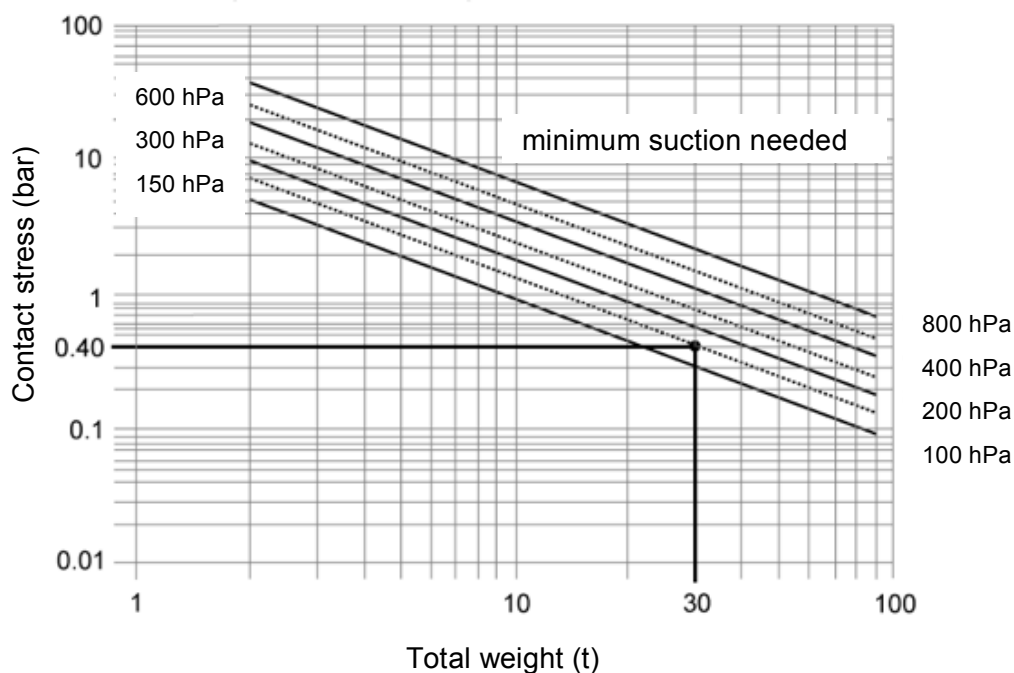
Fig. 2: *Nomogram developped by Urs Vökt in 1993 to read out minimum suction needed to drive on a soil with caterpillar machinery. The minimal soil water pressure required for a machine with total weight 30 t and a contact stress of 0.4 bar to drive on unconsolidated soil is 150 hPa, as displayed in black (modified after BAFU (BUWAL), 2001).*

The use of the nomogram is nowadays well-established on building lots. Whereas they have existed for a few years for forestal purposes (Lüscher et al., 2010), guidelines for soil protection in the agricultural field have only been developed recently (implementation help for soil protection in agriculture by the Bundesamt für Umwelt (Federal Office for the Environment, BAFU) and the

Bundesamt für Landwirtschaft (Federal Office for Agriculture, BLW), 2013). The transfer of the nomogram to tire wheels in agriculture and forestry is unfortunately not that simple. Newer models, such as Terranimo for agriculture (see Section 1.1.1), allow the more complex calculation of minimum suction required for other machinery.

Ever since the introduction of the VBBo (SR 814.12, 2012), its implementation has been delegated to the Cantons in Switzerland. In physical soil protection, which is based in the VBBo, soil water pressure measured with tensiometers on building lots has proven to be a suitable parameter to measure the vulnerability of a soil to compaction and thus has established its use as proxy for soil stability (see also 2.5). To amend these local tensiometer measurements on building sites, many cantonal Soil Protection authorities have released networks recording soil water pressure. The soil water pressure values are divided into 3 to 4 categories (depending on the Canton), which judge the state of a soil with regard to passing over it. The thresholds vary from Canton to Canton, but all agree that the soil must not be passed over if soil water pressure is below 60 hPa and the soil is considered dry above 200 or 250 hPa. The choice of the threshold values is based on experience from the first few building sites with a soil protection concept in the late 1980s and early 1990s.
The first canton to establish such a network was the Canton of Bern in 1996. At these early stations, soil water pressure was measured using manual tensiometers, which are not frost-proof (Matile et
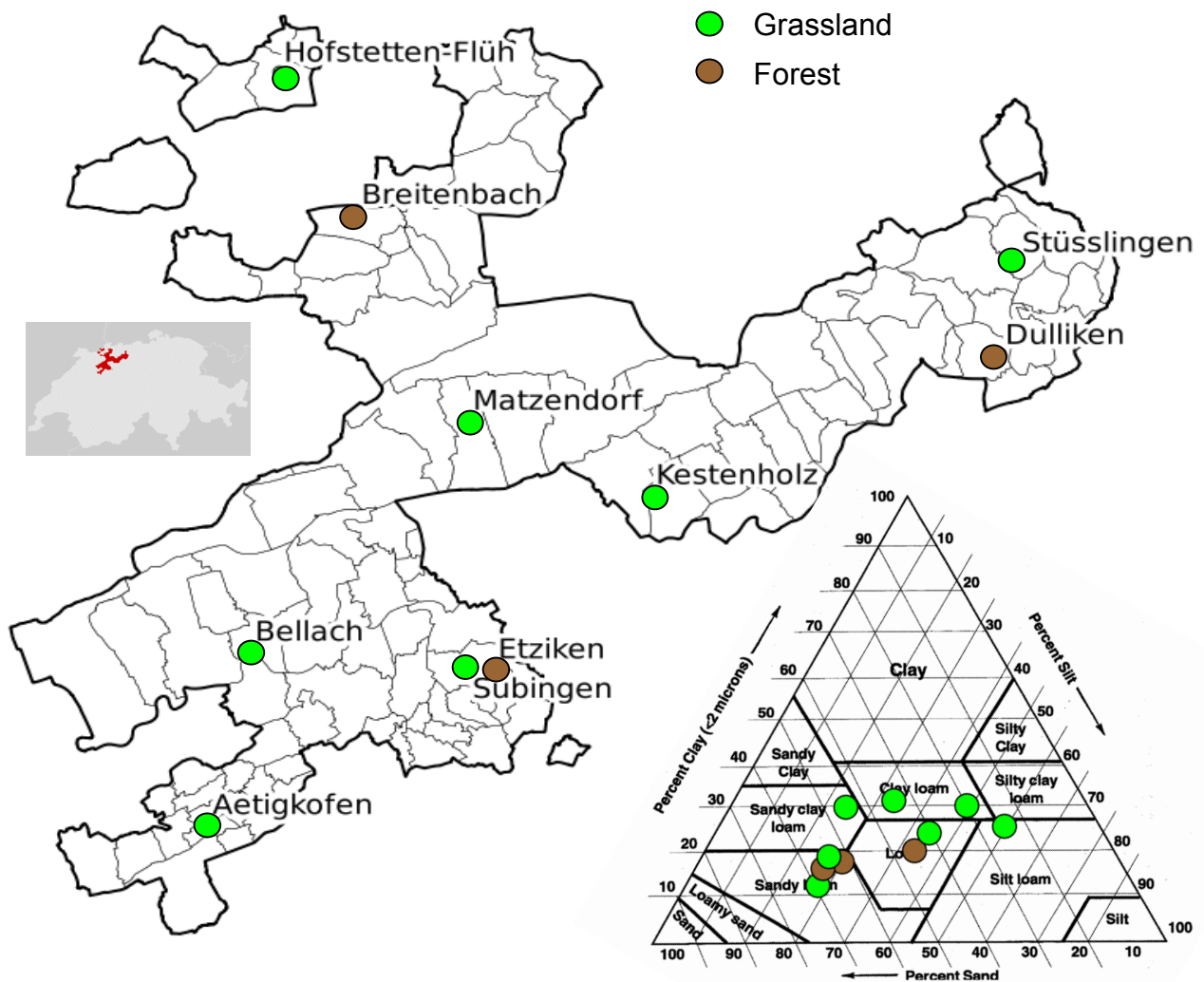
Fig. 3: *Location and texture of ten „Bodenmessnetz" sites in the Canton of Solothurn. Seven of the sites have been installed on grassland, three in a forest. The texture in 20 to 35 cm depth varies around the classical loam, ranging from silt loam to sandy loam. Data: SO!GIS, Canton of SO; BMN.*

al., 2011). Nowadays, some Cantons still use manual tensiometers, while several (AG, BL, LU, SO, TG, TI, UR and ZH) moved on to measuring soil water pressure automatically with the help of pressure transducer tensiometers (mostly the T8 of UMS, UMS 2008). Since these are considered frost-proof below a depth of 20 cm, winter soil water pressure measurements are newly available.

As an example, and because it was one of the first automatic networks, the Bodenmessnetz (soil monitoring network, BMN) in north-western Switzerland (Cantons AG, BL and SO) is described closer here.

1.2   Soil Monitoring Network Canton of Solothurn
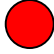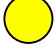
The „Bodenmessnetz" (soil monitoring network, BMN) in north-western Switzerland is operated by the Cantons AG, BL and SO and consists of 25 stations distributed all over the area of the three Cantons. Its goal is to provide real-time soil moisture information for the prevention of soil compaction. Being a supplement to the non-permanently installed tensiometers on building lots, the BMN also serves to indicate trends caused by weather conditions that may help to plan the work in the building industry. It can also be of use to further sensitise farmers and foresters with respect to soil compaction and place a tool judging the actual situation at their disposal, so that the use of heavy machinery can be adjusted to the prevailing weather. Last but not least, the thus obtained long-term data serves to gain further insights into the dynamics of soil water pressure as well as to collect continuous winter measurements.

The network has been started in 2011 by the Canton of Solothurn (SO). The twelve sites in this Canton were chosen to represent a variety of locally typical soil types as well as all regions of the Canton. Since many soils in the Canton of Solothurn suffer from stagnant moisture, some soils with high clay content have also been chosen because they are highly vulnerable to compaction. Fig. 3 shows an overview of ten sites, their position either on grassland or in a forest and their texture, ranging from sandy loam to silt loam. Two of the totally twelve sites have been installed only recently in March 2014, therefore they are neither included in Fig. 3, nor in the analyses. The following parameters are recorded continuously every 15 minutes at each site:

- Soil water pressure and soil temperature in 20 and 35 cm depth (median of 3 sensors at each depth) with the T8 tensiometer (UMS, 2008)
- Soil water content in 20 cm depth with the Stevens Hydra Probe (Stevens Water Monitoring System, 2007)
- Precipitation 1.5 m above ground with a Lamprecht tipping bucket (1 mm resolution, not heated)
- Air temperature and relative humidity 2 m above ground with a Vaisala sensor

Fig. 4 shows a completely equipped BMN station in Kestenholz.

Table 1: *Threshold values for determining soil stability valid for the BMN (Cantons AG, BL, SO).*

🔴	0-60 hPa	„wet"	no passing over, no excavation
🟠	60-100 hPa	„very moist"	no passing over, excavation possible
🟡	100-250 hPa	„moist"	passing over allowed for vehicles with caterpillars, low tire pressure or double wheels respecting the maximal load allowed
🟢	> 250 hPa	„dry"	passing over allowed for all vehicles respecting the maximal load allowed

The soil water pressure measurements are divided into four categories to determine the actual soil stability (see Table 1). The threshold values partly differ between the Cantons and are based on

experienced data of several large building sites (e.g. transit gas pipe, Bahn2000), as mentioned before. Although soil water pressure may reach a certain category, the nomogram (Fig. 2) must always be considered before driving on a soil, since it determines the maximal load allowed.

All data is available to the public on www.bodenmessnetz.ch, a site frequently used by construction site specialists for soil protection (Bodenkundliche Baubegleiter, BBB) as well as farmers or other target group members. Although the measurements are real-time and distributed over the whole Canton, they cannot be looked at as an obliging value because the local variability is not accounted for. That means that the measurements cannot be simply extrapolated to a site which is not represented by a BMN site due to the high spatial variability of soil properties. Tensiometers on building lots to judge the situation on-site are thus still mandatory. Nevertheless, the measurements provided by the Bodenmessnetz and similar networks can be used to get an idea of the soil water pressure distribution at any time.

Fig. 4: *Soil monitoring network (BMN) station in Kestenholz, SO. The station is operated with solar power only and the data is submitted to the server via GPRS mobile network. Picture: FS BS.*

1.3   Problem

Ten of the sites in the Canton of Solothurn (SO) have been recording data since October 2011 and thus were among the first ones to have continuous winter measurements. One annual course for 2013 is displayed in Fig. 5 for two sites. Whereas the soils dry at least once in summer, winter measurements, however, show very low absolute values of soil water pressure, meaning that the soil is close to saturation. In theory, field capacity (definition for Switzerland usually 60 hPa, see also Section 2.1.1) should be reached few days after the last precipitation event (Scheffer and Schachtschabel, 2002). This is, however, not the case for the soils observed. During the winter months (December to February or March), the unfrozen soils do, according to the soil water pressure measurements, not drain to field capacity at 60 hPa even during longer times without precipitation. Also during long dry periods in late autumn (as e.g. in November 2011) and early spring, the soil water pressure measurements did not rise significantly. Furthermore, there is evidence from pedological experts working in the field that the soil may not be as wet as indicated by the tensiometer data. This contradiction has immense consequences for the implementation in

the building industry as well as in agriculture and forest management, because the low soil water pressures recorded theoretically make work with and on the soil impossible during wintertime.
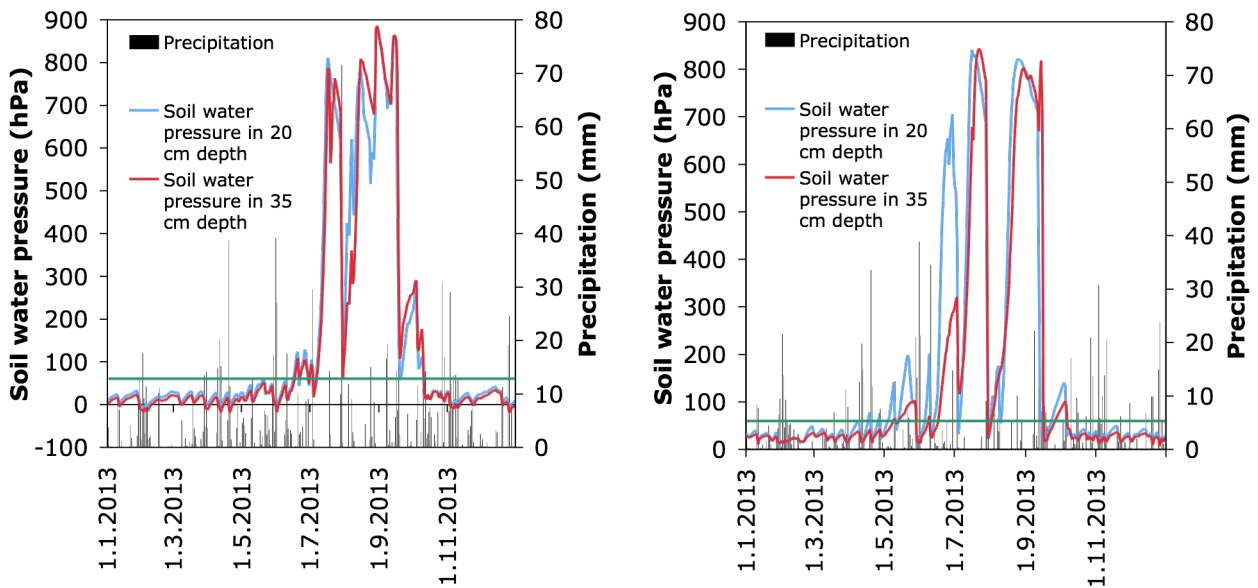
Fig. 5: *Annual course (2013) of soil water pressure measurements and precipitation at two different sites in the Canton of Solothurn: Etziken (sandy loam, forest; left) and Stüsslingen (loam, grassland; right). The threshold above which a soil is allowed to be passed over (60 hPa, green line) is never surpassed from November to March. Data: Bodenmessnetz, Fachstelle Bodenschutz, Canton of Solothurn (further displayed as BMN).*

Due to the datarow providing data of three winters so far as well as the availability of soil water content measurements, most of the data processed in this thesis is from the Canton of Solothurn. The observation of low absolute soil water pressure measurements, however, has not only been reported by the Canton SO.

1.4   Objectives, Hypotheses and Goals

The main objective of this thesis is to find out whether these low soil water pressure measurements represent the situation correctly, because the Soil Protection authorities are interested to know how to interpret the recorded values for the correct implementation and communication.

This main objective will be worked on accordingly by addressing the following research questions:

1. *Are these low absolute soil water pressure values valid only for a limited area, or can they be observed at various Swiss sites during wintertime?*

2. *Are the low absolute soil water pressure measurements possibly influenced by sensor-specific measurement artifacts of the T8 tensiometer?*

3. *Which influence does temperature have on the soil water pressure measurements?*

If large errors due to sensor problems or temperature can be excluded, it will be interesting to find the causes of these low absolute soil water pressures:

4. *Are these dynamics of low soil water pressure determined by atmospheric conditions or rather by hydraulic properties of the soil?*

5. *Which roles do physical soil properties such as macroporosity and hysteresis play?*

6. *How big is the influence of spatial heterogeneity on the soil water characteristics?*

7. *What range of hydromechanical properties is represented by these soil water pressures below 60 hPa?*

Since low absolute soil water pressure measurements have also been mentioned by the Canton of Zurich, they may not be limited to the area of the Canton of SO.

The second question has arisen because all of the Cantons with automatic stations use the T8 tensiometer of UMS (UMS, 2008) for their measurements, meaning that they all rely on it measuring correctly.

„Correctly" also means that a large temperature dependence of the soil water pressure measurements (temperature hindering absolute soil water pressure measurements to rise) can be excluded. The question is outlined for soil water pressure measurements in general as well as specific for the T8 sensor. Many studies have observed the effect of temperature on soil water pressure measurements in general, but most of them dealt with temperatures higher than winter temperatures in Switzerland (e.g. Nimmo and Miller, 1986; Hopmans and Dane, 1986) or focused more on the effect of radiation onto the material than on the difficulty of winter logging (Buchter et al., 1999). Nevertheless, daily fluctuations in soil water pressure due to temperature variation were shown to be larger than the measurements themselves (Buchter et al., 1999). Furthermore, the relationship between water content and soil water pressure has been proven temperature dependent as well (Hopmans and Dane, 1986). The influence of temperature on soil water pressure measurements could thus be of importance.

If large effects of temperature and sensor specific errors can be excluded, it would be helpful to know how these soil water pressure measurements come about, that is to say whether the indicated wet conditions are caused by limited evapotranspiration to the atmosphere or hydraulic soil properties slowing down drainage into deeper horizons.

In aggregated soils, the presence of macropores may lead to preferential flow paths and thus quick drainage of the water collected in these big pores after a heavy rainfall event (Weiler and Naef,
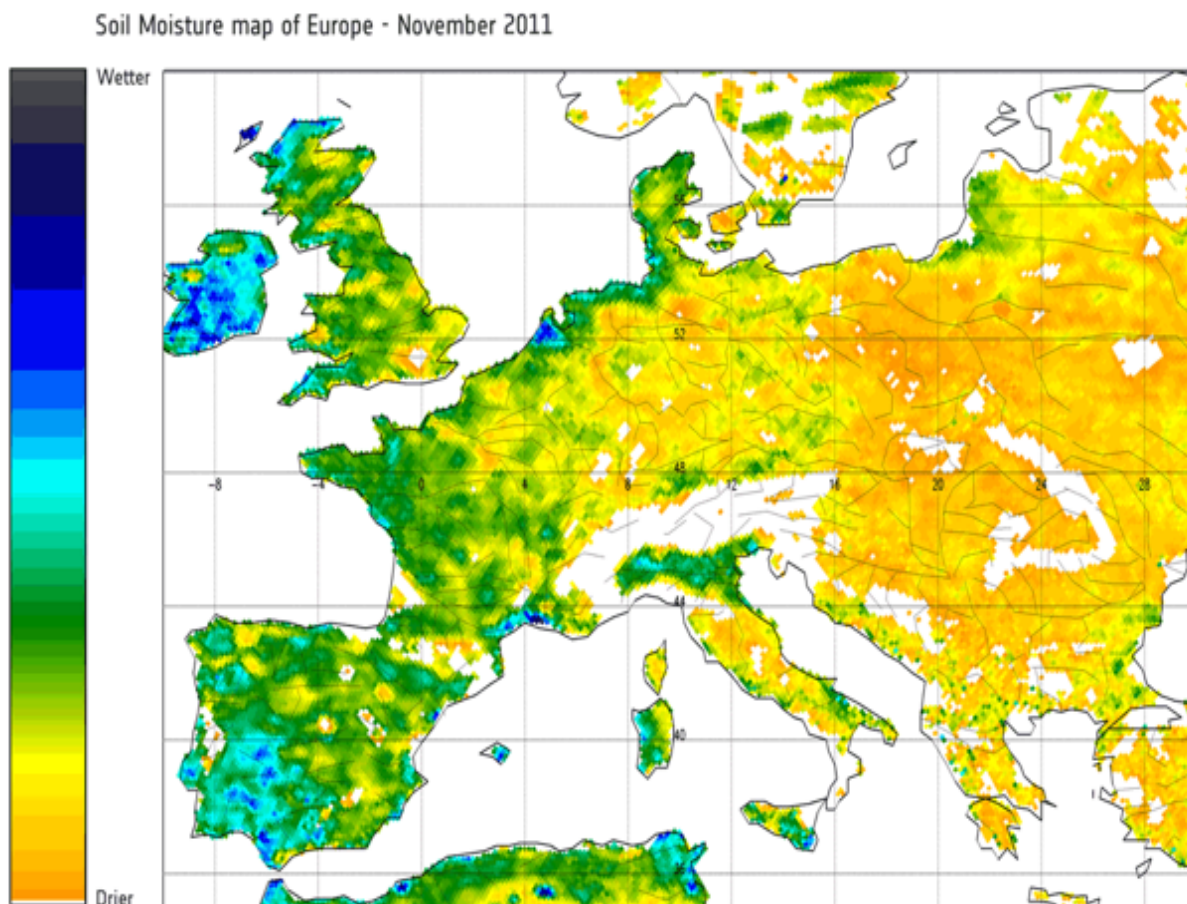
Fig. 6: *Soil moisture map of Europe in the exceptionally dry November 2011 retrieved by the SMOS (Soil Moisture and Ocean Salinity) satellite (CESBIO/F. Cabot/Y. Kerr, 2013).*

2003). Macropores can be formed by soil fauna, by decayed roots, by cracks through wetting and drying or freezing and thawing processes or by erosion from subsurface flow (Beven and Germann, 1982). On grassland in Switzerland, most of the macropores exist due to earthworm activity, which thus significantly influences the infiltration of water in these soils (Weiler and Naef, 2003). Their influence on drainage shall thus be evaluated for some soils of the BMN. As another soil physical property, hysteresis leads to an ambiguity of soil water pressure measurements with respect to the water content they are related to (Scheffer and Schachtschabel, 2002; see also Section 2.1.4). The influence of these hysteretical processes of the soil water characteristics on the recorded soil water pressure values will therefore be discussed.

Finally, it is of interest to know what range of hydromechanical properties these matric suctions below 60 hPa represent. Since soil stability is influenced by soil water pressure and water content (Lu et al., 2010), a relationship between these two variables and the penetration resistance as a proxy for soil stability is hypothesized.

The goal of this thesis is to provide results that guide the Soil Protection authority of the Environmental Department, Canton of Solothurn as well as other Cantons that made the same observation of low absolute soil water pressure with respect to interpretation of measurements indicating persisting wet soil conditions during wintertime.

Besides its obvious benefit in the application of soil sciences for soil protection, the topic covered in this thesis is of interest for local and global purposes. A better understanding of soil water dynamics in winter can lead to better runoff predictions on subcatchment to catchment scale, for soil moisture gives more information on the hydrological behaviour of a catchment (Beven, 2012). Furthermore, the data provided by the Cantonal networks may be included in the International Soil Moisture Network, which provides a data hosting facility for soil moisture information (Dorigo et al., 2011). The data is available for the calibration and validation of land surface models as well as satellite-based soil moisture information, such as the images provided by the SMOS satellite (Dorigo et al., 2011; see Fig. 6; see Section 2.2.1.8 for information on SMOS). This is of interest up to a global scale, because soil moisture has been reported to be an important variable in climate and hydrological science (Seneviratne et al., 2010). Although the International Soil Moisture Network mainly deals with water content data, some networks measuring soil water pressure have already been included (Dorigo et al., 2011). Generally, little studies have been performed on the dynamics of soil water pressure (Rosenkranz et al., 2013).

The topic of soil moisture is also relevant with respect to climate change. Soil moisture data is an important input of climate models and thus the improvement of soil moisture information will advance the prediction of future climate. Air temperatures show a global warming of 0.85°C over the period from 1880 to 2012 including ocean and surface temperatures (IPCC, 2013), for Switzerland even 1.3°C in the last century (OcCC, 2002). According to OcCC (2002), this leads to a higher probability of floods during winter season in Switzerland. It is thus even more important to understand the soil water dynamics now to extrapolate them into future scenarios.

In this thesis, the questions and hypotheses mentioned will be worked on by (i) analysing existing data for seasonal and temperature trends, reproducing the situation with the HYDRUS-1D model, (ii) field work including sensor comparison at one site as well as observation of trends with temperature and penetration resistance measurements and (iii) lab work involving the measurement of the soil water retention curve (SWRC) including hysteresis effects with undestroyed soil samples and the reaction of matric suction under controlled temperatures. All material used and methods applied are described in Section 3. In Section 4, the results are presented and Section 5 discusses the results with respect to other studies. Finally, a conclusion and an outlook including guidelines for the Soil Protection authorities in Switzerland are disclosed.

2   Theory

2.1   *Soil Water*

Soil is a three-phase system including solid bulk material (minerals and organic matter), liquid water as well as air. Typically, the solid material of a soil makes up around 50% of the volume, leaving the remaining 50% to the pores, also called voids (see Fig. 7). The pore space can be completely filled with water, which is the case if the soil is fully saturated. However, most of the time a soil is unsaturated, that is to say the porous phase is partially filled with air and water (Flühler and Roth, 2004).

The presence and amount of water in a soil has many consequences, for example alteration of the hydrological conductivity (see also 2.3), of transport processes or of soil stability (Scheffer and Schachtschabel, 2002; see also 2.5). It is therefore of interest to know about the saturation state of a soil. We can measure two different variables, which are both related to the soil water state: (i) the water content, which is usually a volumetric measure of m^3 water per m^3 soil and (ii) the matric potential, which is a measure of the intensity with which water is bound to the soil (Scheffer and Schachtschabel, 2002).

Fig. 7: Soil as a three-phase system (modified after lecture notes Vadose Zone Hydrology, 2013).

A potential is physically the work that needs to be done to transfer a unit (of volume, mass or weight) to a reference point (Scheffer and Schachtschabel, 2002). The potential of soil water is the product of the mass, gravity and height over a free water surface. It can be expressed as a pressure (Pa) as well as as a length (cm head), see also Section 2.2.2.

The matric potential is one part of the total soil water potential (Scheffer and Schachtschabel, 2002):

$$\psi = \psi_z + \psi_m + \psi_g + \psi_o \tag{1}$$

where ψ_z = gravitational potential (hPa), ψ_m = matric potential (hPa), ψ_g = gas potential (hPa) and ψ_o = osmotic potential (hPa).

The gravitational potential is the amount of work that needs to be done to lift an amount of water from a reference level to an arbitrary height. It is defined as positive going upwards.

The gas potential needs to be considered only if the air pressure inside the soil is not the same as at the reference level.

The osmotic potential is dependent on the amount of dissolved salts in the water. It can thus usually be neglected, unless one is working with a soil that has a high salt content.

The matric potential involves all influences the matric has on the water. It is opposed to the gravitational potential and thus has a negative sign. Although the matric potential can be expressed in different ways, it will be expressed as a positive pressure (hPa; absolute value) in this thesis (Scheffer and Schachtschabel, 2002; see also Section 2.2.2).

2.1.1   Soil Water Retention Curve (SWRC)

To make a statement how much water there is in a soil at which matric potential, the soil water characteristics (SWC) or soil water retention curve (SWRC) is used. It is a curve describing the relationship between the two mentioned parameters of the soil water and characteristic for every soil. The SWRC depends on the pore size distribution (and thus on the texture) of a soil (see Fig. 8), because in a soil with larger grain sizes, the water will run off relatively easy whereas in a clay rich soil, the water will be retained longer due to large capillary and adhesive forces (Scheffer and Schachtschabel, 2002).
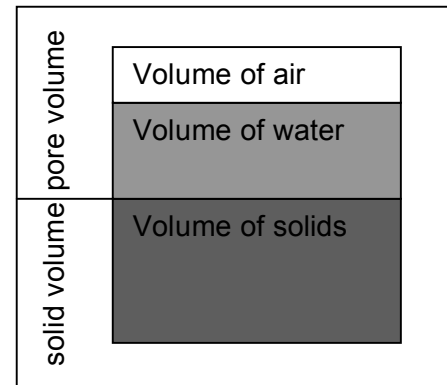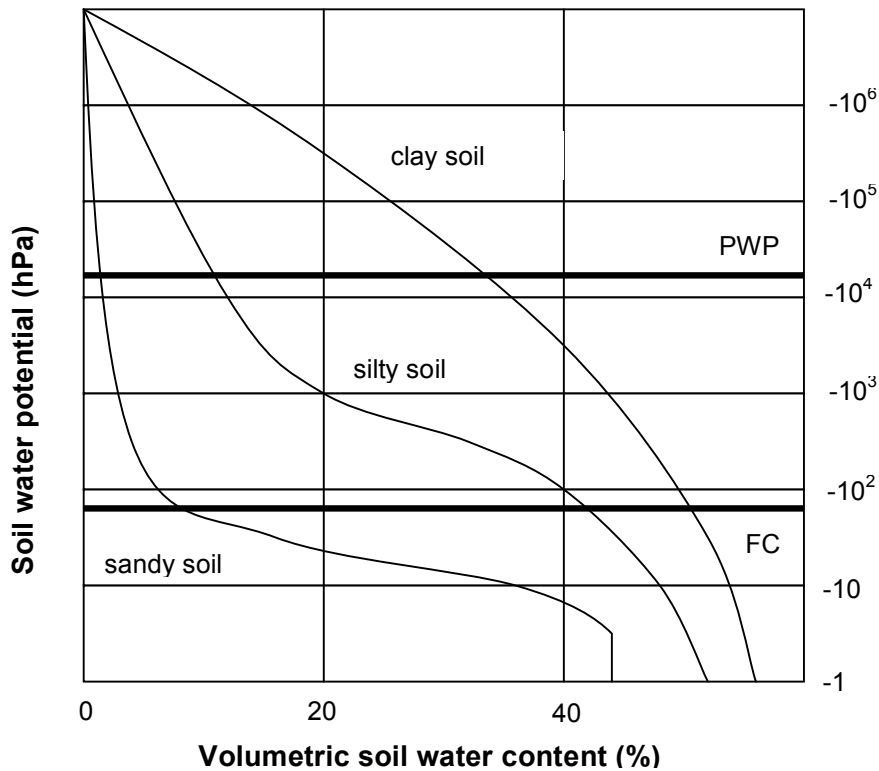
Fig. 8: *Soil water retention curve for three representative soils (sandy, silty and clay). PWP = permanent wilting point, FC = field capacity. The SWRC is characteristic for every soil and depends on the soil texture and structure. For a silty soil (here: a loess), the amount of water available for plants is maximal (modified after Scheffer and Schachtschabel, 2002).*

A sandy soil has a lot of large pores. It therefore drains very quickly and has already lost a big amount of water when it reaches field capacity (60 hPa traditionally, see FC Fig. 8). A soil rich in clay, in contrast, retains more water at field capacity because there are less large pores. Field capacity is traditionally seen as the amount of water present in a soil 2-3 days after the last precipitation (according to 60 – 120 hPa), when gravitational water in the large pores already disappeared (Scheffer and Schachtschabel, 2002). However, there are newer concepts of field capacity, seeing it rather as a dynamic value (Cavazza et al., 2007) or regarding pressure heads as unsuitable to describe it (Twarakavi et al., 2009). In the US, field capacity is defined at 330 hPa (Richards and Weaver, 1944). In this thesis, the European definition will be used.

The gravitational water is considered unavailable for plants. It is theoretically reachable, but usually drains quickly after a precipitation event. Because some soils (especially clays) contain very fine pores, water may also be bound strongly to these fine particles, so that plants cannot make use of it. The soil water potential separating the (not easily, but) available water from the unavailable water has been set to 15'000 hPa according to studies performed with the sun flower. It is called the permanent wilting point (PWP in Fig. 8; Scheffer and Schachtschabel, 2002). For a plant, it is thus relevant how much water a soil can retain between FC and PWP. In Fig. 8, we see that the silty soil in this case provides most water for plants.

2.1.2   Parametrisation of the SWRC

To obtain a mathematical function describing the SWRC, many equations have been developed that allow the fitting of a curve to experimentally determined measurement points. An example for such a parametrisation is the Brooks and Corey (1964) model or the van Genuchten (1980) equation, which is among the most widely used (Flühler and Roth, 2004). The van Genuchten equation is described as follows:

$$h(\theta_e) = \alpha^{-1}\left[\theta_e^{-1/m} - 1\right]^{1/n} \tag{2}$$

$$\text{with } \theta_e = \frac{\theta(h) - \theta_r}{\theta_s - \theta_r} \tag{3}$$

where θ_e = effective saturation (-), $h(\theta_e)$ = soil water pressure at θ_e (hPa), $\theta(h)$ = water content at soil water pressure h (m³/m³), θ_r = residual water content (m³/m³), θ_s = saturated water content (m³/m³) and α (1/m), m, n = parameters.

For many soils, the condition

$$m = 1 - 1/n \tag{4}$$

introduced by van Genuchten (1980) is valid, reducing the amount of parameters to be identified.

Such parametrisations have also been used to determine the unsaturated hydraulic conductivity with the help of the water content or soil water pressure (Flühler and Roth, 2004; see also Section 2.3). With the van Genuchten-Mualem equation (van Genuchten, 1980; Mualem, 1976), a relative K(h) for every effective saturation θ_e can be calculated:

$$k_r(\theta_e) = \theta_e^\alpha \left[1 - \left[1 - \theta_e^{n/(n-1)} \right]^{1-1/n} \right]^2 \tag{5}$$

where $k_r(\theta_e)$ = relative hydraulic conductivity at effective saturation θ_e (-), n and α (1/m) = parameters of the van Genuchten equation (equation 2).

To be able to determine the van Genuchten parameters of a soil and thus mathematically describe its SWRC and water dynamics, measurements of the soil water retention curve are necessary. These measurements can either be obtained in the lab using various apparatus such as pressure plates, hanging water columns or psychometry (dependent on the measurement range desired; Campbell and Shiozawa, 1992; see also Klute, 1986b) or in the field. Field measurements require simultaneous recordings of water content and soil water potential and are thus time-consuming (see also 2.2 Measurement Methods). They are therefore not often used for this purpose. Nevertheless, they are more reliable because a lab SWRC can be subject to many measurement artifactssuch as perturbation or compaction of the sample while sampling, shrinking and swelling of the soil, oversaturation (more than would be possible in nature) or lacking contact to the plate or membrane while draining (DIYS, 2009).

2.1.3   Pedotransfer Functions (PTFs)

As already seen above, the SWRC of a soil depends on its texture. However, there are also other factors that influence the pore size distribution of a soil, as for example aggregation (Scheffer and Schachtschabel, 2002). It is therefore difficult to predict the SWRC if one has only textural information. Nevertheless, many attempts to predict the SWRC have been made, because the soil hydraulic properties are crucial input information for many climatic models, but cannot be measured and extrapolated easily (Schaap et al., 2001). Functions aiming at describing a SWRC with the help of available information are called Pedotransfer Functions (Flühler and Roth, 2004). The goal is to predict parameters of a function describing the SWRC, for example the van Genuchten parameters α, m and n (see Section 2.1.2), with the help of easily available information, such as soil texture (Flühler and Roth, 2004). Many empirical approaches have arisen, among these the database ROSETTA (Schaap et al., 2001), which predicts the van Genuchten parameters of a soil with the help of measured values for soils with similar texture. Of course, the estimation of the SWRC is much easier if one or more points on the SWRC are known from lab or field measurements. Al Majou et al. (2008) showed in their study that the best result could be obtained by using the volumetric water content at field capacity as a predictor when compared to classical variables such as soil texture, bulk density or organic matter content.

2.1.4   Hysteresis

The SWRC is hysteretic, that is to say the water content at a given soil water pressure is not the same for a drying and for a wetting soil. More precisely said, a soil contains less water at the same

soil water pressure when it is subject to wetting than if it is to drying (Pham et al., 2005; see Fig. 9). The reasons for this phenomenon are manifold, as described by Klausner (1991):

1. Irregular cross-sections of the pore passages („bottle-neck effect")

2. The difference in contact angles between advancing and receding menisci

3. Entrapped air having a different volume when the soil water pressure is increasing than when it is decreasing

4. Changes in soil viscosity due to mechanical load („thixotropy") during the wetting and drying history of the soil

Although the hysteretic behaviour of the SWRC has been known for a long time, most applications and models still assume the relationship between the water content and the soil water pressure to be unique (Pham et al., 2005). Some examples for models aiming at predicting the hysteretic behaviour are the Feng and Fredlund (1999) model and two models by Mualem (1974; 1984).

2.2   *Measurement Methods*

Volumetric scale is a very important variable to consider when measuring soil water content or soil water potential. In this chapter, a brief description of the available methods to measure the water content as well as the soil water potential from the profile to the catchment scale is presented. Though it is not complete, literature is mentioned providing a good overview. Some examples of sensor types are given and the commercially available sensors used in the experiments or installed at the BMN sites will be described briefly.

2.2.1   Water Content

The soil water content can be measured directly by taking a soil sample and drying it. The gravimetric water content can then be calculated using the following formula:

$$\theta_m = \frac{M_w}{M_s} \tag{6}$$

Fig. 9: *Hysteresis of the SWRC. The two main curves are the boundary drying and the boundary wetting curve. Curves in between are called scanning curves (modified after Scheffer and Schachtschabel, 2002 and Pham et al., 2005).*

where θ_m = gravimetric water content (g/g), M_w = mass of the water (weight difference between after sampling in the field and after drying in the lab, g) and M_s = mass of the solid parts (weight after drying in the lab, g).

The volumetric water content can be obtained by calculating the bulk density:

$$\rho_b = \frac{M_s}{V_s} \tag{7}$$

$$\theta_v = \theta_m \cdot \frac{\rho_b}{\rho_w} \tag{8}$$

where ρ_b = bulk density (g/cm^3), V_s = volume of the soil sample (cm^3), θ_v = volumetric water content (cm^3/cm^3) and ρ_w = density of water (g/cm^3).

This direct measurement process is destructive and can thus not be carried out over a long timespan. For continuous soil moisture measurements, indirect measurement techniques are predominating (Scheffer and Schachtschabel, 2002).

Indirect water content measurements are usually based on measuring physical properties which differ between water and the other soil parts, namely water and air. Examples for physical properties as indicators for the water content are the electrical conductivity, the thermal conductivity, the neuron diffusion or the debilitation of γ-rays. The propagation velocity of these indicators can then be related to the water content (Scheffer and Schachtschabel, 2002). The most common measurement techniques as well as relevant sensors are described here.

2.2.1.1   Time Domain Reflectometry (TDR)

The TDR-technique uses the propagation speed of electromagnetic waves emitted by the metal sensor to determine the water content. Water has a higher dielectric permittivity (also called „dielectric constant", approx. 81 As/Vm) than soil minerals (approx. 3 to 5 As/Vm) or air (approx. 1 As/Vm) and thus a higher water content leads to a later reflection of the electromagnetic wave (Scheffer and Schachtschabel, 2002).
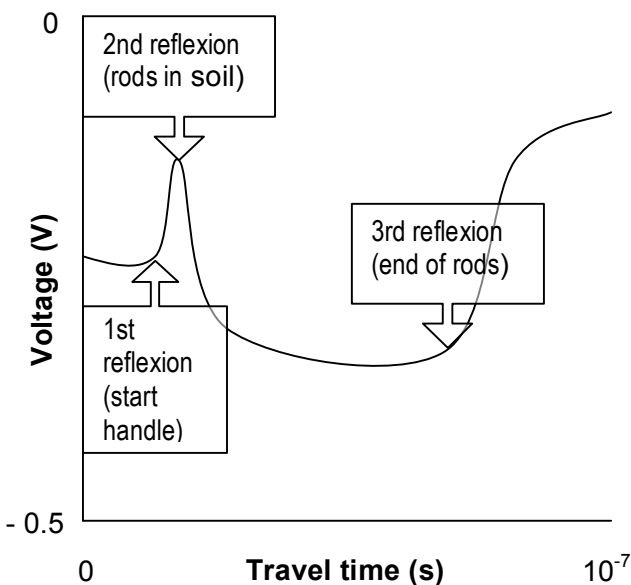
Fig. 10: *TDR-waveform with first, second and third reflection indicated by the arrows (modified after Odegard, 2000).*
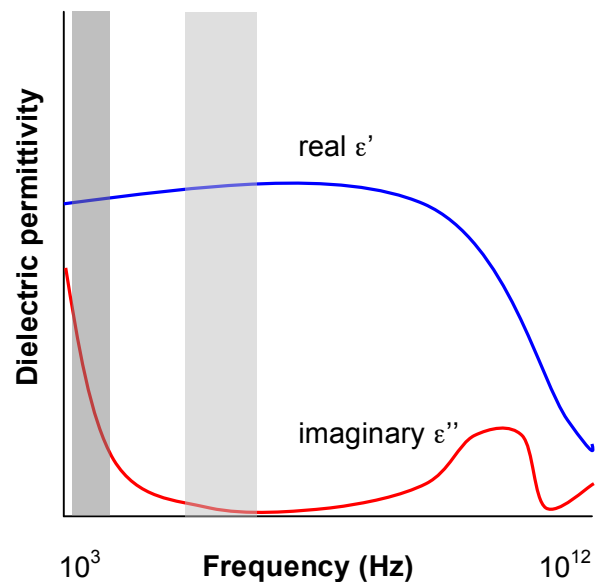
Fig. 11: *Frequency depencence of the real (ε', blue) and imaginary (ε'', red) part of the dielectric constant and frequencies used by the TDR (light grey) and FDR (grey) sensor types. The disturbing imaginary part is at a minimum at TDR frequency (modified after IMKO, 2006).*

The waveform starts with the reflexion of the coaxial cable in the handle. The second reflexion takes place in the beginning of the transition rods in the soil, and the last reflexion is at the end of the rods (see Fig. 10). With the help of the difference between the second and third reflexion, the travel time is calculated and can then be used to deduce the bulk dielectric permittivity. The dielectric permittivity is a number that consists of a real and an imaginary part. The TDR-technique uses a frequency between 600 MHz and 1.2 GHz where the imaginary part is almost 0 and can thus be neglected (see Fig 11). Topp et al. (1980) were among the first ones to describe an empirically based equation to turn the dielectric permittivity into the water content. This equation is still the most widely used and valid up to 50% volumetric water content almost regardless of the soil type as long as we are dealing with mineral soils (lecture notes Vadose Zone Hydrology, Or et al.,2013; see also Section 3.1.2.1 and equation 16). There are also physically based dielectric mixing models that

allow the conversion of the dielectric permittivity to the water content (Roth et al., 1990; Flühler and Roth, 2004). However, for the applicance of this model, the soil porosity needs no be known.

The measuring volume of a TDR probe depends on its construction. Most sensors have 2 to 3 metal rods. Sensors with 2 metal rods destroy the soil less severely and measure the water content over a higher soil volume, making it more robust towards irregularities (Topp and Ferré, 2005).

Many different types of TDR sensors exist on the market. Their high accuracy ($\pm$ 0.013 m^3/m^3 as reported by Topp et al., 1980) as well as the handling without calibration makes them a standard device. However, the price of a TDR is quite high and not affordable for every application. Examples of sensor types on the market are the TRIME-IT (UMS, 2001), TRIME-EZ (UMS, 2001) and TRIME-Pico64 of Imko.

Due to the high price of the TDR probes, a variety of alternative sensors have appeared. Most of the systems available are listed here.

2.2.1.2 Electrical Impedance

Sensors using electrical impedance are part of the Frequency Domain Reflectometry (FDR) group. This group also sends out electromagnetic waves to determine the dielectric permittivity and finally the water content. A standing wave is generated from the reflection of an electromagnetic wave at the propagating wave. The behaviour of this standing wave is then measured and attributed to the dielectric permittivity (Seyfried et al., 2005). The Stevens Hydra Probe (Stevens Water Monitoring Systems, 2007) used at the BMN sites, which uses an emission frequency of 50 MHz, belongs to this group (see Fig. 12; left).

2.2.1.3 Capacitance Measurements

Capacitance sensors also belong to the FDR group and make use of the electromagnetic wave, as the TDR. They also look similar to a TDR probe with metal rods in different shapes available. However, their price lies clearly below the one of a TDR probe making it a popular alternative. By rapidly turning a positive and ground electrode on and off, the probe and the soil form an inductance-capacitance circuit (Kizito et al., 2008). The frequency used is lower than the one of the TDR, namely between 5 and 150 MHz. The charging time of the electromagnetic field is proportional to the capacitance, which can directly be turned into the water content with the help of an inverse square root function (see Topp and Ferré, 2005). However, the relationship has not

Model:	Hydra Probe
Manufacturer:	Stevens
Measured Parameter:	Water content
Type:	Electrical Impedance (FDR)
Accuracy:	$\pm$ 0.03 m^3/m^3
Precision:	$\pm$ 0.003 m^3/m^3
Temperature measurement:	yes
Source:	Stevens (2007)

Model:	10HS
Manufacturer:	Decagon Devices
Measured Parameter:	Water content
Type:	Capacitance (FDR)
Accuracy:	$\pm$ 0.03 m^3/m^3 (Std.)
	$\pm$ 0.02 m^3/m^3 (soil specific calibration)
Temperature measurement:	no
Source:	Decagon (2010)

Fig. 12: *Technical details of the water content sensor installed at the Bodenmessnetz sites (Hydra Probe; left; Stevens, 2007) and the additionally installed 10HS (right; Decagon, 2010).*

proven robust and empirical calibrations according to the soil type are recommended (Topp and Ferré, 2005). Also, at such low frequencies the noise due to temperature or soil electrical conductivity (imaginary part of the dielectric permittivity, see Fig. 11) is higher. Numerous studies have thus come to the conclusion that a high measurement frequency should be used to avoid these noises (more than 70 MHz according to Kizito et al., 2008). Examples of capacitance sensors on the market are the Decagon EC-5, Decagon 5TE, Decagon 10HS (Decagon Devices, 2010; see Fig. 12; right), Delta T ML2x (Theta Probe; UMS, 2004) and Delta T Devices SM200. For further information concerning calibration and use of capacitance probes, see Starr and Paltineanu (2002).

2.2.1.4   Neutron Scattering

One of the eldest systems to measure soil water content is the neutron scattering method. The device consists of an access tube that allows the installation of a neutron probe (source and detector) in a certain soil depth. The probe then emitts neutrons (Americium-241 and Beryllium) which propagate at quite a high speed until they collide with hydrogen atoms. The collision slows the neutrons down, making them „slow" or „thermalised" neutrons. Their number, being proportional to the number of hydrogen present (and thus a proxy of the water content), is then measured by the detector (Johnson, 1962; Flühler and Roth, 2004). Because also other soil properties such as carbon content or other light elements have an influence on the amount of thermalised neutrons, the relationship between thermalised neutrons and water content needs to be calibrated for every soil. Furthermore, the probe contains a radioactive source (Americium-241) and is therefore subject to special regulations (Flühler and Roth, 2004).

2.2.1.5   Gamma Sensor (Transmission)

The gamma sensor works with the principle of density measurement through radiation absorption. The law used hereby is the Beer-Lambert law, which states that the relative decline in radiation intensity is a material constant determined by the absorbance and density of a material. Since these values can be approximately calculated for the soil air and matrix, the soil water part can be obtained by subtracting the known parts from the total decline in radiation density. However, the use of this method is usually limited to the laboratory because it requires the installation of two tubes (source and detector) in a soil. As for the neutron scattering method, the source of the gamma rays are radioactive elements (Americium-241 for layers of a few centimetres, Caesium-137 for layers of 20-30 cm) and therefore special care needs to be taken (Flühler and Roth, 2004).

2.2.1.6   Dual Heat Probe

Campbell et al. (1991) proposed the use of a sensor with two parallel rods, one emitting heat and a thermocouple registering the temperature rise. With the help of the maximal temperature rise, the volumetric heat capacity of the soil can be calculated. The latter is isself related to the water content by the heat capacity of soils and water. For further information see also Bristow et al. (1994).

2.2.1.7   Fibre Optics (DTS)

Recently, Steele-Dunne et al. (2010) came up with a new method to passively measure the water content. Temperature and water content are measured at 1 m resolution with the help of the reflection characteristics of emitted laser pulses. Whereas the methods 2.2.1.1 until 2.2.1.6 mentioned before measured the water content at profile scale and a small soil volume, this method allows a bigger picture with cable lengths up to 10 km.

2.2.1.8   Radiometer Measurements

Surface soil moisture can indirectly be measured with passively emitted microwaves, because it influences the emitted temperature brightness of a surface significantly (Kerr et al., 2001). This relationship has been made use of by the SMOS (Soil Moisture and Ocean Salinity) satellite launched in November 2009. The goal of the SMOS mission is the provision of global data on soil

moisture with a spatial resolution of 35 to 50 km, an accuracy of 4% volumetric soil water content and a revisit time every 1 to 3 days (ESA, 2013). Radiometer measurements can also be performed at a higher spatial resolution by installing an antenna a few metres above the soil surface (lecture notes Vadose Zone Hydrology, Or et al., 2013).

2.2.1.9   Geophysical Methods

The Ground Penetrating Radar (GPR), the Electrical Resistivity (ER) and the Electromagnetic Induction (EMI) techniques form the group of geophysical soil moisture measurements.

The GPR transmits electromagnetic waves into the soil. At the same time it receives the backscattered signals giving hints about subsurface layering as well as the water content. Water content dynamics can be extracted by analysing time shifts, similar to TDR waveform analysis (lecture notes Vadose Zone Hydrology, Or et al., 2013).

When making use of ER mapping, electrodes arrayed in a field provide a cross-section of the electrical resistivity, which can be converted to water content using Archie's law (lecture notes Vadose Zone Hydrology, Or et al., 2013).

The EMI technique maps the electrical conductivity by inducing electromagnetic waves into the soil (lecture notes Vadose Zone Hydrology, Or et al., 2013).

2.2.2   Soil Water Potential

The energy state of the soil water is measured with the soil water potential simplified as the sum of the matric- and the gravitational potential (osmotic and gas potential are usually neglected, see also 2.1). Due to mass conservation, media always flow from regions of higher potential to regions of lower potential. The soil water potential thus drives the movement of water in a soil (Scheffer and Schachtschabel, 2002). It can either be expressed as a pressure (energy per volume of water, Jm^{-3} or Pa) or as a water column length (energy per unit weight of water, J (9810 kg m $s^{-2})^{-1}$ or m). Although the latter is very often used in vadose zone hydrology, hPa will be the unit used in this thesis, because it is independent of temperature changes since it does not include the temperature dependent density of water (Flühler and Roth, 2004). Even though the matric potential is physically a negative pressure, the values in this thesis are treated absolutely (meaning positive values when dry, negative values when extremely wet) for practical reasons (see also 2.2.2.1).

There is no single matric potential sensor that is capable of measuring the full range of interest (Durner and Or, 2005). Tensiometry is the method used for the wet range up to approximately 1000 hPa. It is the most widely used and generally regarded as being accurate if done properly (Durner and Or, 2005). In the intermediate range, the use of reference porous media such as gypsum blocks, granular blocks or filter paper, or alternatively of heat dissipation sensors, is recommended. However, they need to be calibrated with the help of the water content of the soil (Durner and Or, 2005; Topp and Ferré, 2005). For measurements of the soil water potential in the dry range (>100'000 hPa), the dew-point temperature is measured by a thermocouple psychrometer and then related to the relative humidity, which is proportional to the amount of water present in the soil (Durner and Or, 2005). Since the range of interest in this thesis, namely the application of the soil water potential as a proxy to determine soil stability, lies within the wet range, the focus in this theory part lies on tensiometry.

2.2.2.1   Tensiometry

A tensiometer is a device to measure the sum of the pneumatic (= gas) and matric potential. For most applications, the pneumatic potential is assumed to be equal to zero since the air pressure in the soil is usually equal to the atmospheric pressure (Durner and Or, 2005). The matric potential thus measured is the pressure difference between the atmospheric air pressure and the pressure of the soil water. It has a negative sign with respect to atmospheric pressure. By the term „suction" or „tension", we refer to the absolute value of this pressure difference (Durner and Or, 2005). The

matric potential, which is measured by the tensiometer, is the sum of the capillary and adhesive forces present in a soil (Scheffer and Schachtschabel, 2002).

The measurement principle of a tensiometer is relatively simple. A tube filled with water is installed with contact to the soil through a membrane at its end (usually a ceramic cup). The water inside the tube and the soil water are thus at equilibrium, because the membrane is permeable to water but not to air. If the matric potential of the soil lowers (that is to say it becomes more negative), water is sucked out of the tensiometer by the soil until an equilibrium state is reached. Water flowing out creates an underpressure inside the tensiometer tube. The underpressure can then be measured with a manometer. The first tensiometers suggested by Livingston (1908, 1918), Gardner et al. (1922) and Richards (1928) were connected to a simple U-manometer filled with water or mercury. They had a rather long response time and were therefore later replaced by mechanical pressure gauges and pressure transducer tensiometers (Durner and Or, 2005; see also Vachaud and Thony, 1971; Bianchi, 1962 or Watson, 1967). Although, there are other measurement techniques, such as, for example, the Septum Tensiometers, which are stiched through for every measurement (Marthaler et al., 1983), the pressure transducer tensiometers are mostly used today. A pressure transducer consists of a metal membrane, which deforms with pressure change. This process produces an electrical response, which can be measured and related to a pressure (Tandeske, 1991). The pressure transducer system can also be used for automated logging (Durner and Or, 2005). Nowadays, the most advanced tensiometers got the pressure transducer installed inside the ceramic cup (Durner and Or, 2005). This construction allows a shorter water column, which leads to a shorter response time and diminishment of the temperature sensitivity (Sisson et al., 2002). The T8 tensiometer (UMS, 2008) installed at the sites of the BMN is of this type (see Fig. 13 and 14).

The most important limitation of tensiometers is their limited measurement range already mentioned above. It is restricted by the air entry pressure of the membrane as well as by the boiling point of water. The first restriction can be influenced by the choice of the pore diameters of the ceramic cup (Durner and Or, 2005). The second one is physically based, since water starts to boil at the underpressure of -927 hPa (at 20°C and 950 hPa atmospheric pressure; UMS, 2008). Due to this physical property of water, a tensiometer cannot show an absolute value higher than approximately 927 hPa even though the soil might be drier. In the field, the measurement range can even be lower (up to 850 hPa; UMS, 2008). For the data of the BMN, this restriction needs to be considered in summer when soils are dry.

Tensiometer readings can further be negatively influenced by missing soil-tensiometer contact, by the formation of gas bubbles inside the water column (both leading to longer response times), by

Fig. 13: T8 tensiometer with 1) water-filled cup 2) fibreglass reinforced shaft 3) pressure transducer and 4) refill tubes (UMS, 2008).

Model:	T8
Manufacturer:	UMS
Measured Parameter:	Soil water pressure
Type:	Advanced Tensiometer
Accuracy:	± 0.5 hPa
Temperature measurement:	yes
Source:	UMS, 2008; BMN

Fig. 14: Technical details of the T8 sensor installed at the Bodenmessnetz sites (UMS, 2008).

temperature (leading to wrong data interpretation, see also next paragraph) and by frost (freezing of the water in the tube) (Durner and Or, 2005). However, tensiometers installed in 20 cm depth or more that have no water column above the soil surface (e.g. the T8) are considered to be frostproof, because in these depths the freezing front usually penetrates slowly (UMS, 2008).

Tensiometer measurements are influenced by temperature. The physical effect of the capillary tension being influenced by the surface tension of the soil water has been reported by Richards and Gardner (1936). The surface tension of water declines with rising temperatures, making surface tension decline, too (see Section 5.3.1). Furthermore, radiation and temperature effects have been observed causing diurnal fluctuation structures characterised by a drop in absolute values at first and a rise afterwards, starting usually around midday (Buchter et al., 1999). The exact physical reasons for this observation remain unknown, because the change is much larger than expected when looking at the temperature dependence of the surface tension. These air-temperature fluctuations have been attributed to the head space of the tensiometer, where possible gas bubbles are formed (Durner and Or, 2005). The fluctuations also depend on the type of shaft materials used: CAB appears to be more robust than PVC (Buchter et al., 1999). Horizontally installed tensiometers have proven to be most robust against temperature fluctuations, but a vertical installation is also possible if the shafts are insulated (Buchter et al., 1999). Due to the upcoming Advanced Tensiometers mentioned before, which only have a small water column inside the ceramic cup, these thermally affected fluid movements could be minimised (Sisson et al., 2002).

2.2.2.2 Reference Porous Media

In the intermediate pressure range, reference media such as gypsum blocks, fiberglass or nylon are used to determine the matric potential by measuring their water content with the help of electrical resistance. The matric potential measurements are thus indirectly obtained by their relation to the water content inside the media. A site-specific calibration is needed in any case. Other disadvantages of these methods are the temperature dependence, the difficulty of obtaining a good contact with the soil matrix and a relatively long response time (Durner and Or, 2005). Recent developments go into the direction of measuring the water content of the reference porous media with the help of the dielectric permittivity (Durner and Or, 2005).

2.2.2.3 Heat Dissipation Matric Potential Sensors

The heat dissipation matric potential sensors work in a similar way to the dual heat probes described under 2.2.1.6. However, the measurement obtained is converted into a matric potential through a laboratory calibration (Scanlon et al., 2002). The range of measurable matric potentials lies between 100 and 10'000 hPa (Reece, 1996). The advantage of this method is that its measurement is (in contrast to the electrical resistance and dielectric permittivity measurements) independent of the osmotic potential, making it robust also in salt-rich soils (Scanlon et al., 2002).

2.2.2.4 Thermocouple Psychrometry

To measure the water potential, psychrometry relies on the water potential in the air phase, which is in equilibrium with the water potential and related to relative humidity (Durner and Or, 2005). Two thermocouple junctions measure the temperature difference between the ambient temperature („dry bulb temperature") and the temperature of an evaporating surface („wet bulb temperature"). This difference can then be used as input for the psychrometer equation and thus the relative humidity can be calculated (Durner and Or, 2005). The temperature needs to be determined with very high accuracy in order to detect fine changes in the soil water potential up to -10^6 hPa. Therefore thermocouple psychrometers do not perform well if installed close to the surface, where thermal gradients are important (Durner and Or, 2005).

2.3 *Soil Water Flux*

Water flux in a soil is driven by a potential gradient. The potential referred to is the soil water potential. Water flux always occurs from regions of higher potential to regions of lower potential because of energy conservation (Flühler and Roth, 2004). To obtain a flux (rate of mass flow across a unit of area), the gradient is multiplied by the hydraulic conductivity of a soil.

2.3.1 Saturated Flow

Darcy (1856) was the first one to describe saturated flow as the product of the hydraulic gradient and the saturated hydraulic conductivity. Here is the formula of Darcy's law:

$$Jw = -Ksat \cdot \frac{\Delta H}{\Delta z} \qquad (9)$$

where Jw = water flux density (cm/d), Ksat = saturated hydraulic conductivity (cm/d), H = total pressure head (includes soil water pressure and gravitational pressure) (m), z = flow course (length of column, gravitational head) (m).

Ksat is a constant depending on material properties of the soil, overall the pore space geometry (Flüher and Roth, 2004). It is not easy to predict and therefore usually measured newly for every soil (Flühler and Roth, 2004). Even for the same soil, the difference between different measurement methods applied may lead to variation in the order of two magnitudes (Mohanty et al., 1994). Nevertheless, trials to obtain Ksat empirically from the texture have been made, for example by Schaap et al. (2001) with the help of a large database considering various soil textures (ROSETTA). Darcy's law is only valid for laminar flows, a constraint that is usually given under natural conditions in a soil (Scheffer and Schachtschabel, 2002).
The result obtained with Darcy's law is a flux over the whole cross sectional area of a soil, including solids and pores (Flühler and Roth, 2004).

2.3.2 Unsaturated Flow

Most of the time, a soil is not fully saturated, and flow conditions are influenced considerably by the saturation state of a soil. This effect is mainly due to the hydraulic conductivity depending on the amount of water in the system (Flühler and Roth, 2004). The more a soil desaturates, that means the more air it contains in its pores, the harder it is for water to penetrate. Therefore, we need to take into account the actual water content to calculate the flow in a soil. Whereas Ksat introduced in Darcy's law was a constant, K(h) defined as the unsaturated hydraulic conductivity is a function depending on h (matric potential) or θ (water content). Usually the water content is taken as the driving parameter, because it describes the volume of the water phase and is thus closer to the flow pathways than the matric potential (Flühler and Roth, 2004).
A formula to calculate the flow of water in unsaturated soils has been introduced by Buckingham in 1907 who extended Darcy's law by replacing Ksat by K(h):

$$Jw = -K(h) \cdot \frac{\Delta H}{\Delta z} \qquad (10)$$

where Jw = water flux density (cm/d), K(h) = unsaturated hydraulic conductivity (cm/d), H = total pressure head (includes soil water pressure and gravitational pressure) (m), z = flow course (length of column, gravitational head) (m).

Since the unsaturated hydraulic conductivity is difficult to measure and highly dependent on the pore size distribution of a soil, attempts to predict K(h) with the help of the soil water characteristics have arisen. The most famous among these developped models are, as partly already mentioned under 2.1.2, the Jackson model (1972), which is physically based or the Brooks and Corey (1964), the van Genuchten-Mualem (1980; 1976) and the Kosugi (1996) model as parametric models (Flühler and Roth, 2004; lecture notes Vadose Zone Hydrology, Or et al., 2013).

All of the models include simplifying assumptions, such as that the pore space geometry can be characterised by a bundle of continuous cylindrical capillaries, that the flow must occur through these capillaries and that the length of these is larger than the length of the corresponding soil column. To account for the latter effect, the tortuosity factor determining the length ratio between the length of a pore and the length of the probe has been introduced (Flühler and Roth, 2004).

The Buckingham-Darcy equation (equation 10) can be used to calculate vertical steady state unsaturated flow. However, a parametrisation of the function K(h), as described above, has to be chosen, to solve the problem.

The calculation of unsaturated and unsteady flow needs the introduction of a continuity equation into Buckingham-Darcy's flux law. The achieved combination is the so-called Richards equation proposed by Richards (1931):

$$\frac{\Delta \theta_w}{\Delta t} - \frac{\Delta}{\Delta z}\left[k(\theta_w)\frac{\Delta H}{\Delta z} \right] = 0 \tag{11}$$

where θ_w = volumetric water content (m^3/m^3), t = time and the rest of the variables as for equation 10.

The Richards equation is, although very generally describing the movement of water in soils, based on a few assumptions: The temperature during the flow is not changing, the parameters θ_w and H are in an equilibrium status, the matrix is not subject to swelling or shrinking and there is contact between the air in the soil and the atmosphere (Flühler and Roth, 2004).

Solving the Richards equation is not trivial because it is a nonlinear partial differential equation. By stepwisely replacing the differentials by differences and discretizising space and time, an explicite numerical solution can be obtained. To solve it, however, the SWRC and soil hydraulic properties must be known. Nowadays, the Richards equation can relatively easily be solved with the help of computational software, such as for example the program HYDRUS-1D (Šimunek et al., 2013), which works with finite elements (Beven, 2012).

In practice, classical soil water flow calculations are challenged because of the presence of macropores. Macropores are large pores in between aggregates (Weiler and Naef, 2003). Macropore flow may be accompanied by turbulent flow processes, for which Darcy's law is not valid (Jarvis, 2007; see also Section 5.4.2). Since HYDRUS-1D is based on the Richards equation (equation 11), the largest pores draining quickly after a precipitation event are not taken into account by the program (Šimunek et al., 2013).

2.4   Soil Water Balance

The general form of the water balance equation, valid also for large areas, is described as follows (Scheffer and Schachtschabel, 2002):

$$P = R + ET + \Delta S \tag{12}$$

where P = precipitation (m^3), R = runoff (m^3), ET = evapotranspiration (m^3) and ΔS = change in water storage (m^3).

Equation 12 is based on mass conservation, therefore the input (precipitation) must be equal to the output (runoff and evapotranspiration). For a certain time and area chosen, input and output may not even out. Then, the difference is assigned to a storage, which has been emptied or filled. When considering a bigger time scale and area, the storage term can be neglected (Scheffer and Schachtschabel, 2002). For Switzerland, the mean annual components of the water balance (mean values of the years 1961-1990) are 1458 mm precipitation, 469 mm evapotranspiration and 991 mm runoff. The storage term, consisting of ice, snow, ground water, surface water bodies, soils and plants, is thus equal to -2 mm (Schädler and Weingartner, 2002).

Soil acts as important water storage. The quantitative description as well as the dynamics of soil water are thus of interest for the understanding of the hydrological cycle (Flühler and Roth, 2004). As already seen in Section 2.2.1, the water content of a soil volume can be measured with various sensors covering a different volumetric scale. The inputs and outputs of this soil volume are usually considered fluxes (water volume per time unit and area) as introduced in Section 2.3.

When looking at a soil volume, the soil water balance is characterised by the following fluxes: Infiltration into the soil, evaporation and drainage out of the soil, capillary rise within the soil and lateral flow into or out of the soil volume looked at (Flühler and Roth, 2004; see Fig. 15).
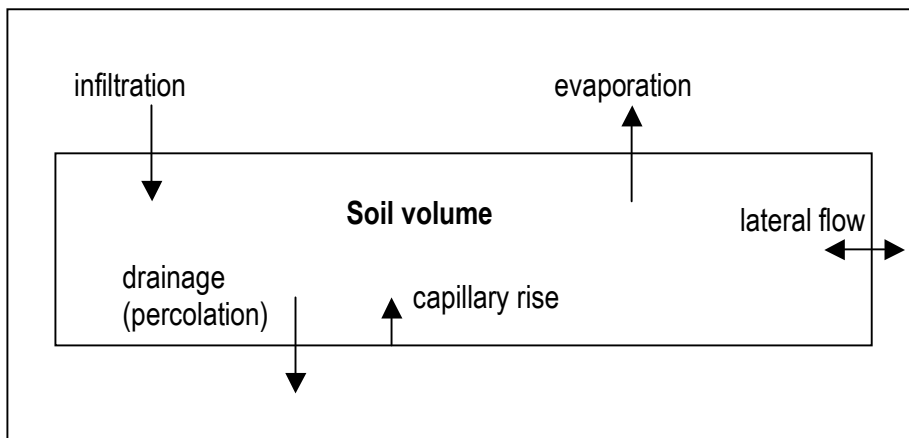
Fig. 15: *Water fluxes determining the soil water balance of a certain soil volume (modified after Flühler and Roth, 2004).*

Often, soil cannot be looked at independently of the vegetation covering it, because plants also take out water of the soil (transpiration) and hinder precipitation to infiltrate by interception (Flühler and Roth, 2004). The same situation as in Fig. 15 for a site including vegetation thus looks more complex (see Fig. 16).
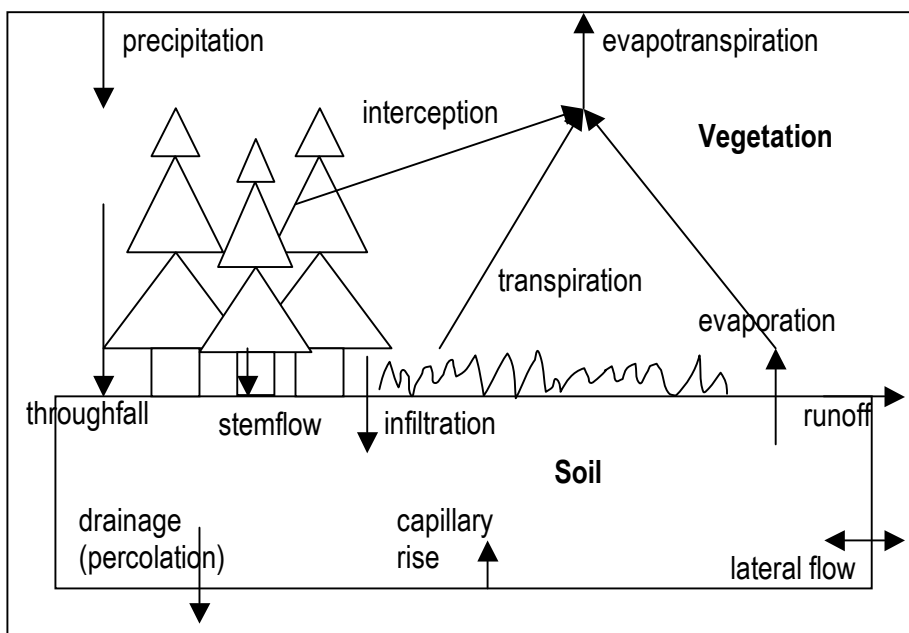
Fig. 16: *Water fluxes determining the soil water balance of a site including the vegetation cover (modified after Flühler and Roth, 2004).*

Precipitation is separated into interception (water retained by vegetation) and throughfall, of which interception is further divided into stemflow (precipitation reaching the soil surface by flowing along the stem) and intercepted water that evaporates. Stemflow is mostly relevant for forests. To obtain the infiltration, interception and surface runoff must thus be subtracted from the total precipitation at a site (Flühler and Roth, 2004).

The other relatively complex variable, evapotranspiration, is defined as the sum of evaporation by the bare soil surface and transpiration by plants (Flühler and Roth, 2004).

If all these components are known, a very detailed soil water balance can be calculated. However, the measurement of some of these fluxes requires a lot of effort. For many applications, a simpler estimation by calculation may serve as well (Flühler and Roth, 2004). An example is the calculation of evapotranspiration with the help of an empirical equation (Scheffer and Schachtschabel, 2002) instead of measuring all the fluxes that form part of it as seen in Fig. 16.

2.5   Soil Mechanical Properties

To determine the shear strength of saturated soils, the effective stress approach by Terzaghi (1943) is often used:

$$\sigma = \sigma' + u \tag{13}$$

where σ = total stress (force per area) (hPa), σ' = effective stress (pressure of the solid parts) (hPa) and u = pore water pressure (hPa).

After equation 13, the shear strength for saturated soils is only dependent on the soil water pressure (Scheffer and Schachtschabel, 2002). The concept of effective stress has then been extended for unsaturated soils by Bishop (1954; 1959):

$$\sigma' = \sigma - \chi u \tag{14}$$

where χ is a factor dependent on the saturation state (1 for saturated soils, 0 for completely dry soils).

The effective stress is the stress that a soil can bare under the current conditions (Scheffer and Schachtschabel, 2002). It has been applied more often in practice than the alternative independent state variables approach (Khalili and Khabbaz, 1998). However, the determination of χ is not trivial and several attempts have been made to find a relationship between χ and the degree of saturation (Khalili and Khabbaz, 1998; Lu et al., 2010).

When looking at equation 14, we can see that the highest stability of a soil can be reached if the pore water pressure (the matric potential) gets more negative (that is to say the soil dries), but at the same time the water content θ does not change that quickly and χ thus stays closer to 1 (Scheffer and Schachtschabel, 2002). The reasons for the general increase in stability for a dry soil are i) the higher rigidity with increasing contact points between the soil particles and ii) the strong capillary forces in the menisci of the pores (Moitzi and Boxberger, 2007). The stability of a soil is thus dependent on both soil water pressure and soil water content (Gallipoli et al., 2003).

In practical applications, the concept of precompression stress is often used to determine the maximum amount of pressure that can be applied without causing a plastic deformation (Scheffer and Schachtschabel, 2002). The precompression stress depends on soil properties as well as actual saturation (Horn and Fleige, 2003) and determines the frontier between elastic (and thus reversible) and plastic deformation (Moitzi and Boxberger, 2007). It can be seen in the loading curve of a soil (see Fig. 17). The loading curve describes change of the void ratio (volume of pores divided by volume of solids) with change of vertical stress for laterally unlimited load (Scheffer and Schachtschabel, 2002). As long as the soil is compacted the first time, the change is linear, which means the comprimation state of the soil is equal to the load. The soil is deformed plastically. If the soil has been stressed and stabilised at a certain level (e.g. by the pressure of a glacier during the ice

age), a new relationship between the vertical stress and the void ratio is generated. It is called „re-compaction" or secondary compaction (see Fig. 17). A new stress up to the maximal vertical stress that had been applied before results in an elastic deformation on the re-compaction line. The precompression stress is thus the maximal stress that can be exerted on the soil at a given time without leading to a new first compaction (Scheffer and Schachtschabel, 2002), so it is the intersection point of the first compaction and the re-compaction line. Qualitatively said, the soil can bear a stress that is smaller or equal to its precompression stress with little or no negative consequences.
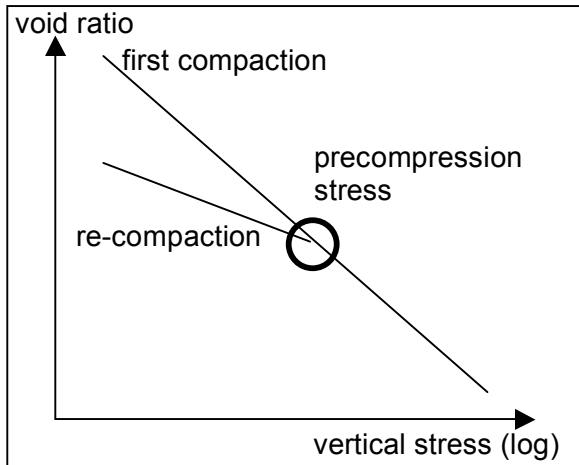
Fig. 17: Loading curve with precompression stress (black circle) where first compaction and re-compaction intersect (modified after Scheffer and Schachtschabel, 2002).

One way to measure the loading capacity of a soil (that is to say its compression strength) is by measuring the penetration resistance (Flühler and Roth, 2004). Soil water pressure has been shown to be an indicator for the penetration resistance (Taylor et al., 1966). However, this parameter is also influenced by soil skeleton content, soil texture and aggregation because they determine the cohesion (Hartge, 1978; Hartge and Horn, 1989). The penetration resistance is measured with the help of a penetrometer consisting of a metal tube with a cone at the front. The tube is inserted into the soil either manually or with the help of an engine. Simultaneously, the pressure exerted on the cone (= cone point resistance) as well as the penetration depth are recorded (Bradford, 1986). The device needs to be calibrated for the cone area and cone angle because they influence the force applied and the friction during the insertion. Penetration resistance is also a recommended parameter for the estimation of soil compaction (Buchter and Häusler, 2009).

3 Material and Methods

3.1 Field Work

3.1.1 Sites

3.1.1.1 Site Selection

Since the main constraint for the field work (especially the sensor comparison) was the availability of closeby meteorological and soil-specific measurements, the location was given to be one of the BMN sites in the Canton of Solothurn. For the selection, the following criteria were relevant:

- reasonable field data of both soil water pressure and water content
- broad range of water contents at the same soil water pressure in the soil water pressure range relevant in winter (0 to 100 hPa)
- reliable data provision
- fairly common soil texture
- landcover grassland rather than forest (because of its relevance for the building industry as well as agriculture)
- contact to land owner

Three sites (Aetigkofen, Subingen and Stüsslingen) could thus be identified, of which Stüsslingen (loam) was chosen for most of the field work (sensor comparison, cone penetrometer measurements) due to its easy accessibility. To have an additional soil type, soil samples were also taken at the Aetigkofen (sandy loam) site.

3.1.1.2 Stüsslingen

Figure 18: *Position of the BMN-site in Stüsslingen (SO). Map: map.geo.admin.ch.*

The BMN site in Stüsslingen is located on the edge of Stüsslingen village close to a farmhouse (see Fig. 18 and 20) at 451 m above sea level. The soil was classified as „Regosol" (Swiss classification system, type 1323; BGS and FAL, 2002; see Fig. 19) and has a loamy texture according to the FAO

soil texture classification (FAO, 2006; see Table 2). It contains a small amount of soil skeleton since its underground is of alluvial origin (data: FS BS 2011).

Figure 19: Soil profile in Stüsslingen.
Picture: M. Brotschi/M. Carizzoni (provided by FS BS).

Figure 20: BMN station in Stüsslingen.
Picture: M. Brotschi/M. Carizzoni (provided by FS BS).

Table 2: Soil profile description of the Stüsslingen loam. Horizon names are according to the Swiss classification system (BGS and FAL, 2002). Numbers in brackets are estimates by experts (pH: Hellige), the others represent lab measurements. Data: FS BS Solothurn (2011).

Depth (cm)	Horizon	Organic matter (%)	Clay (%)	Silt (%)	Sand (%)	pH
0-14	Ah 1	6.1	29.2	39.2	31.6	7.2
14-33	Ah 2	2.4	22.1	45.4	32.5	7.5
33-54	Cg (cn)	0.9	17.1	34.5	48.4	7.6
54-71	bIICBg(g), cn	(0)	(24)	(40)	(36)	(7.3)
71-87	Cg(g),cn	(0)	(28)	(28)	(36)	(7.5)
87-109	Cg,cn	0.3	22.0	52.9	25.1	7.4

3.1.1.3 Aetigkofen

The BMN site in Aetigkofen is located on the western edge of Aetigkofen village (see Fig. 21 and 23) on 601 m above sea level. The soil was classified as „Parabraunerde" (Swiss classification system, type 1323; BGS and FAL, 2002; see Fig. 22) and has a sandy loam texture according to the FAO soil texture classification (FAO, 2006; see Table 3). As in the case of the Stüsslingen loam, it contains a small amount of soil skeleton, because it has been formed over a moraine (data: FS BS, 2011).
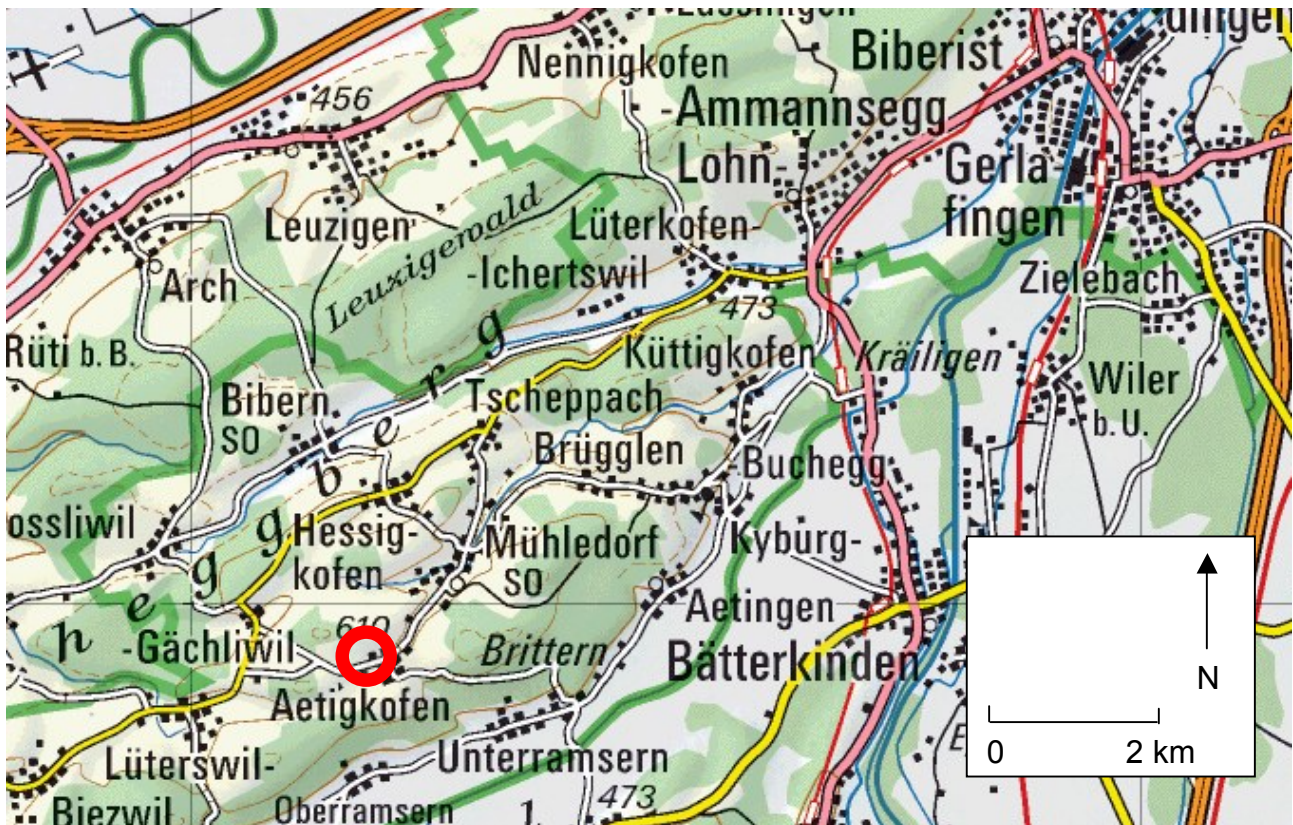
Figure 21: *Position of the BMN-site in Aetigkofen (SO). Map: map.geo.admin.ch.*

Figure 23: *BMN station in Aetigkofen.*
Picture: M. Brotschi/M. Carizzoni/Ch. Hauert (provided by FS BS).

Figure 22: *Soil profile in Aetigkofen.*
Picture: M. Brotschi/M. Carizzoni/Ch. Hauert (provided by FS BS).

Table 3: *Soil profile description of the Aetigkofen sandy loam. Horizon names are according to the Swiss classification system (BGS and FAL, 2002). Numbers in brackets are estimates by experts (pH: Hellige), the others represent lab measurements. Data: FS BS Solothurn (2011).*

Depth (cm)	Horizon	Organic matter (%)	Clay (%)	Silt (%)	Sand (%)	pH
0-7	EAh,(g)	4.8	14.1	28.3	57.6	5.4
7-26	EAh,cn,(g)	1.5	12.6	28.3	59.2	4.6
26-39	EB(x),cn	(0.5)	(9)	(32)	(59)	(4.8)
39-65	BW,x	(0)	(11)	(32)	(57)	(5)
65-97	BWlt 1	0.2	15.6	20.2	64.2	4.7
97-140	BWlt 2	(0)	(16)	(32)	(52)	(5)

3.1.2   Sensor Comparison

3.1.2.1   Technical Setup

Since most of the low soil water pressure measurements among the different cantons have been recorded with the T8 tensiometers of UMS (UMS, 2008), additional soil water pressure measurements are desirable to exclude sensor-specific bias. These have been performed by custom-built pressure transducer tensiometers from the ETH STEP group (details of installation see Section 3.1.2.2). Eight pressure transducers have therefore been numbered and connected to a Campbell Scientific AM416 Relay-Multiplexer. To convert their measurements from mV to bar (and later hPa), a specific calibration with the help of a vacuum pump was performed in the lab. As an example, the equation for the third pressure transducer is the following:

$$y = -0.1204\,x + 0.0747 \tag{15}$$

where y = pressure (bar) and x = reading of pressure transducer (mV).

To be able to compare the measurements of the Stevens Hydra Probe to other water content measurements, six TDR-Sensors (self-made by the technicians at the STEP research group) and four Decagon 10HS-Sensors (Decagon Devices, 2010) were chosen to be installed in Stüsslingen in 20 and 35 cm depth (see Section 3.1.2.2). The reason for the selection of the TDR-Sensors is that these sensors are looked at as state-of-the-art for water content measurements and are also often used as a standard reference if various sensors are compared (Mittelbach et al., 2012; Rosenkranz et al., 2013). The TDR-Sensors installed measure using the quite robust and texture-independent Time Domain Reflectometry method (see Section 2.2.1.1) and consist of a plastic case with two metal rods of 18 cm length. However, a TDR-Sensor is rather expensive to acquire. The Decagon 10HS-Sensors (Capacitance sensor, see Section 2.2.1.3) have been chosen for comparison as a less costly alternative, which the STEP research group also uses for simple soil moisture analysis. They have an accuracy of ± 0.03 m³/m³ (Mittelbach et al., 2012).

Fig. 24: *Em50-Datalogger recording measurements of the 10HS-sensors.*

All six TDR100-Sensors were numbered and connected to a Campbell Scientific SDMX50 Multiplexer. To convert the dielectric measurements to volumetric water content measurements, the Topp equation (Topp et al., 1980) has been used:

$$\theta = 10^{-4}(0.043\varepsilon^3 - 5.5\varepsilon^2 + 2920\varepsilon - 530) \tag{16}$$

where θ = water content (m^3/m^3) and ε = dielectric constant (As/Vm) measured by the TDR).

The five Decagon 10HS-Sensors have been connected to an ECH$_2$O Em50-Datalogger, which is operated by 5 AA-Batteries (see Fig. 24). The ECH$_2$O datalogging system is quite easily applicable and the measured values are automatically converted to volumetric water content.

The data acquisition system for the TDR-Sensors and the tensiometers consisted of a Campbell Scientific CR1000 datalogger fed either directly by a solar panel or, if the power supply of the solar panel was not enough, by a 12V car battery held by a PS12E case of Campbell Scientific. The datalogger was programmed in CRbasic to measure every 15 minutes (see Appendix A). All the technical devices except for the ECH$_2$O Em50-Datalogger were stored in a metal case (see Fig. 26).

Figure 25: *Installation of the water content sensors in the middle hole (10HS on top, TDR on bottom).*

Figure 26: *Metal case with data logging system and power supply.*

3.1.2.2 Sensor Installation

The devices were installed on December 4th, 2013 and started measuring that day at 2:30 p.m..

The metal case was screwed to two wood plugs approximately 25 cm above the ground surface (see Fig. 26). The ECH$_2$O Em50-Datalogger already has a plastic case coming with it, which was installed separately approximately 1 m above ground (see Fig. 24).

The water content sensors were installed in three different holes dug in front of the long-term T8 tensiometers. Two TDR-Probes have been inserted horizontally in every hole, one in 20 cm and one in 35 cm depth respectively. Right next to them, a 10HS-Sensor has been installed in the eastern hole in 20 cm depth, in the western hole in 35 cm depth and at both depths in the hole located in the middle (see Fig. 25 and 28).

The tensiometers were chosen to be mounted as close to the long-term T8 tensiometers as possible. At every location (east, middle, west; see Fig. 28) two tensiometers have been installed, one in 20 cm and one in 35 cm depth respectively. Therefore, there were three tensiometers in every depth, which is the recommended minimum number (Matile et al.,

Figure 27: *Tensiometer after the installation without (left) and with foam radiation shields (improved version).*

2011; Webster, 1965). The installation included the drilling of a hole (slightly narrower than the diameter of the porous cup to guarantee a good contact with the soil matrix), the insertion of the PVC-pipe with the ceramic cup at the bottom, the filling with 2/3 deareated water and 1/3 ethanol (coloured yellow with food colouring), the closure with a plug connected to the pressure transducer and the coverage with a blue lid as well as a plastic bag. To prevent rainwater from flowing downwards along the tensiometer pipe, fango loam has been dispersed around the tensiometer pipe. For the protection against solar radiation, foam radiation shields were put over the installed tensiometers (see Fig. 27). The first version of the radiation shield protection installed on December 4th, 2013 appeared to be insufficient in height since all soil water pressure measurements showed huge oscillations during sunny days. The protection has thus been improved on December 12th.

The measured values were downloaded to a laptop by cable with the help of the LoggerNet program on every field day. A detailed description of the weather and work done on the field days can be found in the field journal in Appendix B. The tensiometer data were, after their automatic processing to bar, converted into hPa and corrected for the height of the tensiometer shaft with the help of the tensiometer equation:

$$\psi_m = \psi_{pt} + (z_{pt} - z_{cup}) \tag{17}$$

where ψ_m = matric potential (negative) (hPa), ψ_{pt} = reading at pressure transducer (negative) (hPa), z_{pt} = height of pressure transducer above soil surface (positive) (cm), z_{cup} = height of cup below soil surface (negative) (cm).
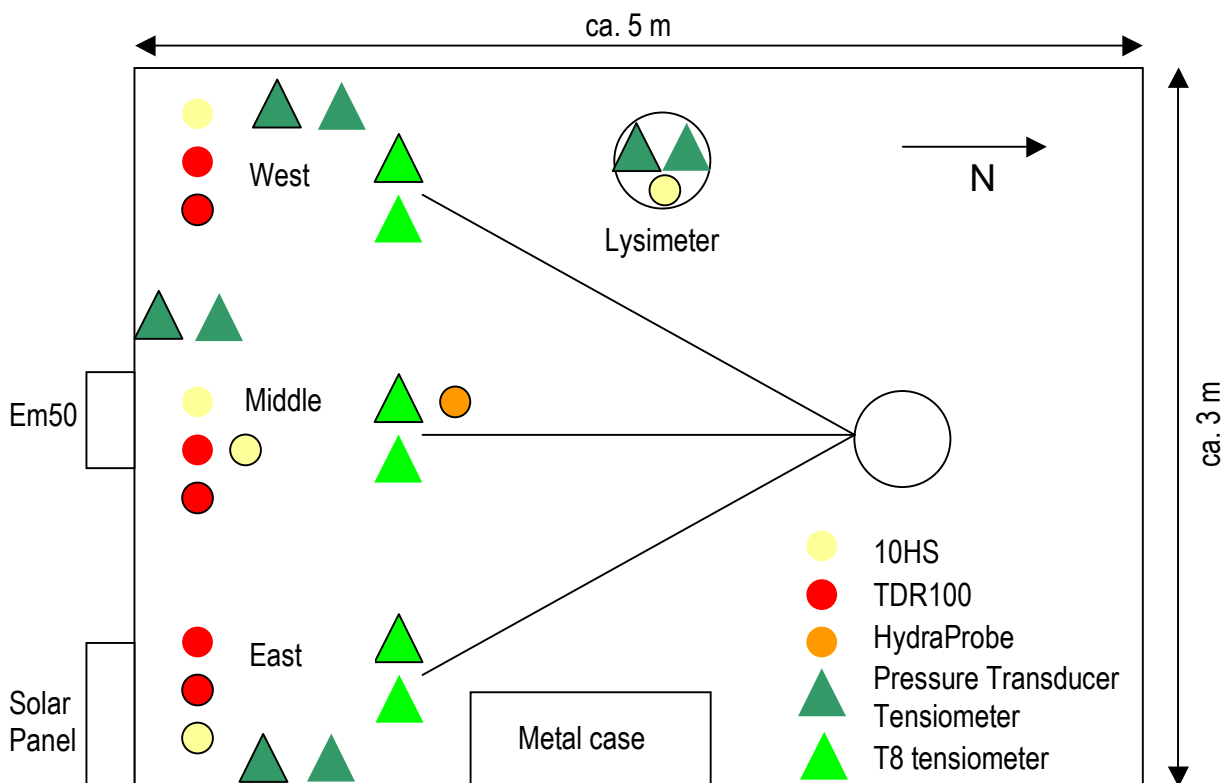
Figure 28: *Plan of the station setup. T8 tensiometers and Hydra Probe had been installed before (sensors BMN). Black rim around symbol means installation in 20 cm depth, no ring means installation in 35 cm depth.*

Since in this thesis, soil water pressure values are looked at as positive values, the negative matric potential obtained was then multiplied by -1.

The data recorded was then looked at and obvious measurement errors, such as negative water contents or water contents >1, have been deleted manually. For sensors with jumping values (as for

example the TDR in the eastern hole in 20 cm depth in the beginning), all measurements that exceeded a change of 6 Vol. % within the 15 minutes interval have been erradicated.

After the installation of the lysimeter (see Section 3.1.2.3), some measurement problems among the tensiometers could be observed. Whenever one sensor measured either a positive pressure or a pressure out of range, all other pressure transducers appeared to jump approximately 20 to 30 hPa, either in a positive or a negative direction. They still had a reasonable reaction, but the absolute values could not be trusted. Obvious measurement errors have been deleted during data processing and the periods taken for further analyses have been chosen carefully with respect to these measurement problems.

3.1.2.3   Lysimeter

Additionally, a lysimeter (here defined as a closed system where no mass exchange occurs) has been installed on December 19th, 2013 close to the western location (see Fig. 28). It is a simple construction of a metal bucket that has been filled with local soil and densely sealed with tree wax (see Fig. 29). Three holes in the lid allowed the installation of two tensiometers and one Decagon 10HS sensor inside the bucket. The aim of this installation was the isolation of temperature as factor influencing the soil water pressure measurements by excluding water content changes through precipitation and evapotranspiration. The bucket has a height of 25.5 cm and has been installed in 38 cm depth, so that the two tensiometers could be placed at about the same depths as the other ones (20 and 35 cm respectively). Although no big differences between the measurements of the two tensiometers are to be expected, small water fluxes in the beginning as well as minor fluctuations due to temperature differences between the two depths could be extracted. The water content sensor has been installed almost vertically in the uppermost 10 cm of the bucket as a control for possible water content changes.

Figure 29: *Installation of the lysimeter (from left to right): 1) digging a hole and filling the bucket, 2) insertion of sensors, sealing and placing of bucket in whole, 3) closing hole and complete installation of tensiometers.*

However, the tensiometer installed about 35 cm below soil surface ran empty every few days. After one refil without avail, it has been replaced on December 27th, 2013. The water content increased slightly during the first week. This observation could be either due to leaking of the sealed bucket in the upper part or due to the small amount of water that has been released through the tensiometer. After the replacement of the tensiometer the leakage had vanished. Nevertheless, ever since the replacement some measurement errors among all tensiometers could be observed. The tensiometer, which has been installed deeper in the bucket showed strange measurements, even after replacement of the pressure transducer. Its results could therefore not be further processed. The other tensiometer ran empty quite a few times and did not always provide reliable measurements either. For the plots in the Results Section 4.3 and 4.5, sequences with reasonable measurements have been chosen.

To get some additional measurements, a T8 sensor has been installed on March 4th, 2014 at 20 cm depth in the lysimeter and connected to a computer with the help of a TensioLink adapter (UMS, 2005). However, there is only data of approximately 6 hours since the power supply was limited to the computer accumulator.

3.1.3   Cone Penetrometer Measurements

To measure the penetration resistance during wintertime under different soil water pressure and water content conditions, cone penetrometer measurements have been performed weekly at the Stüsslingen site. A soil cone penetrometer is the standard method to measure penetration resistance (ASABE, 2004, see also Section 2.5). The CP40II device used herefore measures the penetration resistance in kPa that the cone faces when being inserted manually at a constant speed (see Fig. 30). The depth below soil surface is simultaneously recorded with the help of ultrasonic waves and the recorded penetration resistance measurements are immediately averaged for every 2.5 cm depth interval by the device. This averaging accounts for small local changes in the soil matrix (pores, stones, soil aggregates). More information about the CP40II can be found in the operation manual (ICT International, 2012).

Figure 30: *CP40II cone penetrometer inserted half-way in the soil.*

On every measurement day, at least six insertions of the CP40II (calibrated for a maximum depth of 75 cm and the smallest cone with an area of 130 mm^2) were executed at random locations within the perimeter of the station. Insertions reaching less than 35 cm depth were deleted. These were mostly due to hitting of a stone since the soil contains some gravel-sized stones (see Section 3.1.1.2). Values of zero in between other values have been manually eliminated. The obtained values have then been downloaded onto a computer with the help of the CP40II retrieval software and averaged over all measurements at the same depth of the same day.

On the last field day, a 1 m^2-plot about 2 m outside the station perimeter has been irrigated to estimate the behaviour of the penetration resistance for a saturated soil. To control the effect, a 10HS sensor has been installed in the uppermost 10 cm and 6 insertions according to the standard procedure have been made i) before the irrigation, ii) shortly after the irrigation of about 30 l water and iii) about 20 minutes later.

3.1.4   Soil Sampling

Figure 31: *Soil sampling (from left to right): 1) hammering the closed ring holder into the soil, 2) removed ring holder with sample inside, 3) cutting off the excessive soil of the aluminium ring by knife.*

To determine the saturated conductivity and the absolute water content as well as to extract the soil water retention curve in the lab, soil samples were taken at the Stüsslingen as well as at the Aetigkofen site. The sampling method was chosen so that the aggregates remain as undisturbed as possible. All samples have therefore been collected using an Eijkelkamp sample ring kit (Eijkelkamp, 2013) where an aluminium ring of 5 cm diameter and 5 cm height is inserted in a closed ring holder (see Fig. 31; middle). The ring holder then needs to be connected to a metal pole with a hammerhead on top. After the drilling of a 15 cm deep hole with a riverside auger, the closed ring holder is hammered approximately 9 cm into the soil (see Fig. 31; left). The soil samples retained in the aluminium rings have thus been taken from a depth between 17 and 24 cm. As soon as the closed ring holder had been removed from the soil, it was opened and the excessive soil on both sides of the aluminium ring was cut off with a knife (see Fig. 31; right). To prevent evaporation, the sample was immediately closed with plastic lids, put into a plastic bag and numbered.

3.2   Laboratory Methods

3.2.1   Absolute Water Content Determination

Four of the five soil samples collected on December 12th, 2013 at the Stüsslingen site were weighted (after removal of the plastic lids, weight1) and then oven dried according to the standard methods (24 hours at 105°C; Scheffer and Schachtschabel, 2002). Afterwards the samples were weighted again (weight2) and with the help of the volume V of the aluminium ring (98.175 cm³), the weight loss could be translated into the volumetric water content with the following formula:

$$\theta = \frac{(weight1 - weight2)}{V} \tag{18}$$

where θ = water content, weight1 = weight before drying (g), weight2 = weight after drying (g), V = volume of aluminium ring (cm³).

Equation 18 is valid if the density of water is assumed to be constant and 1 cm^3 = 1 g. For different water densities, equation 8 (2.2.1) can be used.

3.2.2   Ksat Measurements

The saturated hydraulic conductivity (Ksat) has been determined using the constant head method (Klute, 1986a) for the Stüsslingen loam. Using this method, a constant head is maintained and the volume of flow V through a sample is measured and converted to Ksat applying Darcy's law.

Before the saturated hydraulic conductivity can be measured, the soil sample needs of course to be saturated. Therefore, the soil sample with length L (in our case 5 cm) and cross sectional area A (in our case 19.635 cm^2) is placed onto a water-saturated ceramic plate and thus saturated with an upward flow through the soil column. Once the soil surface is glossy, the tempe cell is closed and a constant head H is exerted on the soil sample (see Fig. 32). An outflow volume V can be measured for the time t, then the flux density Jw can be calculated and multiplied by the reciprocal of the gradient H/L to obtain Ksat according to Darcy (1856):

Fig. 32: *Constant head lab setup with Mariotte flask (left top), tempe cell with soil sample (middle) and outflow (right).*

$$Jw = \frac{V}{A \cdot t} \tag{19}$$

$$Jw = -Ksat \cdot \frac{H}{L} \qquad -> \qquad Ksat = -Jw \cdot \frac{L}{H} \tag{20}$$

where Jw = water flux density (cm/d), V = volume of outflowing water (cm^3), A = cross sectional area of soil sample (cm^2), t = time (d), Ksat = saturated hydraulic conductivity (cm/d), H = constant head (cm), L = length of the soil column (cm).

3.2.3   Soil Water Retention Curve Measurements

The soil water retention curve has been measured for six undisturbed soil samples, three from the Stüsslingen loam and three from the Aetigkofen sandy loam. The method used herefore was the relatively simple pF laboratory station by ecoTech, which has a hydrophilic plastic membrane and can be used from 10 to 750 hPa. It is a suction cell type apparatus, where the soil is kept at atmospheric pressure and the soil water pressure is reduced into a vacuum, so that water flows out of the sample until an equilibrium state is reached (Haines, 1930; Klute 1986b). Since an underpressure is generated, this method is limited to a suction of -1000 hPa (1 bar), because then, the water starts to boil (Klute, 1986b). These suction cells are also called pressure plates and have already been mentioned by Richards (1948; 1965; see also Dane and Hopmans, 2002). They are the most commonly used method to derive the SWRC in
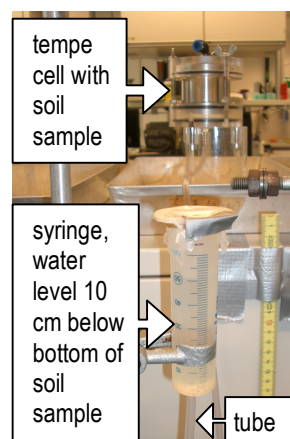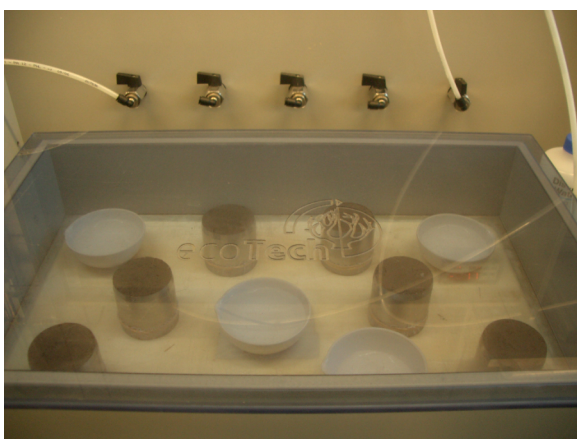
Fig. 33: *pF laboratory station with soil samples on it for drainage (left) and tempe cell system for wetting installed at 10 cm (right).*

the wet and intermediate range (Solone et al., 2012).

The soil samples were first covered with an artificial silk tissue. Then they were saturated overnight in a water bath before being put onto the membrane along with bowls of distilled water and closed up to prevent evaporation. The drainage was started by applying a suction of 0 hPa on the soil samples (equal to 5 hPa suction on the upper rim of the sample). Although the sampes have been weighted at full saturation, some water may already have been lost in this sensible phase. At the pressure of 0 hPa, the samples were weighted from time to time until the weight change was so small that an equilibrium state could be assumed, then they were put back onto the membrane (see Fig. 33; left). The same procedure has been applied for the following pressure values: 10, 20, 30, 40, 60, 80 and 100 hPa. The pressure was left on one level at least overnight, according to the minimum required equilibration time (Klute, 1986b). The aparatus sometimes had trouble to maintain a constant pressure, leading to values of e.g. 48 hPa in the morning when 40 hPa were set. These measurement problems have been accounted for by correcting the lost weight from a pressure of 40 hPa to a pressure of 48 hPa. After 100 hPa, the apparatus was set to 500 hPa and a longer time was left to equilibrate (10 days).

As a next experiment, the drainage procedure was repeated in a climate chamber at 2-3°C at 20, 40, 60 and 80 hPa to estimate the temperature dependency of the SWRC, which has been reported by Hopmans and Dane (1986). The saturation occured at room temperature. Because the weight after saturation and drainage of macropores differed quite a bit from the one before, the results have been displayed with the effective saturation on the x-axis (equation 3, 2.1.2) calculated with θ_s as water content after drainage of the macropores (different for each sample and experiment) and θ_r as the minimum water content measured in the field for the data available so far.

The last experiment was the reproduction of the wetting curve in the lab to see if hysteresis can be observed. Therefore, the soil samples were placed in the same tempe cell as for the Ksat measurements (Section 3.2.2) with a water-saturated ceramic plate at the bottom which was connected to a water reservoir (a syringe) with a water-filled tube. The samples were first saturated, then drained to 80 hPa and after that rewetted at 40, 20 and 10 hPa (see Fig. 33; right) before being saturated again. Since absolutely no air could be tolerated during the wetting, because it would cut off water transportation, this experiment was rather difficult to execute. The samples were not left to equilibrate for too long, because then the change of air entering also rose. For the data procession, the observed inflow was added to the water content observed at 80 hPa during drainage, because the samples were not weighted during wetting and thus no absolute weight could be extracted.

Fig. 34: *Plastic box with Winzlerboden soil, T8 and HydroSense open (left) and sealed with plastic tape inside the climate chamber (right).*

3.2.4   Temperature Dependence of T8 Measurements

To be able to quantify the reaction of T8 tensiometer measurements to temperature changes, a test in a Versatile Environmental Test Chamber (type MLR-350H, Sanyo) climate chamber has been performed. Therefore, a well-filled T8 tensiometer has been installed in a plastic box of about 22 cm height filled with Winzlerboden soil (loamy sand, sand content about 83% in the uppermost 40 cm, see also Richard and Lüscher, 1983) because it is well documented and available for lab experiments, which has been watered layer for layer and then let equilibrate for 4 days until the water content remained stable at 14%. To control the water content, a HydroSense CD620 sensor (Campbell Scientific, 2010) has been installed in an angle of about 35 degrees from the surface to the bottom of the box (see Fig. 34; left). The box was then covered with a lid and sealed with isolation tape to prevent evaporation (see Fig. 34; right). The tensiometer values were read out with the help of the TensioLink device by UMS (UMS, 2005) that allowed the connection to and power supply by a laptop. The HydroSense CD620 sensor was not continuously logging, but used as a control during the experiment. Temperature settings were chosen to start at 12°C and then decrease in 2°C steps until 0°C were reached. In between the temperature steps, the system was allowed to equilibrate for one day. To further prevent evaporation, a rather high relative humidity of 55% was chosen. More was not possible with the chosen system due to technical limitations of the climate chamber.

During the logging, the water content rose from 14 to 16%. However, after the equilibration of the system at an ambiance temperature of approximately 21°C, the water content was at 14% again.

3.3   Data Analysis

3.3.1   Data Preparation

The data already recorded by the BMN sites was, although available at 15 minutes intervals, mostly used on a daily basis. Daily averages have been generated automatically during the download on the website www.bodenmessnetz.ch. The reliability of these values has been compared to manually generated daily averages. A very good agreement has been found, so that the analysis has been carried out with the automatically generated data. Nevertheless, some errors had to be removed. Thus, daily averages of days with less than 12 hours of data have been deleted manually. Also, obvious sensor measurement errors have been erradicated.

The data from the FaBo of the Canton of Zurich has also been searched for implausible values and they have been deleted manually. Then the daily average has been generated using the „average" function in MS excel.

Unless mentioned explicitly, all analyses have been carried out using the mentioned daily average values.

3.3.2   Frequency Analysis of Soil Water Pressure Measurements

For the initial idea for this thesis came from the Canton of Solothurn, a first analysis of the situation of low soil water pressure measurements in winter among other Cantons seemed appropriate to be able to estimate the importance of this phenomenon. A list of all data sets available for this thesis and thus processed in the frequency analysis can be found in Appendix C, Table C.1. Manually read tensiometers have not been included because of their insufficient data provision in winter (either none or one value per week).

For the frequency analysis of the soil water pressure measurements, the daily average values in 20 cm depth of all sites mentioned in Table C.1 from October 2011 to March 2012, October 2012 to March 2013 and October 2013 to February 2014 (unless available and with the exception of the data of Agroscope) have been analysed with a cumulative frequency function for monthly as well as

spatial distribution of soil water pressure measurements. The 20 cm depth was chosen because it was available for all data processed.

3.3.3 Field Soil Water Retention Curves

Since both water content and soil water pressure have been measured in 20 cm depth at all sites in the Canton of Solothurn, field desorption curves could be plotted for the two years data row. Not all sites delivered curves that made sense, but four sites (Aetigkofen, Etziken, Stüsslingen, Subingen) had curves with a reasonable shape. Only these were thus used in further analyses involving water content and soil water pressure.

3.3.3.1 Comparison with Other Sensors

All these SWRC from the Canton of Solothurn were obtained by measurements of the T8 tensiometer and the Stevens Hydra Probe (as mentioned in Section 1.2). To exclude possible sensor artifacts at this first step, they have been compared to SWRC measured with other sensors, such as the ThetaProbe ML2x (UMS, 2004) in combination with the T8 tensiometer at the Reckenholz station, Canton of Zurich (data: FaBo), the trime-EZ water content sensor (UMS, 2001) in combination with the T8 tensiometer at the Pfaffenmatt Station in Erstfeld, UR (data: Amt für Umweltschutz, UR) or the Tektronix cable tester TDR (Tektronix, 2000) in combination with manually operated septum tensiometers (see Durner and Or, 2005) also at the Reckenholz in the Canton of Zurich (data: Agroscope). Except for the Agroscope data, the data processed was the same as listed in Table C.1, Appendix C. Of Agroscope, another data set (ASTO, November 1991 until October 1994) was used.

3.3.3.2 Seasonal Trends in the SWRC

The curves of the sites chosen have been plotted with a seasonal resolution for the two years December 2011 until November 2012 and December 2012 until November 2013, such that the data points were shown which season (winter, spring, summer, fall) they belong to. The obtained graphs were qualitatively analysed for seasonal trends in the SWRC. The plotting for two years was assumed to account for interannual trends as well.

3.3.4 Temperature Influences

The data obtained by the BMN sites in the Canton of Solothurn has been analysed for the temperature conditions under which the measurements were made. At first, simple plots such as the soil water pressure as a function of soil and air temperature were compiled. Additionally, the field SWRC have been divided into sections of different temperatures as done with the seasons previously (see Section 3.3.3.2). To obtain a good representation of wintertime, a high resolution of 2°C steps has been chosen for cold temperatures between 0 and 10°C.

To get an idea of possible temperature influences on the measurements, for certain soil water pressure ranges (e.g. from 25 to 35 hPa) the corresponding soil water content has been plotted as a function of temperature. The same has been done the other way round: for a certain soil water content region, simultaneous soil water pressure values have been charted against temperature.

Additionally, the physical effect of temperature changes onto soil water pressure through surface tension and density changes of water has been quantified by applying the following formula (Sachs and Meyn, 1995):

$$h = \frac{2 \cdot \gamma(T)}{\rho(T) \cdot g \cdot r} \tag{21}$$

converting to $r(T_1) = r(T_2)$ for two different temperatures T_1 and T_2:

$$\frac{2 \cdot \gamma(T_1)}{\rho(T_1) \cdot g \cdot h(T_1)} = \frac{2 \cdot \gamma(T_2)}{\rho(T_2) \cdot g \cdot h(T_2)} \tag{22}$$

solving for $h(T_2)$:

$$h(T_2) = \frac{\gamma(T_1) \cdot \rho(T_1)}{\gamma(T_2) \cdot \rho(T_2)} \cdot h(T_1) \tag{23}$$

where h = soil water pressure (hPa), γ = surface tension of water (N/m), ρ = density of water (kg/m^3), g = gravity acceleration (m/s^2), r = pore radius (m), T_1 = temperature 1 (°C) and T_2 = temperature 2 (°C).

With the help of tables showing the temperature dependent values of the surface tension and the density of water (Weast, 1969), the factor in front of h(T_1) = 0°C has been calculated for h(T_2) = 5°C, 10°C, 15°C, 20°C and 25°C. Surface tension decreases with increasing temperature (see Fig. 35; left). After its highest density at 4°C, the density of water decreases with temperature, too (see Fig. 35; right).
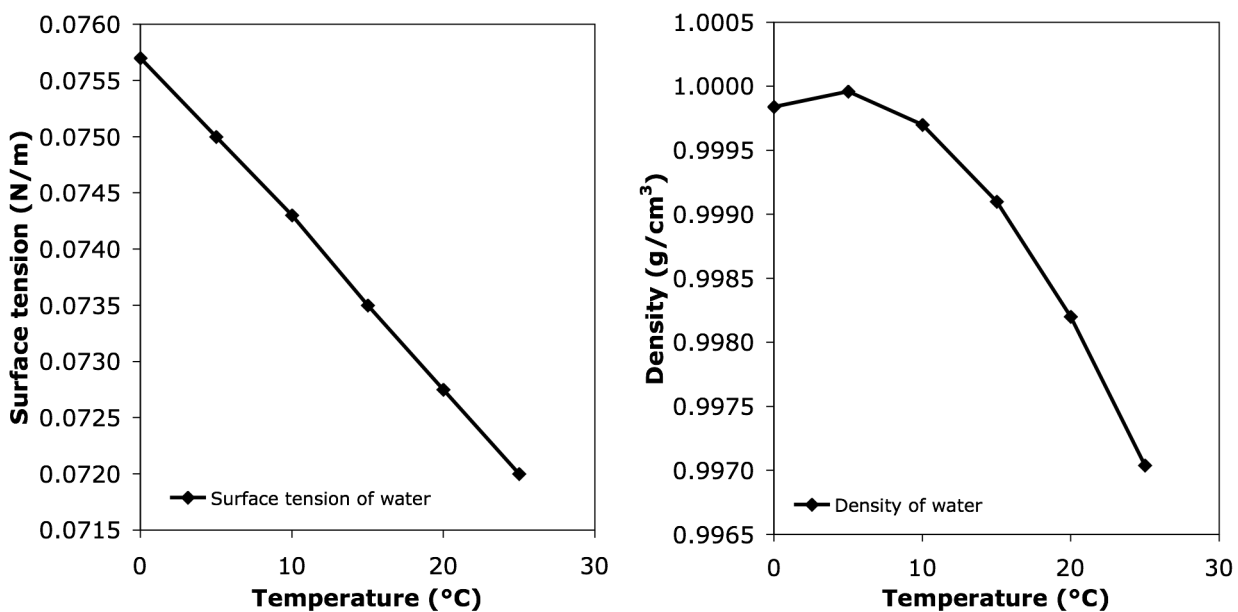
Fig. 35: *Change of surface tension (left) and density (right) of water with temperature. Whereas the surface tension declines linearly with rising temperature, the density shows a more complex shape with a maximum at 4°C. Data: Weast (1969).*

Furthermore, the physical effect of temperature change onto soil water pressure only through surface tension without density changes of water has been calculated with the following formula (Flühler and Roth, 2004):

$$p(T) = \frac{2 \cdot \gamma(T)}{r} \tag{24}$$

converting to $r(T_1) = r(T_2)$ for two different temperatures T_1 and T_2:

$$2 \cdot \gamma(T_1) \cdot p(T_2) = 2 \cdot \gamma(T_2) \cdot p(T_1) \tag{25}$$

solving for $p(T_2)$:

$$p(T_2) = \frac{2 \cdot \gamma(T_2) \cdot p(T_1)}{2 \cdot \gamma(T_1)} \tag{26}$$

where p = soil water pressure (hPa), γ = surface tension of water (N/m), r = pore radius (m), T_1 = temperature 1 (°C) and T_2 = temperature 2 (°C).

The surface tension has been taken out of the same table (Weast, 1969) and the factor in front of p(T_1) = 0°C has been calculated for p(T_2) = 5°C, 10°C, 15°C, 20°C and 25°C, too.

3.3.5   Relative Humidity Influences

As for temperature, similar plots were computed for relative humidity. Relative humidity plays a key role in drying of soils because it determines the evapotranspiration (and thus the loss of soil water to the air) significantly. Soil water pressure as well as daily change in soil water pressure defined as value of the present day minus value of the previous day was plotted against the vapor pressure deficit of the atmosphere defined as 100%-RH (in %).

3.3.6   Flux Calculation

With the help of soil water pressure measurements in two depths, namely 20 and 35 cm in the case of the BMN sites of the Canton SO, a potential gradient can be calculated. This gradient can then be applied in the Buckingham-Darcy equation (equation 10, see Section 2.3.2) to get a flux.

Since the hydraulic head H (as seen under 3.2.2) is defined as the sum of the pressure head h and the gravitational head z, the soil water pressure measurements need to be corrected for their height difference with respect to the soil surface:

$$H(20) = h(20) + z(20) \tag{27}$$

$$H(35) = h(35) + z(35) \tag{28}$$

The gradient can then be calculated as the difference between the two measurements divided by the depth difference in cm:

$$grad = \frac{H(20) - H(35)}{z(35) - z(20)} \tag{29}$$

where h(x) = pressure head in x cm depth (hPa), H(x) = hydraulic head in x cm depth (hPa), z(x) = gravitational head (equal to depth of the measurement; cm), grad = dimensionless.

The unsaturated hydraulic conductivity K(h) has been calculated dependent on θ using the van Genuchten-Mualem parameterisation for three of the soils (van Genuchten, 1980; Mualem, 1976), which were chosen to be Aetigkofen (sandy loam. grassland), Dulliken (loam, forest) and Stüsslingen (loam, grassland) because of their vicinity to a MeteoSchweiz site with evapotranspiration data available. The van Genuchten-Mualem parameterisation is at the moment the most commonly used to calculate K(h) (Flühler and Roth, 2004). Before the flux has been calculated, the van Genuchten parameters n and α were obtained by fitting to the lab SWRC data (data: FS BS, 2011). As saturated water content θ_s the water content at 60 hPa from the lab SWRC data was assumed to be correct, because lab saturation tends to overestimate the saturation possible in the field (DIYS, 2009). The residual water content, θ_r, has been obtained by entering the exact soil texture values in the Rosetta database (Schaap et al., 2001) because otherwise it was always fitted zero by the van Genuchten equation (equation 2). With the help of these values, the effective saturation $\theta_e(t)$ could be computed for every day (see equation 3). The effective saturation could then be used as input to calculate the relative hydraulic conductivity, as mentioned before (van Genuchten, 1980; Mualem, 1976; equation 5).

Since the value obtained is just a relative value stating what fraction of Ksat is active, it needs to be multiplied with the saturated hydraulic conductivity to obtain the actual daily K(h):

$$k(\theta_e) = k_r(\theta_e) \cdot Ksat \tag{30}$$

where $k(\theta_e)$ = unsaturated hydraulic conductivity at effective saturation θ_e (cm/d) and Ksat = saturated hydraulic conductivity (cm/d).

For Ksat, various values have been tested. As a first approximation, the value proposed by the Rosetta database for the exact texture has been used. Furthermore, measured values could be tested for the Stüsslingen loam.

Finally, the flux was obtained by multiplication of gradient and unsaturated hydraulic conductivity:

$$flux = grad \cdot k(\theta_e) \qquad\qquad (31)$$

where flux = flux (cm/d).

As a convention, fluxes with a negative sign are pointing downwards. This has been accounted for by the choice of the gradient sign.

The obtained daily fluxes were then summed up for the whole winter and compared to the expected percolation to see if mass balance is more or less fulfilled using the following formula (see also Section 2.4):

$$perc = P - ET \qquad\qquad (32)$$

where perc = expected (absolute) amount of percolating water, P = precipitation sum over winter (data: BMN) and ET = evapotranspiration data of a nearby MeteoSchweiz site (data: IDAWEB, MeteoSchweiz) calculated with the empiric Primault formula (Primault, 1962 and 1981) summed up over winter.

3.3.7   Reproduction of Situation with HYDRUS-1D

The HYDRUS-1D-Model (Šimunek et al., 2013) is a soil physics model that can calculate flows at any time and place by solving the Richards equation (see Section 2.3.2) with the help of finite elements. It is commonly used for modelling purposes among soil physicists.
In this thesis, the HYDRUS-1D-Model has been used to check if the observed soil water pressure values can be reproduced with classical soil physics.

In order to get a van Genuchten-Mualem parameter set (van Genuchten, 1980; Mualem, 1976) that fits the observed soil water pressure measurements in summer (April to September 2012), the Inverse Solution has been used (Hopmans et al., 2002). With the help of it, one can define the observed values as input data and choose parameters to be fitted to obtain the best approximation possible of the calculated to the observed values.
All simulations have been carried out for the Stüsslingen site using daily precipitation of the BMN data and evapotranspiration of the nearby Gösgen station (data: IDAWEB, MeteoSchweiz) calculated with the empiric Primault formula (Primault, 1962 and 1981) as time-variable boundary conditions. For the Inverse Solution, daily soil water pressure measurements in 20 cm depth of the BMN of the respective months have been used as input for the fit. If possible, all van Genuchten-Mualem parameters (θr, θs, α, n and Ksat) were chosen to be fitted. However, most of the time it did not work out for all. Then the parameters that could be fitted together were fitted in combination and the others were left according to the standard parameter set for loam. If only one parameter could not be fitted automatically, the model has been run with the fitted parameters and the unfittable parameter optimised manually. This was the case for n for the summer fit. For the winter fit, just α and n could be fitted. Since trials to optimise the other three parameters always ended in a lower Rsquare for the regression of predicted versus observed values, the other three were left according to the standard loam values.
As soil hydraulic property model, the classical van Genuchten model (1980) has been chosen due to its limited amount of parameters to fit. As a control, the analysis has also been carried out for other models, but no big differences were found. The water flow boundary conditions were chosen as atmospheric with surface runoff for the upper boundary and free drainage for the lower one.
The obtained parameter set with the best summer fit has then been applied to simulate winter conditions (input data: precipitation of BMN and evapotranspiration data of Gösgen, MeteoSchweiz from October 2012 to March 2013). The same procedure has then been repeated for the reverse case: The optimal winter fit parameter set has been applied to the summer conditions. The fit to the observed values has thus been qualitatively analysed.

The robustness of the best winter (October 2012 to March 2013) and summer (April to September 2012) fit has been validated by applying the same parameter set to other years of the same season (October 2011 to March 2012; October 2013 to February 2014; April to September 2013).

4   Results

4.1   *Soil Water Pressure Frequency Distribution*
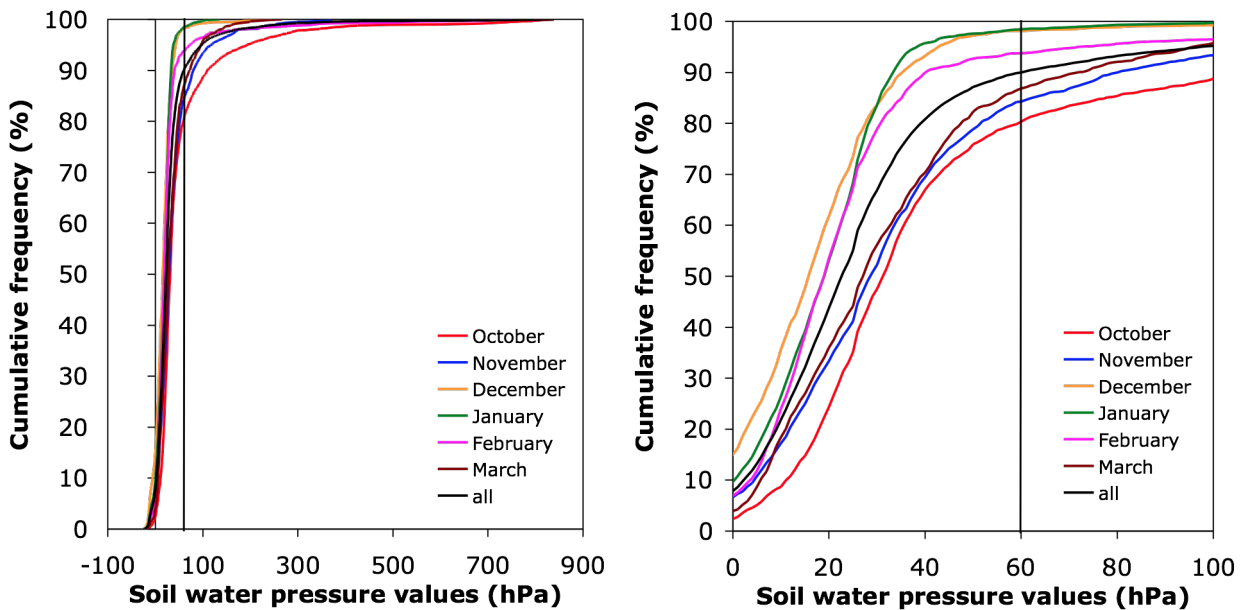
Fig. 36: *Monthly cumulative frequency distribution of soil water pressure measurements over all years and all sites as mentioned in Table C.1 with available data for the winter semester. The black line represents the critical threshold at 60 hPa. Most of the soil water pressure measurements lie below it (90% over all data and all months; see zoom between 0 and 100 hPa on the right). Data: see Table C.1, Appendix C.*

The cumulative frequency distribution derived from all soil water pressure data available from October 2011 until February 2014 shows that 90% of the soil water pressure measurements in Switzerland lie below the critical threshold of 60 hPa during the winter half year (see Fig. 36). December and January as well as February have the most very low soil water pressure measurements (about 85% below 30 hPa). February, however, reaches the highest values together with October. The very high values in October above 400 hPa were reached at one single site in Breitenbach SO, which is located in a forest. Breitenbach showed such high soil water pressure measurements in the beginning of the month October in 2011 and in 2013 while no other site did. Fig. 37 (left) shows the cumulative frequency of all soil water pressure measurements in the winter half year for the sites in Erstfeld UR, Hofstetten-Flüeh SO and Möhlin AG, which all have a silty loam texture. In spite of their similar texture, the soil water pressure measurements differ considerably. Erstfeld UR is the driest of the three locations reaching more than 60 hPa about 61% of all days in wintertime. The other two sites hardly ever dry up to the threshold, they both show around 96% of the measurements below 60 hPa. The average winter precipitation of the three years considered (Möhlin: only 1 year due to limited datarow; Erstfeld: precipitation of Altdorf UR by IDAWEB, MeteoSchweiz) does not vary much between the three sites.
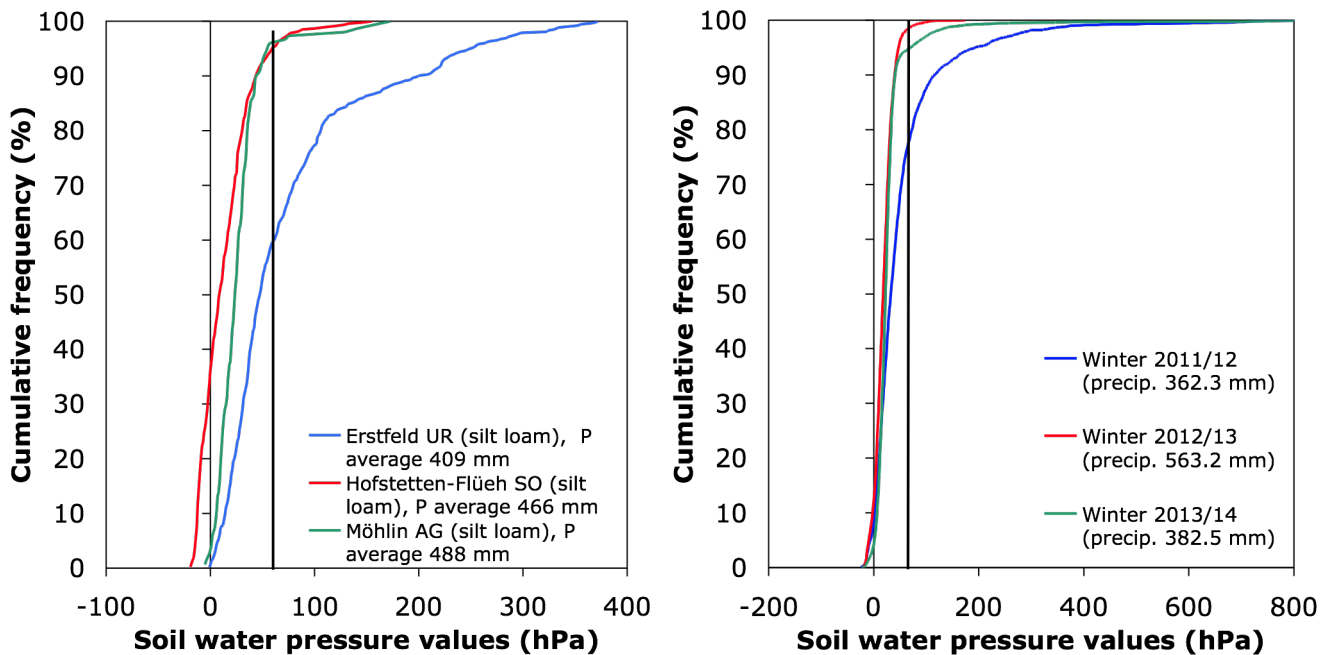
Fig. 37: *Left: Cumulative frequency of all available soil water pressure measurements in the winter half year for three different sites. Although their texture is the same and the average precipitation P at the site (Erstfeld: precipitation of Altdorf) lies within a similar range, the behaviour varies considerably. Right: Cumulative frequency of soil water pressure measurements over all sites for three consecutive winters (Oct-Mar, 2014 until Feb) according to data in Table C.1. 2011/12 was clearly the driest winter resulting in higher absolute soil water pressure measurements. The black line represents the critical threshold (60 hPa) in both graphs. Data: precipitation of Altdorf and Zurich, Fluntern: IDAWEB, MeteoSchweiz.*

Fig. 37 (right) shows the cumulative frequency of all sites over the last three winters (October to March, 2014 only until end of February) with the precipitation sum for the site Zurich Fluntern over the respective months (data: IDAWEB, MeteoSchweiz). The curve for winter 2011/12 is by far the driest with respect to soil water pressure measurements, overall in the drier range above 60 hPa. This can be attributed to the dry autumn 2011, when soil water pressure could still reach high values. The difference between the winters 2012/13 and 2013/14 is negligible and limited to the uppermost measurement range, which is due to dry values in the very beginning of October 2013. Nevertheless, even in the dry winter 2011/12 nearly 80% of all daily mean soil water pressure measurements were below 60 hPa.

Looking at these cumulative frequency curves, it can be made out that the phenomenon of low absolute soil water pressure measurements is not limited only to the Canton of Solothurn, but represents the common case for the sites analysed in Switzerland. Few sites can outreach the threshold at 60 hPa under unfrozen conditions for a longer time in winter, among these are the sites in Erstfeld UR, Rafz ZH and Wädenswil ZH.

4.2   Soil Water Retention Curves

4.2.1   Data Analysis of Field SWRC

To get a first impression of what the relationship between soil water pressure and water content for the data obtained by the BMN sites in the Canton of Solothurn looks like so far, the SWC have been plotted for every site. While some had shapes that seemed somehow unrealistic, four of the sites provided reliable curves shown in Fig. 38.
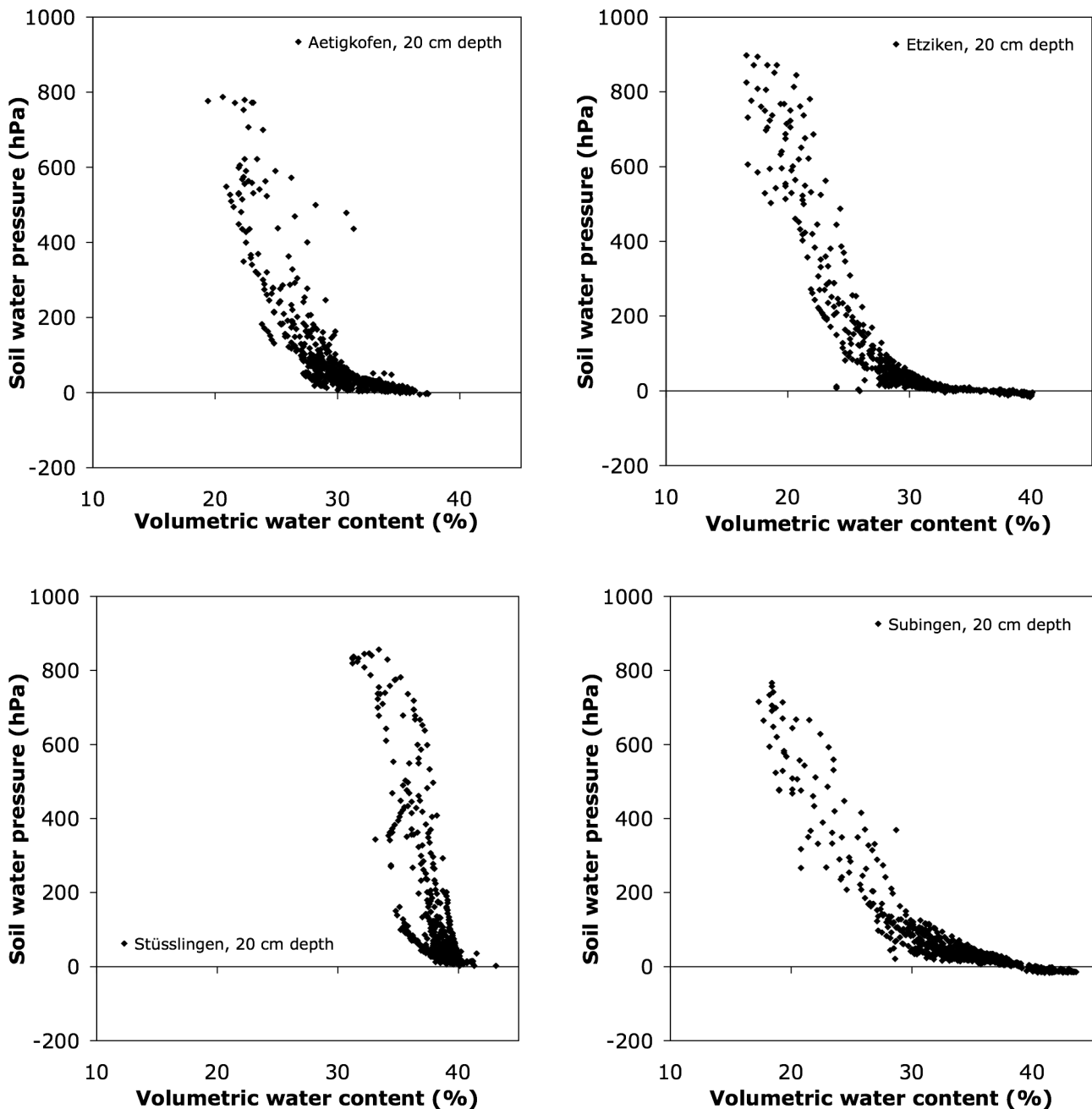
Fig. 38: *Soil water retention curves for four sites in the Canton of Solothurn: Aetigkofen (sandy loam, grassland), Etziken (sandy loam, forest), Stüsslingen (loam, grassland) and Subingen (sandy loam, grassland). Each site has its individual curve shape, ranging from quite narrow (Stüsslingen) to wide (Subingen). Data: BMN.*

All SWRC shown in Fig. 38 follow more or less the trend suggested by the theory (see also Section 2.1.1 and Fig. 8). It is clearly visible at all four sites that, for whatever reason, the relationship between soil water content and soil water pressure is not unique, meaning that various water content values can be attributed to the same soil water pressure measured. This effect will be looked at closer further on in this section (see Fig. 40 and 41).

Most of the curves, however, have datapoints in the very wet range that consist even of negative soil water pressure measurements and form a kind of „tail". This curve shape will be further analysed and discussed later. While some of the sites cover a wide range of water content measurements, such as Subingen, the water content of others seems to stay in a similar region for a

wide range of soil water pressure values (see for example Stüsslingen). The soil water pressure measurements all cover similar ranges.

To compare the SWRC obtained with different sensors, data of the Canton of Zurich (measuring soil water content with the ThetaProbe ML2x, (UMS, 2004)), the Canton of Uri (measuring the water content with the trime-EZ sensor (UMS, 2001)) and Agroscope (measuring soil water pressure with septum tensiometers and the water content with Tektronix cable testers (Tektronix, 2000)) has been analysed additionally. For the Reckenholz site of the FaBo and the Erstfeld site, only winter measurements as mentioned in Table C.1 have been processed. Since for the Agroscope data winter values were rather sparse, the values recorded during the ASTO experiment from November 1991 to October 1994 (all year round) have been presented. The resulting SWRC with daily average values can be seen in Fig. 39.

Although there are some outliers, especially on the wetting branch with relatively low water contents measured compared to the soil water pressure, all curves have a reasonable shape. A „tail", as described for the curves of the BMN before, could also be made out at both Reckenholz sites. The two Reckenholz soils, although both of sandy loam texture, appear to have a fairly different SWRC. The data by the FaBo ZH (Fig. 39; left) varies quite in its water content although soil water pressure measurements range only up to 90 hPa. The Agroscope data (Fig. 39; right) shows about the same water content variation, but soil water pressure was measured up to almost 800 hPa. Although measured with different sensor types, these SWRC all have a reasonable shape and can be compared to the SWRC obtained with the BMN data. The BMN measurements thus once more seem to be reliable and ready-to-use for further analyses.
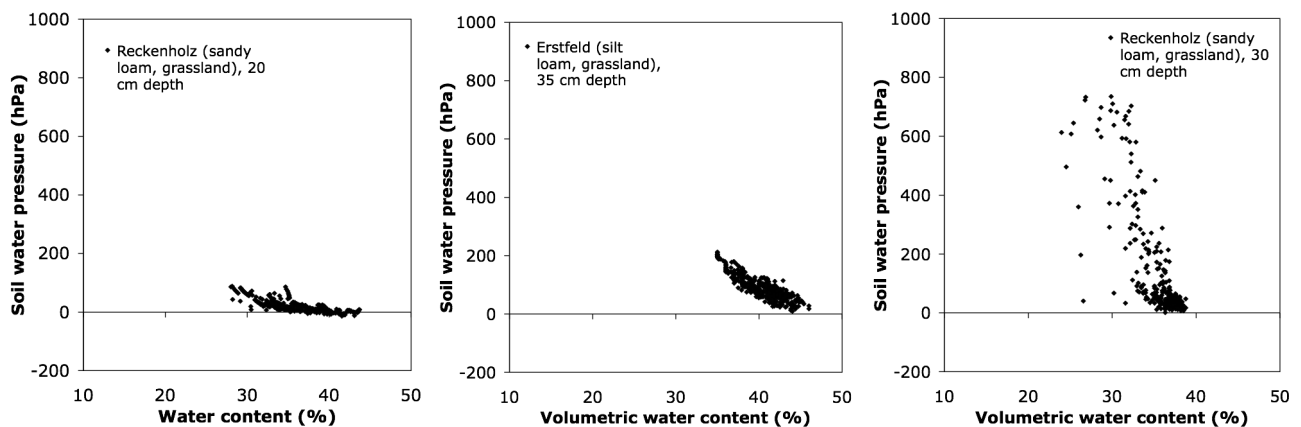
Fig. 39: *SWRC obtained with different sensors than at the BMN. Left: Data from the Reckenholz station (data: FaBo) measured with T8 (soil water pressure) and ThetaProbe ML2x (water content). Middle: Data from the Erstfeld station (data: Canton of Uri) measured with T8 (soil water pressure) and trime-EZ (water content). Right: Data from the Agroscope ASTO experiment (data: Agroscope) measured with septum tensiometers (soil water pressure) and Tektronix cable testers (water content). In spite of the different sensor types used, especially for the water content, the curve shapes are comparable to the ones of the BMN.*

In addition, the SWRC of the BMN have been analysed with respect to seasonal patterns in order to find out more about the difference in water content values observed at the same soil water pressure as seen in Fig. 38. Fig. 40 therefore shows the SWRC in Etziken (sandy loam, forest) with a seasonal resolution of the years 2012 and 2013.
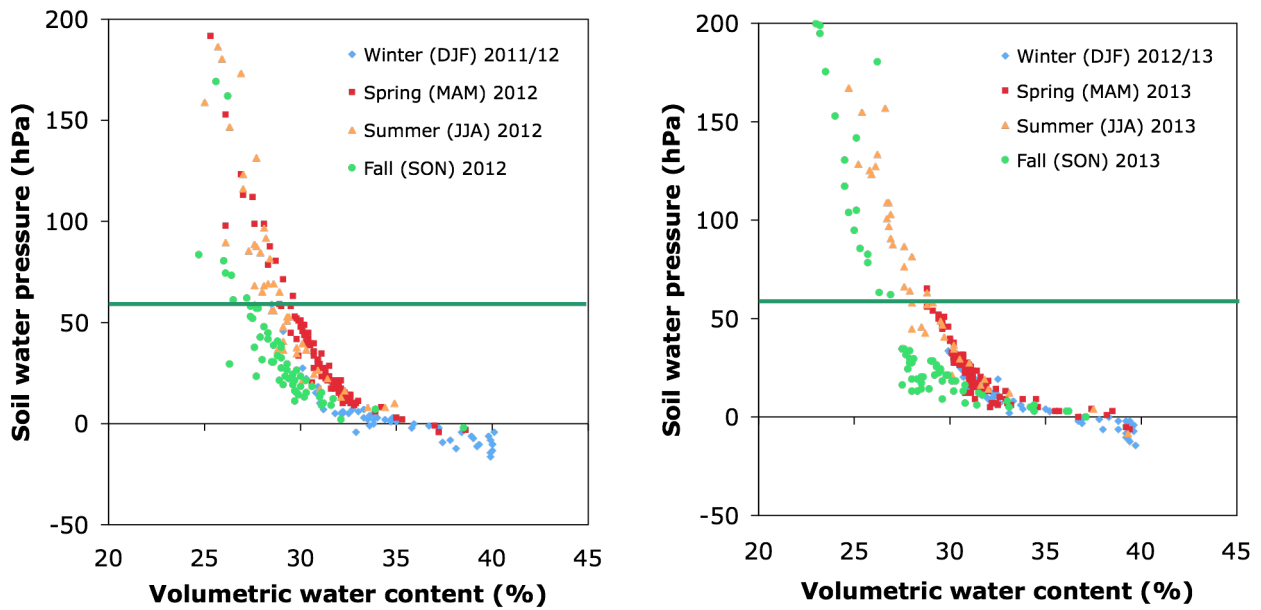
Fig. 40: *SWRC at the Etziken (sandy loam, forest) site displayed for every season of the years 2012 (left) and 2013 (right). The data points show a seasonal trend: higher water content values are measured at the same soil water pressure in spring and summer, than in fall. The threshold, which allows no passing over bare soil is shown in green (60 hPa). Data: BMN.*

For both years, a clear distinction can be made the seasons within the SWRC pattern. The wettest values with respect to both water content and soil water pressure were recorded in winter (December to February) as well as in spring 2013, which was quite cold and wet (MeteoSchweiz, 2014). The daily mean values in spring then lie on the very right side, meaning that during that season the measured water content values were highest at a given soil water pressure. The summer data lies very close to it, but a little more to the left, indicating a slightly drier condition at the same soil water pressure. The lowest water content values at a given soil water pressure value have been recorded in autumn. Although it was not always as clear as for Etziken in Fig. 40, the general pattern could be confirmed when looking at the SWRC of other sites of the year 2013 (see Fig. 41).
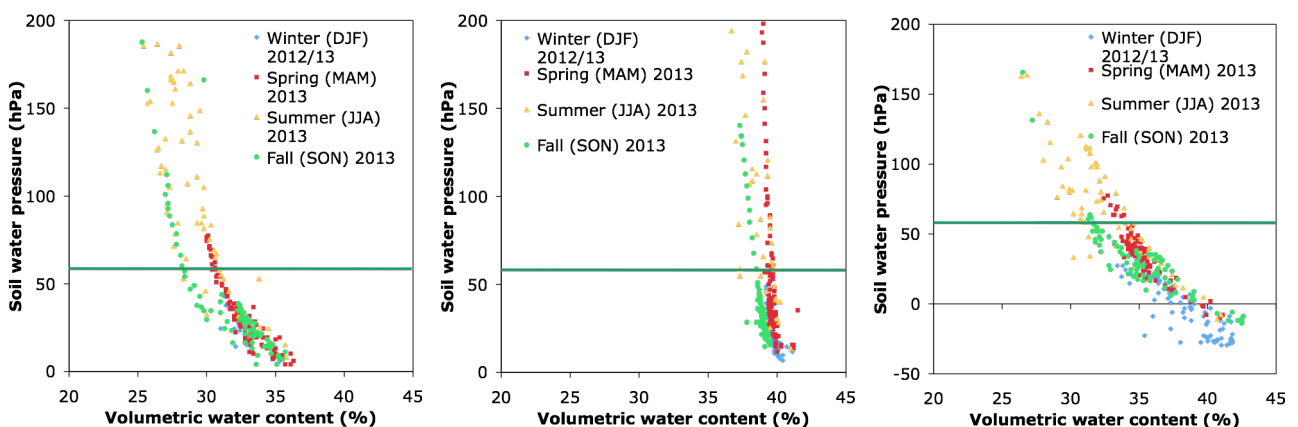
Fig. 41: *SWRC at the Aetigkofen (sandy loam, grassland; left), Stüsslingen (loam, grassland; middle) and Subingen (sandy loam, grassland; right) displayed for every season of the year 2013. Although it is not always as clear as for Etziken in Fig. 40, the SWRC do show the same pattern. Data: BMN.*

4.2.2 Lab SWRC

The soil water retention curve was measured in the lab with undisturbed soil samples to be able to compare it to lab data obtained with disturbed samples as well as to field values. The curve obtained for three samples of the Aetigkofen sandy loam and the Stüsslingen loam respectively at ambiant temperature (about 21°C) is displayed in Fig. 42.
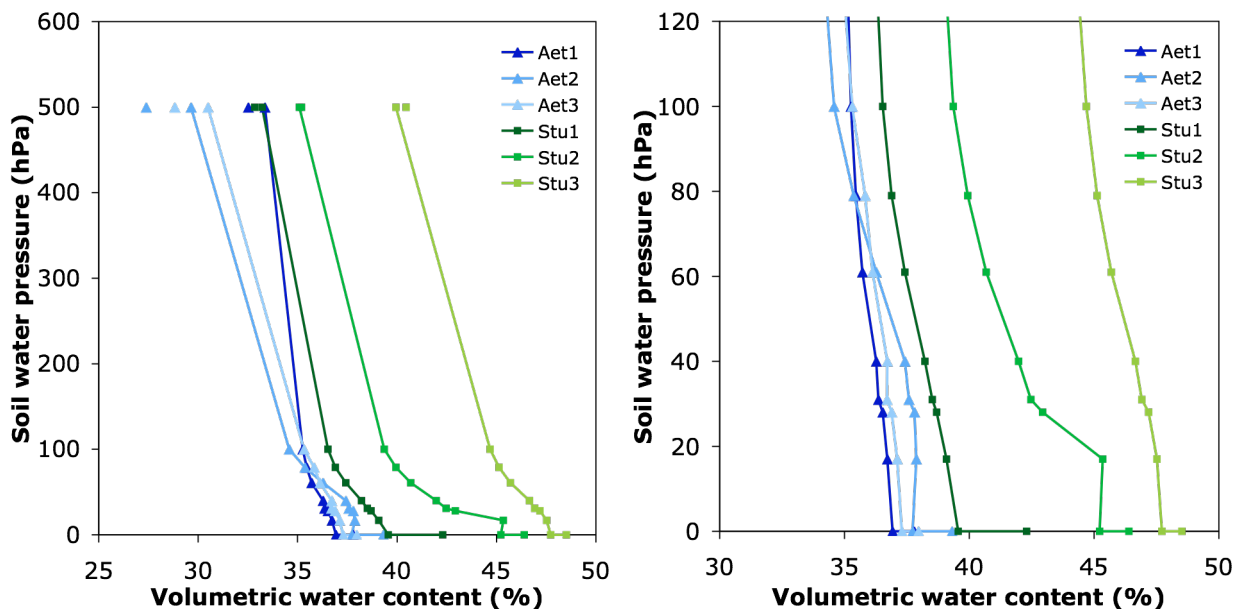
Fig. 42: *Lab SWRC for three samples of the Aetigkofen sandy loam (blue) and the Stüsslingen loam (green) respectively. The right figure shows the detail from 0 to 100 hPa. The first dot at 0 hPa represents the measurement right after saturation, the second dot at 500 hPa a second measurement that has been obtained. For the Aetigkofen soil, all three measurements lie close to each other. The Stüsslingen soil appears to have a higher water content and a higher variability between the samples. Both soils show little change in water content up to 100 hPa.*

The results show that the Stüsslingen loam (displayed in green) has generally a higher water content than the Aetigkofen sandy loam (displayed in blue). Also, its variability between the samples is higher with a difference in water content up to almost 10 Vol. %. Nevertheless, its reaction to rising soil water pressure is, except for one outlier of the Stu2 sample, very similar between the three samples analysed. The samples of the Aetigkofen sandy loam appear to be more homogenous with respect to water content. Their change in water content with rising soil water pressure is, however, not the same for all samples. A big difference could be made out especially at 500 hPa, where one sample still shows quite a high water content. The second dot represents a second measurement at 500 hPa, which appeared to be associated with lower water content at the Aetigkofen site. For the Stüsslingen site, the difference between the two measurements was fairly small.
The first dot at 0 hPa was the water content right after saturation, the second one the value at which the samples had stabilised at a soil water pressure of 0 hPa at the bottom of the sample. The loss between the two points is just the drying of the very largest pores. It appears to be slightly bigger at the Stüsslingen than at the Aetigkofen site.

The comparison between the lab SWRC measured with undisturbed soil samples and the one where the aggregates were destroyed and the samples were repacked (data: FS BS, 2011) can be seen in Fig. 43 (left).
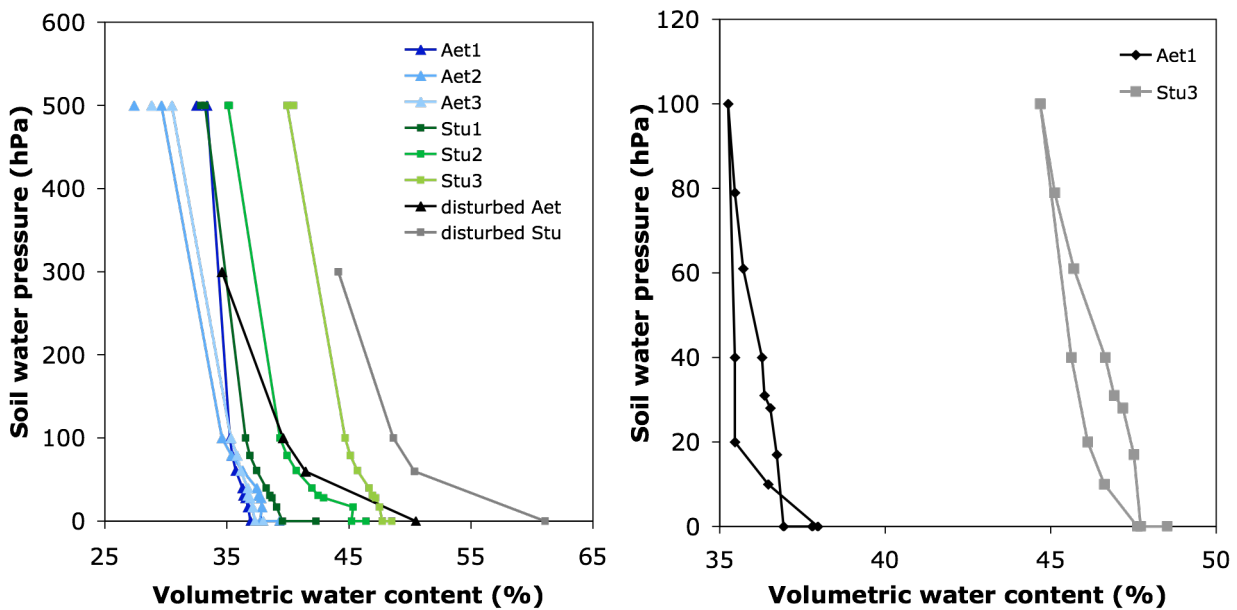
Fig. 43: *Left: Lab SWRC comparison between undisturbed and disturbed soil samples (disturbed: median of 5 measurements) at the Aetigkofen (blue/black) and Stüsslingen (green/gray) site. For both soils, the disturbed samples have a higher water content than the undisturbed samples at the same soil water pressure. Right: SWRC drying and wetting branch reproduced in the lab for one sample of the Aetigkofen and one of the Stüsslingen soil. The lower water content at a given soil water pressure on the wetting branch could be reproduced well for both samples. Data disturbed SWRC: FS BS (2011).*

Obviously, the SWRC measured with samples that have been disturbed yield much higher water contents at the same soil water pressure. The difference between Stu1 and the disturbed Stu (Stüsslingen) curve at saturation makes out as much as 19 Vol. %. For the Aetigkofen site, the differences are a little smaller. However, it can also be judged better, because the three Aetigkofen sample curves lie closer to each other. For both of the soils, the decrease in water content with rising soil water pressure is larger between 0 and 60 hPa for the disturbed SWRC than for the undisturbed one.

The results of the hysteresis experiment performed in the lab are shown in Fig. 43 (right). Because of some measurement problems mentioned in Section 3.2.3, the results shown here are only from two samples, one of each soil analysed in the lab. The draining curve (right branch) is the same as displayed in Fig. 42, and for the wetting branch, the water content at 80 hPa as obtained with the draining experiment was taken as a reference for the inflow values measured. Although the experiment setup included a hanging water column and the unit cm or m head would be more suitable, the standard hPa was maintained because of the presentation together with the drying branch. Both samples show the typical pattern also seen in Section 2.1.4, where the water content at a given soil water pressure is lower during a wetting phase than during a draining phase (see Fig. 43; right). Also, the water content was about the same in the end as in the beginning.

4.2.3   Comparison Lab/Field SWRC

The Stüsslingen lab SWRC as already seen in Fig. 43 (right) is, except for the overall higher water content, quite similar to the data measured in the field (see Fig. 44; left). The width of water content values measured at a certain soil water pressure approximately corresponds to the effect observed in the lab. For the Aetigkofen sandy loam, the SWRC obtained in the lab is flatter with respect to the

slope, that means the change in water content with soil water pressure rise is much smaller than expected when looking at the field data (see Fig. 44; right). Due to this narrowness in water content measurements, the hysteresis effect shown in the lab is also much smaller than the one observed in the field (assuming that the variability of water content measurements in the field at a given soil water pressure can be attributed solely to hysteresis).
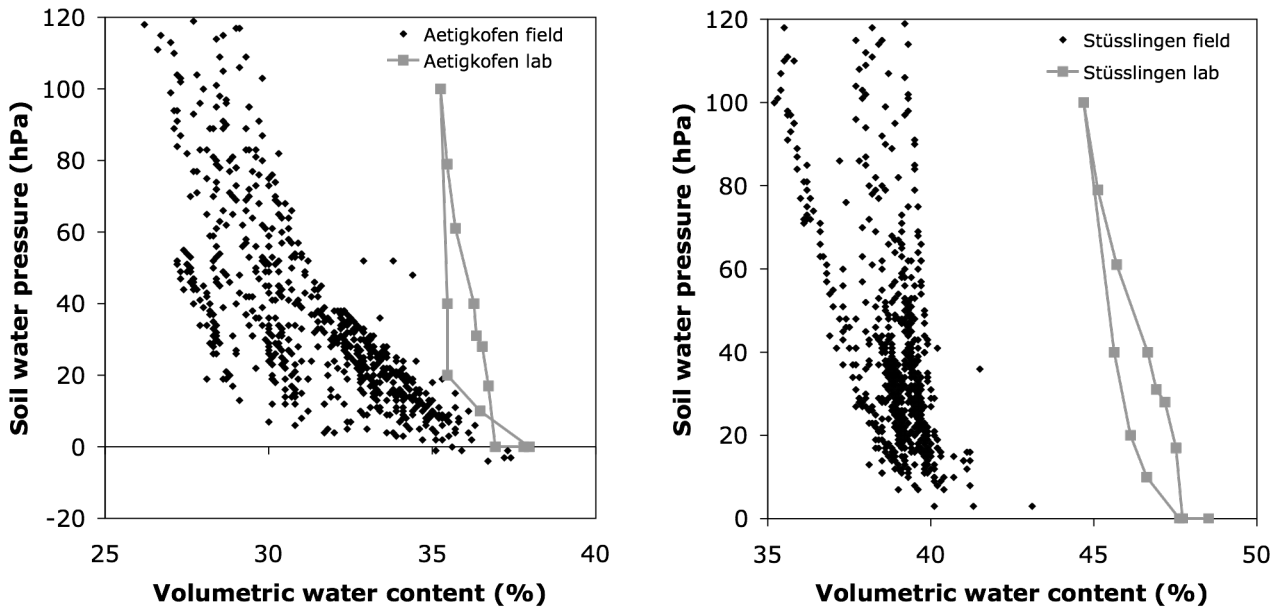
Fig. 44: *Lab hysteresis experiment in comparison with the field SWRC of the respective soil (Aetigkofen left, Stüsslingen right). The shape of the Stüsslingen lab SWRC is quite similar to the data obtained in the field. In Aetigkofen, the lab SWRC seems to underestimate the water loss with rising soil water pressure and therefore the hysteresis experiment cannot reproduce the spread observed in the field data. Data field: BMN.*

Also, a comparison between the SWRC measured in the field as well as the lab data from disturbed soil samples (data: FS BS) has been made. The described SWRC for the Aetigkofen, Etziken, Stüsslingen and Subingen site can be seen in Fig. 45.

The lab saturation values are usually about 10 Vol. % too high, but with rising soil water pressure the difference between the lab and the field values gets smaller. For Etziken and Subingen, the lab values are always higher than the recorded values in the field. In Aetigkofen and Stüsslingen, the prediction of the water content at 1000 hPa seems more or less appropriate, but it cannot be said with certainty because an extrapolation is needed for this statement due to 1000 hPa being out of the tensiometer measurement range.
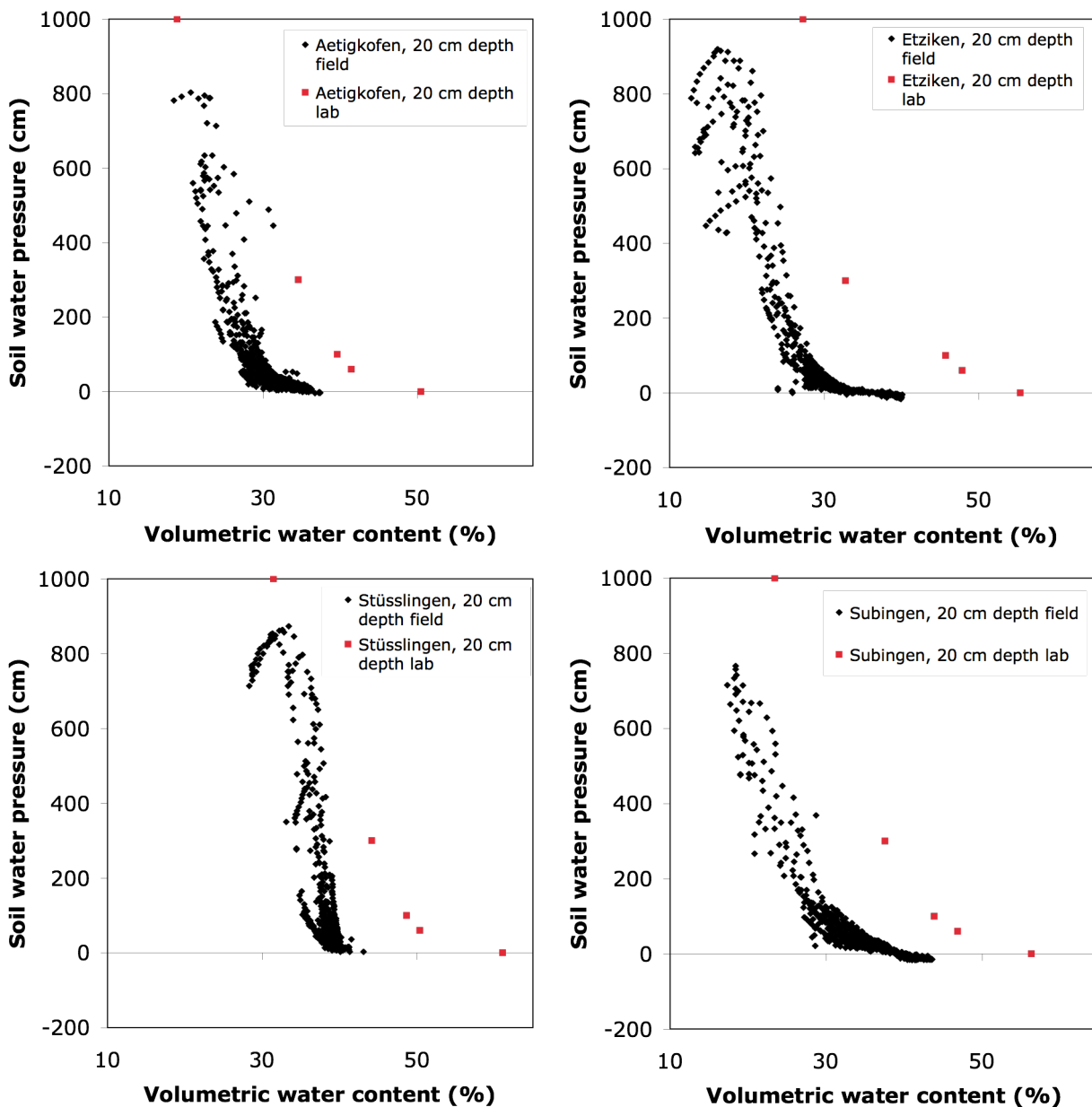
Fig. 45: *SWRC for four BMN sites in Aetigkofen (sandy loam, grassland; top left), Etziken (sandy loam, forest; top right), Stüsslingen (loam, grassland; bottom left) and Subingen (sandy loam, grassland; bottom right). The black dots represent measurements made in the field (data: BMN) and the grey dots are from destroyed lab samples (data: FS BS, 2011). The lab curves have a similar shape to the field values, but constantly predict too high water contents at the respective soil water pressures (0, 60, 100, 300 and 1000 hPa). The overestimation is usually largest for the saturated water content, declining towards a pressure of 1000 hPa.*

4.3   Temperature Dependence of Soil Water Pressure

To get a first idea of how the soil water pressure measurements at the BMN sites depend on temperature, they have been plotted against both soil and air temperatures available (see Fig. 46 and 47). For both sites displayed exemplarily here, Etziken and Stüsslingen, a threshold phenomenon of higher soil water pressure measurements occuring only at higher temperatures is visible. The scatter and the temperature range is bigger for the air temperature than for the soil temperature, which was to be expected because soil temperature gets more dampened the deeper in the soil it is measured.

For these two sites, the soil never froze during the measurement period (October 2011 until February 2014). Whereas Etziken does not include a single exception and shows that all higher soil water pressure measurements above 150 hPa were recorded at air temperatures above 8°C and soil temperatures above 12°C, in Stüsslingen there are few measurements that do not follow this rule. Nevertheless, it is clear that higher soil water pressure measurements were only recorded at higher air and soil temperatures.
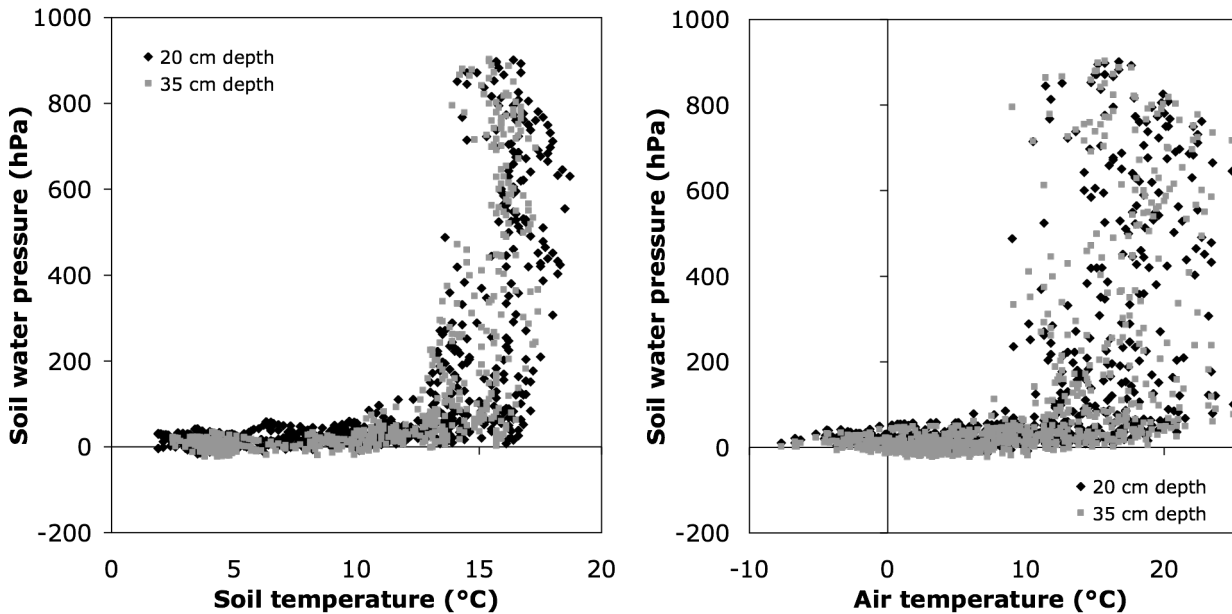
Fig. 46: *Dependence of the soil water pressure on the soil temperature (left) measured in the respective depth and on the air temperature in 2 m height (right) at the Etziken site (sandy loam, forest). A threshold phenomenon of higher soil water pressure occuring only at higher temperature can be made out for both soil and air temperature. The air temperature scatters more than the soil temperature, as expected. Under about 8°C air temperature and 12°C soil temperature, soil water pressure does not rise above 150 hPa. Data: BMN.*
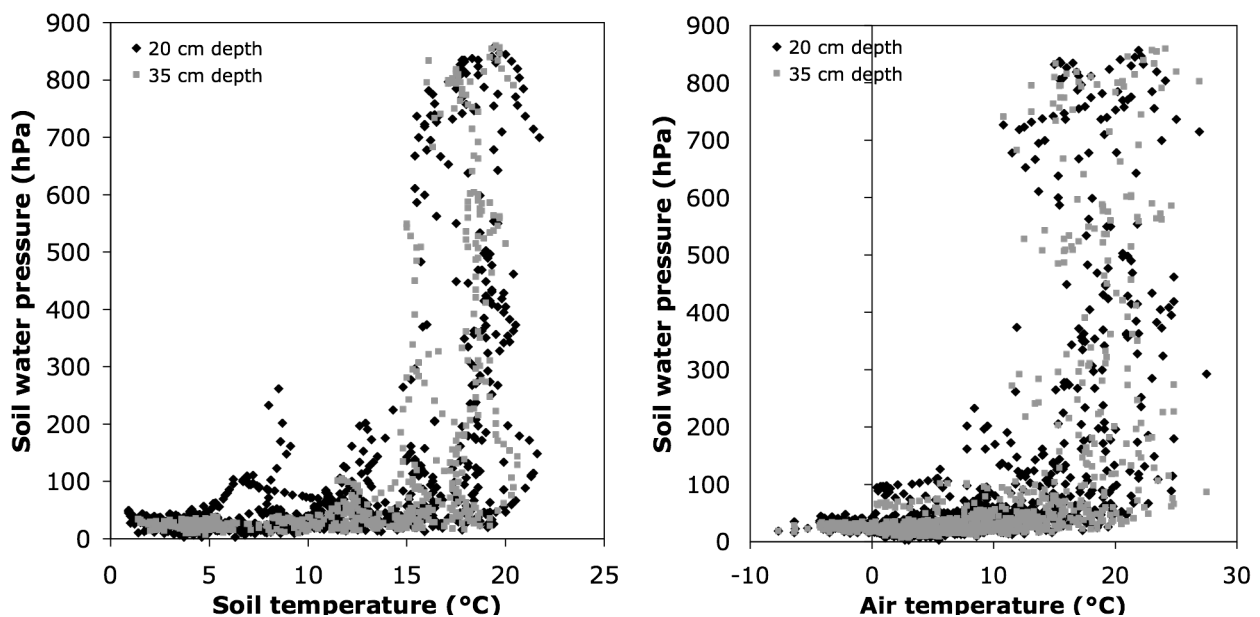
Fig. 47: *Dependence of the soil water pressure on the soil temperature (left) measured in the respective depth and on the air temperature in 2 m height (right) at the Stüsslingen site (loam, grassland). As for Etziken, most of the higher soil water pressure measurements occured at higher air and soil temperatures. An exception are the few datapoints indicating conditions clearly above 60 hPa at only about 7-8°C soil temperature in 20 cm depth. Data: BMN.*

However, all the analyses regarding temperature so far do not serve to tell whether the higher soil water pressure measurements were caused by the temperature difference or whether they are due to a change in the prevailing conditions in general that were acompanied by a rise of temperature. Soil water pressure measurements are of course influenced by other factors than temperature, such as water content, relative humidity, radiation and precipitation. Since the water content is for sure the most important of these variables, the influence of soil water pressure on both water content and temperature will be looked at closer.
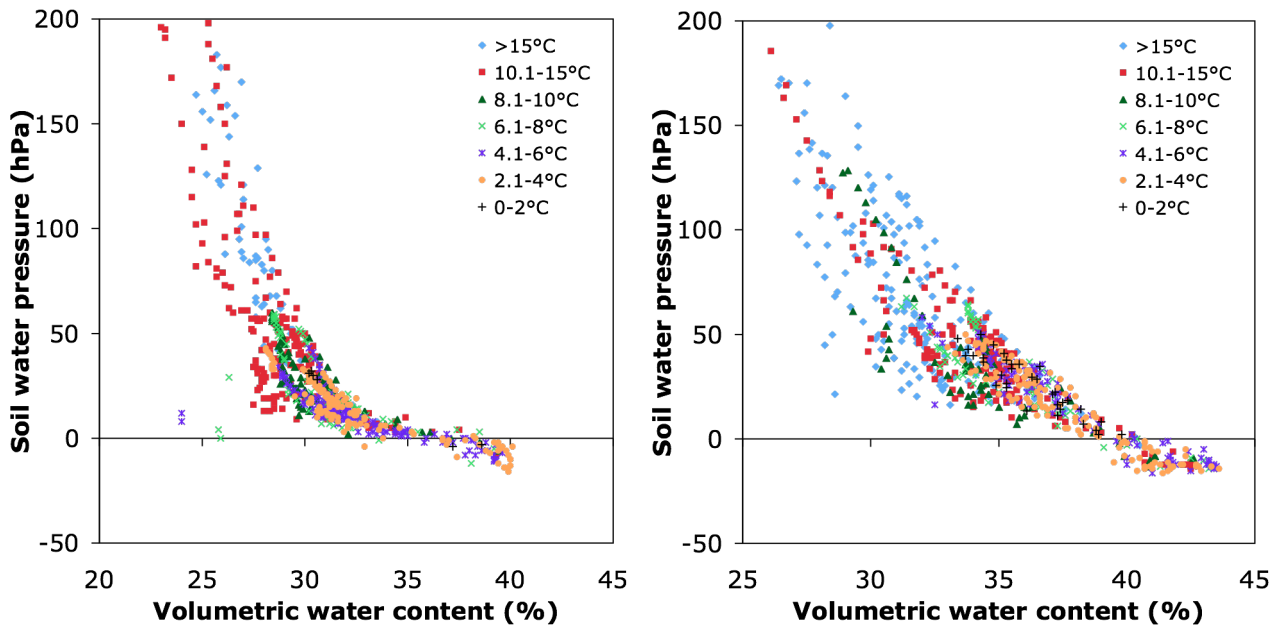
Fig. 48: *Field soil water retention curves depicted with their respective soil temperature in 20 cm depth at the Etziken site (sandy loam, forest; left) and at the Subingen site (sandy loam, grassland; right). Higher absolute soil water pressure is only reached at higher soil temperatures, but in the lower regions no clear temperature dependency can be made out. Data: BMN.*

The SWRC of several sites has been plotted depending on soil temperature to get an impression of what temperature changes mean for the relationship between soil water pressure and soil water content. In Fig. 48, two examples of the Etziken and Subingen site are displayed.
As expected from Fig. 46 and 47, absolute soil water pressure values clearly above the first threshold at 60 hPa occur only if soil temperatures are above 10°C at the Etziken site or above 8°C at the Subingen site. However, in the wet range no distinct trend with temperature can be seen. The values rather form a cluster, and for some temperature classes, as for example 2.1-4°C (orange) in Etziken, different parallel curves within the data cloud can be made out.

Fig. 49 and 50 show the water content depending on soil and air temperature for two different ranges of soil water pressure measurements. Inspite of there being a slight trend of decreasing water content at about the same soil water pressure with increasing air temperature at the Subingen site, generally no clear trend with temperature could be established.
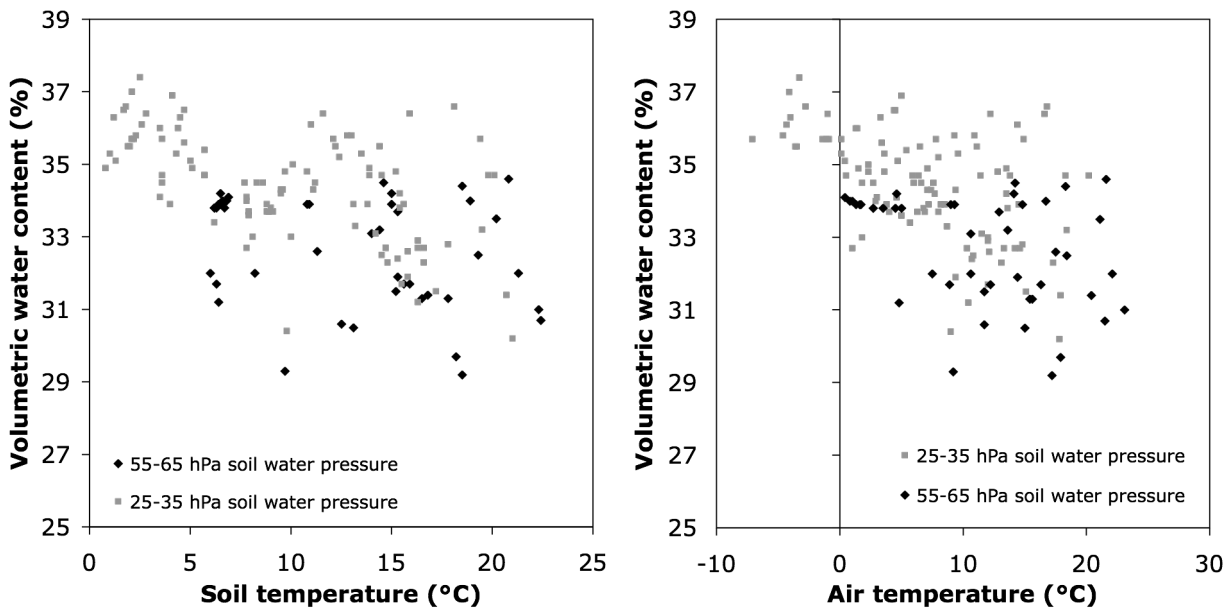
Fig. 49: *Volumetric water content of soil water pressure measurements in a similar range plotted against soil temperature measured in the respective depth (left) and air temperature 2 m above soil (right) at the Subingen site (sandy loam, grassland). Whereas no trend with temperature can be seen for soil temperature, both soil water pressure measurements series show a tendency towards lower water contents at the same soil water pressure with increasing air temperature. Data: BMN.*
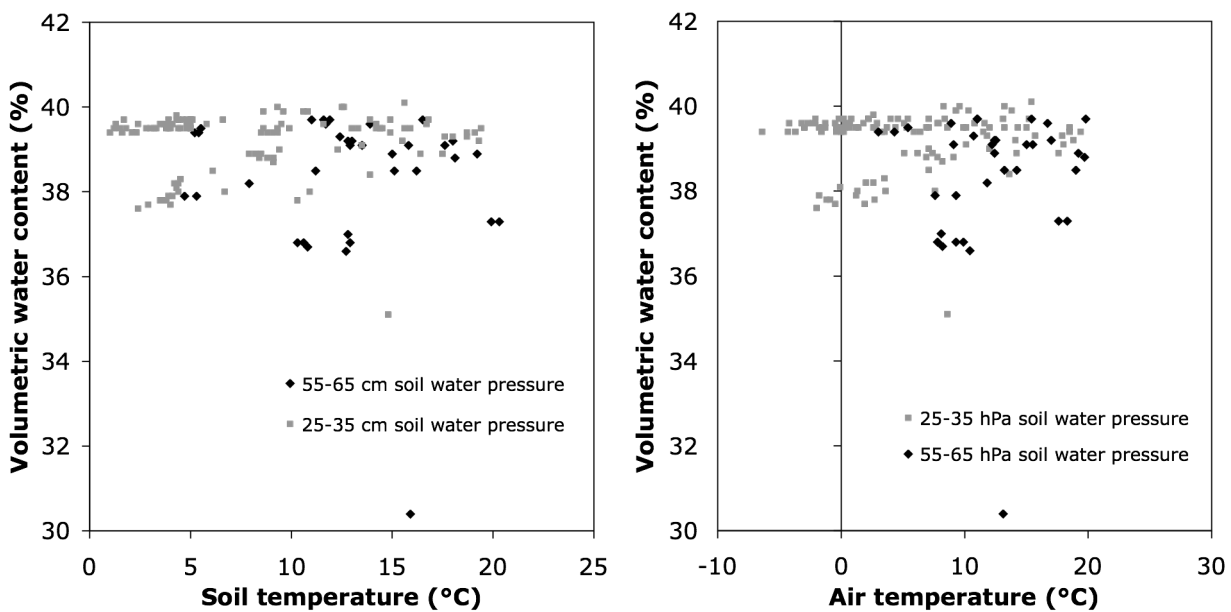
Fig. 50: *Volumetric water content of soil water pressure measurements in a similar range plotted against soil temperature measured in the respective depth (left) and air temperature 2 m above soil (right) at the Stüsslingen site (loam, grassland). Inspite of some ambiguity in the data, no trend regarding water content for a given soil water pressure with temperature can be observed. Data: BMN.*

The same graphs displayed vice versa, that means the soil water pressure at a similar water content dependent on soil and air temperature, can be found in Fig. 51 and 52.
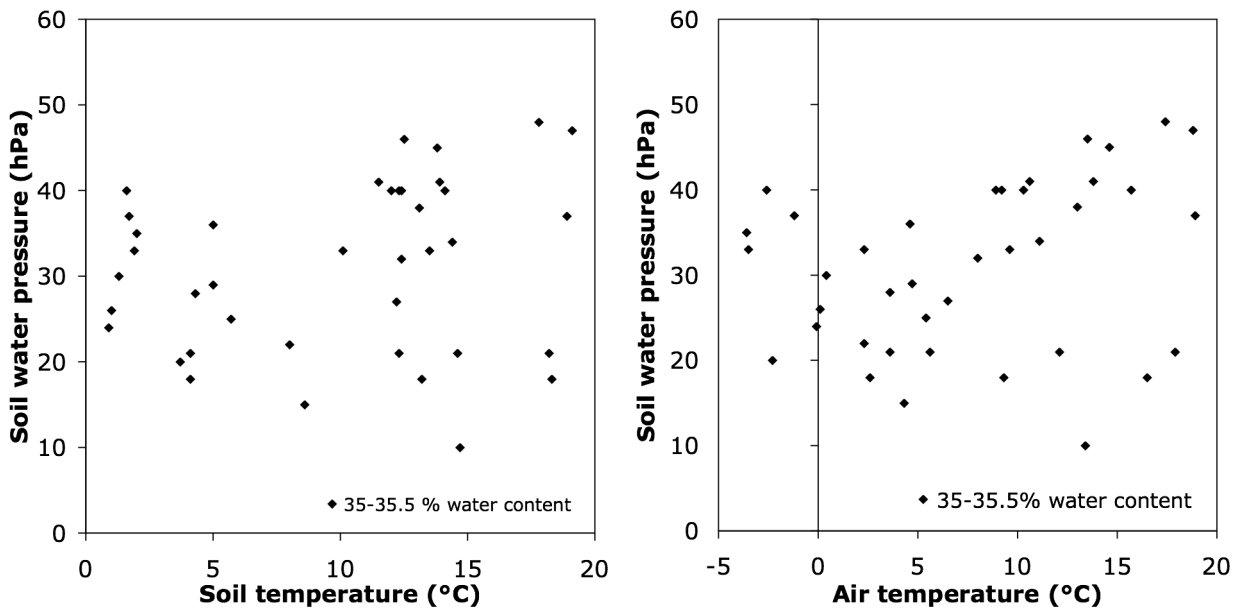
Fig. 51: *Soil water pressure measurements of a similar water content plotted against soil temperature measured in the respective depth (left) and air temperature 2 m above soil (right) at the Subingen site (sandy loam, grassland). Although the variability augments with rising temperatures, no clear trend is visible. Data: BMN.*
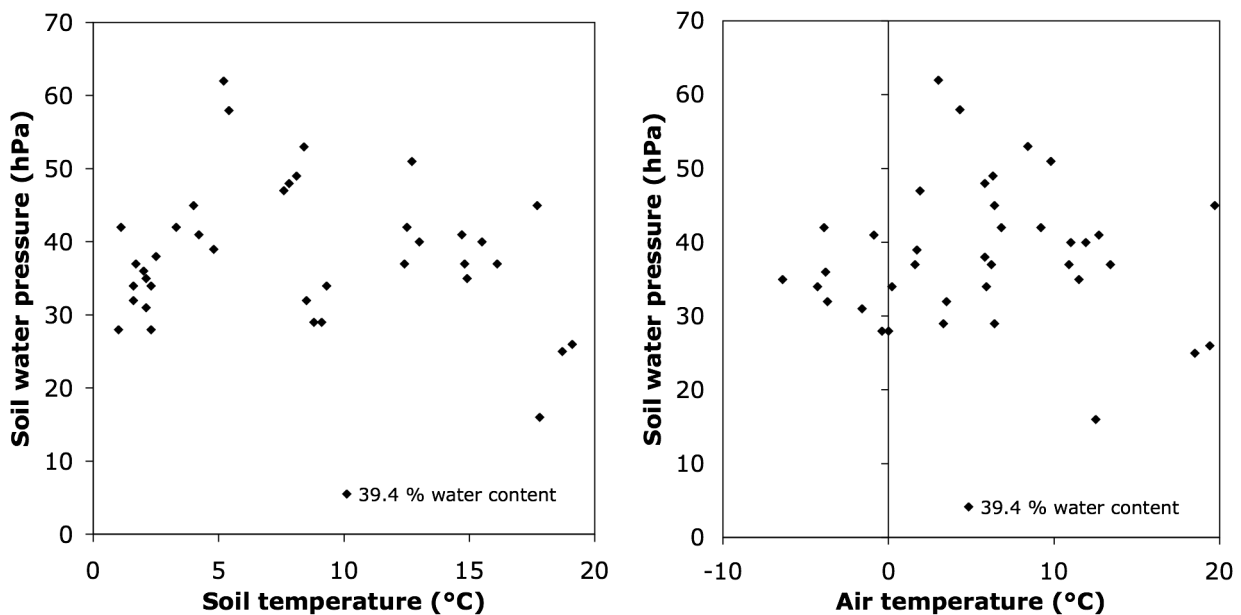
Fig. 52: *Soil water pressure measurements of a similar water content plotted against soil temperature measured in the respective depth (left) and air temperature 2 m above soil (right) at the Stüsslingen site (loam, grassland). The soil water pressure decreases slightly at higher soil and air temperatures, but the relationship is very weak. Data: BMN.*

Of Fig. 51 and 52, none of the data series shows a distinct relationship with temperature. However, in Stüsslingen a slight trend towards lower soil water pressure measurements at higher temperatures can be made out. In Subingen, this trend can be seen, too, but only until a soil temperature of about 10°C respectively an air temperature of about 5°C. Then, a positive trend between absolute soil water pressure measurements and temperature is depicted. Nonetheless, these trends are all of very weak nature. Furthermore, the variability in Subingen grows with increasing temperature, making a prediction even more difficult.

The T8 measurements appear quite robust to short-term temperature change in general, because in the field the raw data 15-minutes median (of three measurements) value stays rather constant. The self-installed tensiometers in constrast with a higher water column above the ground showed very high oscillations during daytime (see Fig. 53), although they were protected against radiation. On December 12th, the radiation shield was improved, leading to a reduction of the oscillations for the tensiometers installed in 35 cm depth and almost a disappearance of them in 20 cm depth. It is interesting to see that during the day the soil water pressure measurements in 20 cm depth almost exclusively rise, while the ones in 35 cm depth decline first and then show a sharp rise. Although the oscillations cannot be clearly attributed to radiation or temperature, since both were strong on these sunny days, they clearly coincide with the rising temperatures in the morning (see Fig. 54).
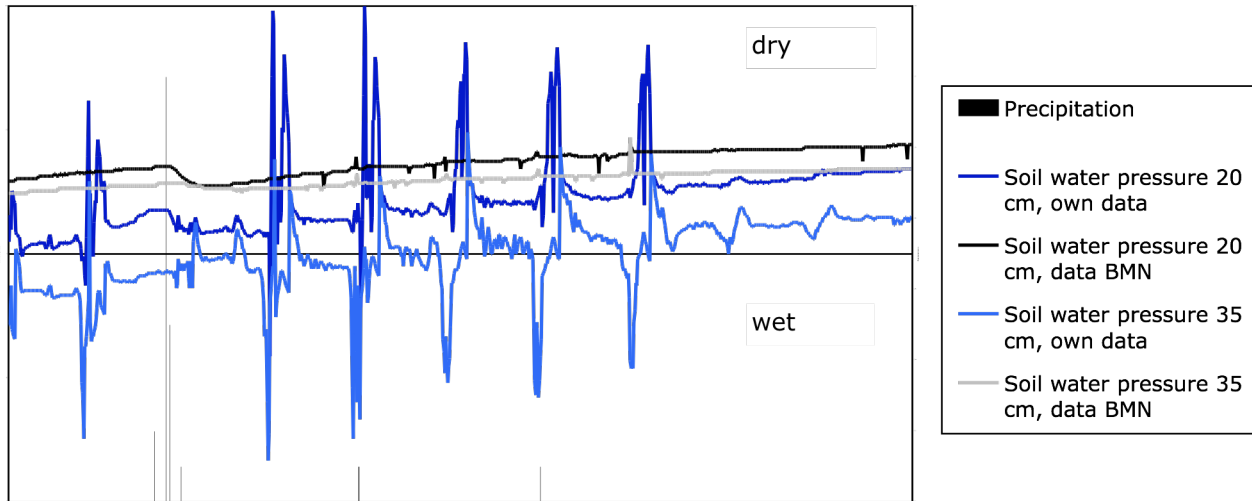
Fig. 53: *Raw data (15 min. values) of soil water pressure measured at the Stüsslingen site by the T8 of the BMN and the self-installed tensiometers. Every line represents the median of three measurements. The tensiometers show the same trends, but the T8 sensors prove to be much more robust against temperature and radiation fluctuations than the self-installed tensiometers. The protection shield was improved on December 12th, leading to a reduction of the oscillations. Data soil water pressure (partly) and precipitation: BMN.*
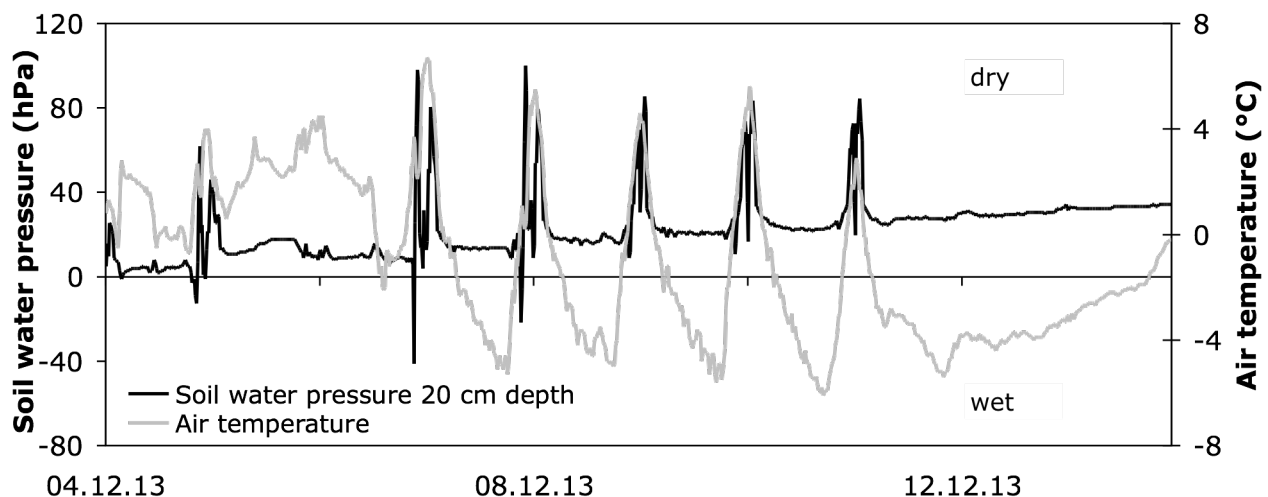
Fig. 54: *Raw data (15 min. values) of soil water pressure measured at the Stüsslingen site by the self-installed tensiometers and temperature measured by the BMN station. The soil water pressure line represents the median of three measurements. The self-installed tensiometers react clearly to temperature and/or radiation changes although protected against radiation. The protection shield was improved on December 12th, leading to a reduction of the oscillations. Data temperature: BMN.*

All these values recorded were, as mentioned before, not only influenced by temperature, but by other factors characterising the moment of the measurement as well. The goal of the experiment in a climate chamber with a T8 tensiometer as well as the installation of a lysimeter in the field was to (almost) exclude other factors influencing the soil water pressure measurement and quantify but the influence of temperature. This was achieved by constructing a closed system, so that the water content stayed constant during the measurements (details see under Methods, Sections 3.1.2 and 3.2.4). The results of the climate chamber experiment are depicted in Fig. 55.
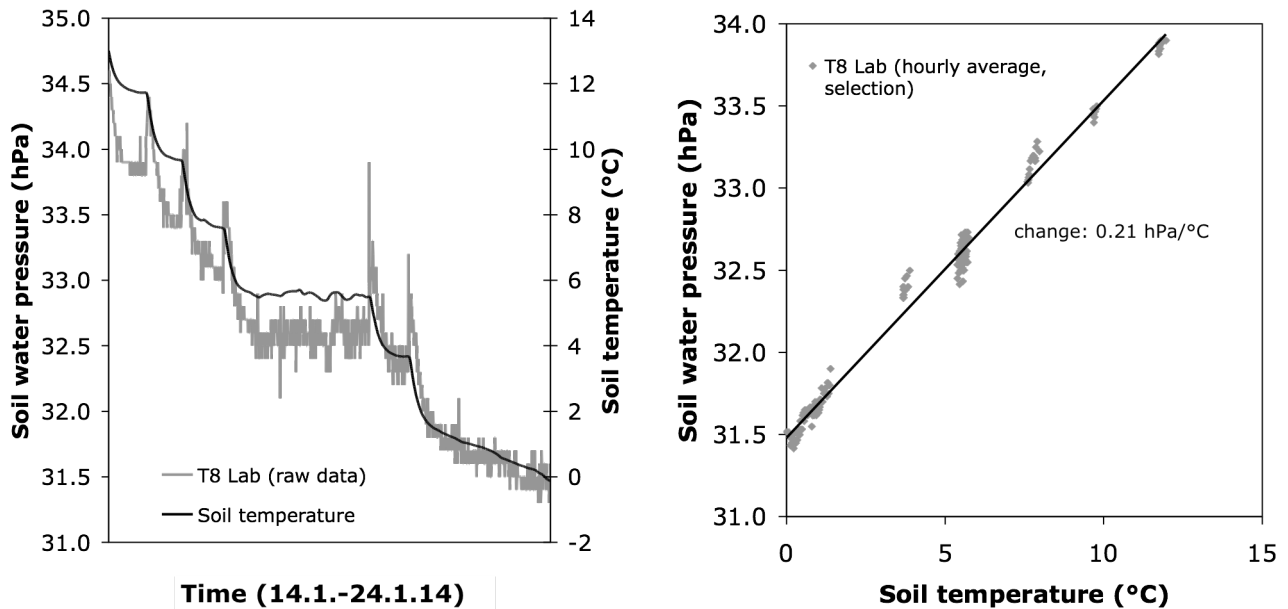
Fig. 55: *Temperature influence on soil water pressure measurements of the T8 tensiometer in a closed system in the lab. Raw data is shown on the left and an extraction of the soil water pressure measurements at constant temperature on the right. Although the water content remained constant, the soil water pressure showed an increasing trend with rise in temperature. However, the trend is relatively small (0.21 hPa/°C).*

The results shown in Fig. 55 state clearly that there is a trend of increasing soil water pressure with rise in temperature. It is approximately linear in the range tested (0 to 12°C). The measurements of the T8 cannot be considered completely robust against temperature changes since they showed a decrease of 0.21 hPa/°C at a constant water content when the system was cooled. The T8 raw data further shows a quick rise of soil water pressure shortly after the temperature started to drop (see Fig. 55; left).

A similar experiment has been undertaken in a lysimeter in the field, where two tensiometers were installed in a sealed bucket. Because of measurement problems with the tensiometers, only a short time period of four days is shown for one tensiometer in Fig. 56. Nevertheless, it can be seen clearly that the soil water pressure measurements reacted with air temperature, but not with soil temperature. Therefore, the measurements have been plotted dependent on air temperature in Fig. 56 on the right-hand side. The figure shows a slight linear trend towards higher soil water pressure measurements with higher air temperatures. Still, the variance is quite big and the slope is only 1.19 hPa/°C.
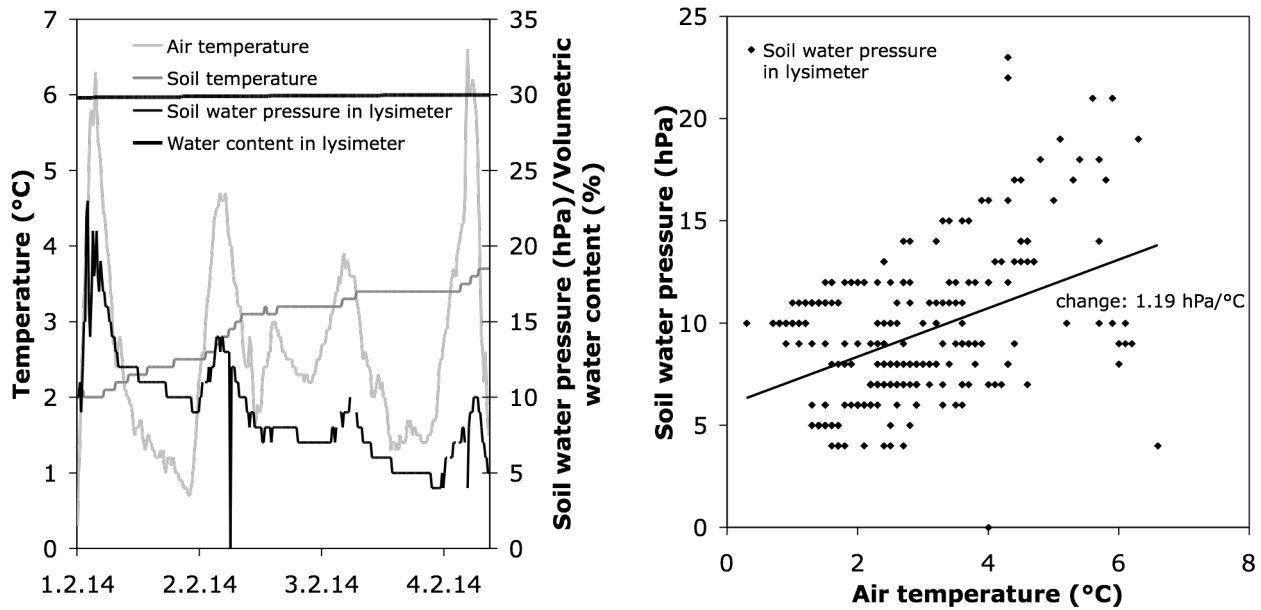
Fig. 56: *Temperature influence on soil water pressure measurements of a self-installed tensiometer in a lysimeter in the field. The curves over four days (left) show a reaction of the soil water pressure to air temperature, but not to soil temperature. The dots (right) indicate a trend of higher soil water pressure measurements with higher air temperatures (slope 1.19 hPa/°C). Data temperature: BMN.*

As a final experiment with respect to temperature influence, the SWRC measurement (drainage curve) in the lab has been repeated at 2-3°C.

The results in Fig. 57 are displayed as effective saturation values, that means their respective water content at 0 hPa after drainage of the macropores is assumed to be 1 (fully saturated soil) and the other values are displayed as portion of this full saturation if the lowest water content observed in the field is taken as 0 (see Section 3.2.3 for details). They show that for all soil samples, the water content measured at a given soil water pressure decreases with falling temperature. The difference is about 0.025 to 0.035 (fraction of effective saturation), variing between the samples. The high variation of the Stüsslingen samples, which could already be observed in Fig. 42, could be confirmed with this second experiment: the curves of the respective samples show a similar course for the two experiments. The same can be observed for the Aetigkofen sandy loam, although in general the change of the effective saturation (equation 3) varies less between the samples.
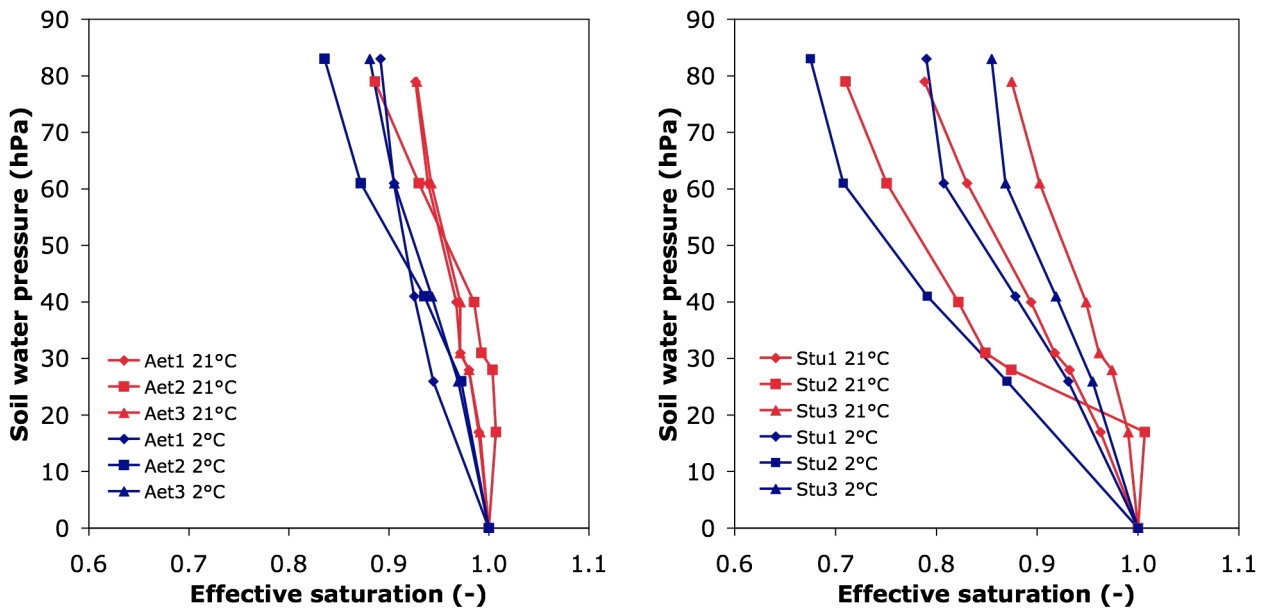
Fig. 57: *Lab SWRC (drainage) for the Aetigkofen sandy loam (left) and the Stüsslingen loam (right) measured at two different temperatures: approximately 21°C and approximately 2°C. In general, the water content measured at a given soil water pressure is lower at lower temperature. The difference between the two temperatures is about the same for all soils (approximately 0.025 to 0.035 fractions of effective saturation).*

4.4   Relative Humidity Influence

The relationship between daily mean soil water pressure and vapor pressure deficit (defined as 100% minus relative humidity in %) can be seen for Aetigkofen and Stüsslingen in Fig. 58.
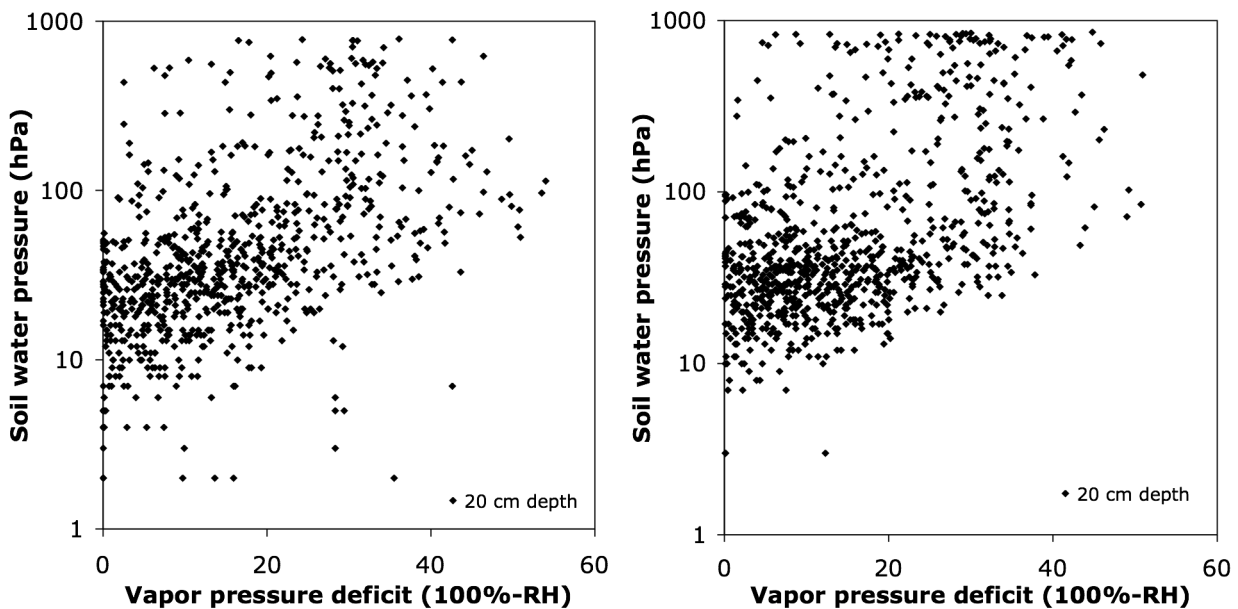
Fig. 58: *Soil water pressure plotted against vapor pressure deficit of the atmosphere for the Aetigkofen (sandy loam, grassland; left) and the Stüsslingen site (loam, grassland; right). For both sites, a relationship is visible, although high soil water pressure measurements may also occur when the vapor pressure deficit is low. Negative values (observed only at the Aetigkofen site) could not be displayed due to the logaritmic scale. Data: BMN.*

In this half-logaritmic representation, a weak trend of higher soil water pressure measurements at higher vapor pressure deficits can be made out. Generally, low soil water pressure measurements in the wet range (0-60 hPa) seem to be accompanied by a relatively high atmospheric humidity. However, the scatter is very high and it appears for both sites that high soil water pressure measurements may also occur at low vapor pressure deficits.
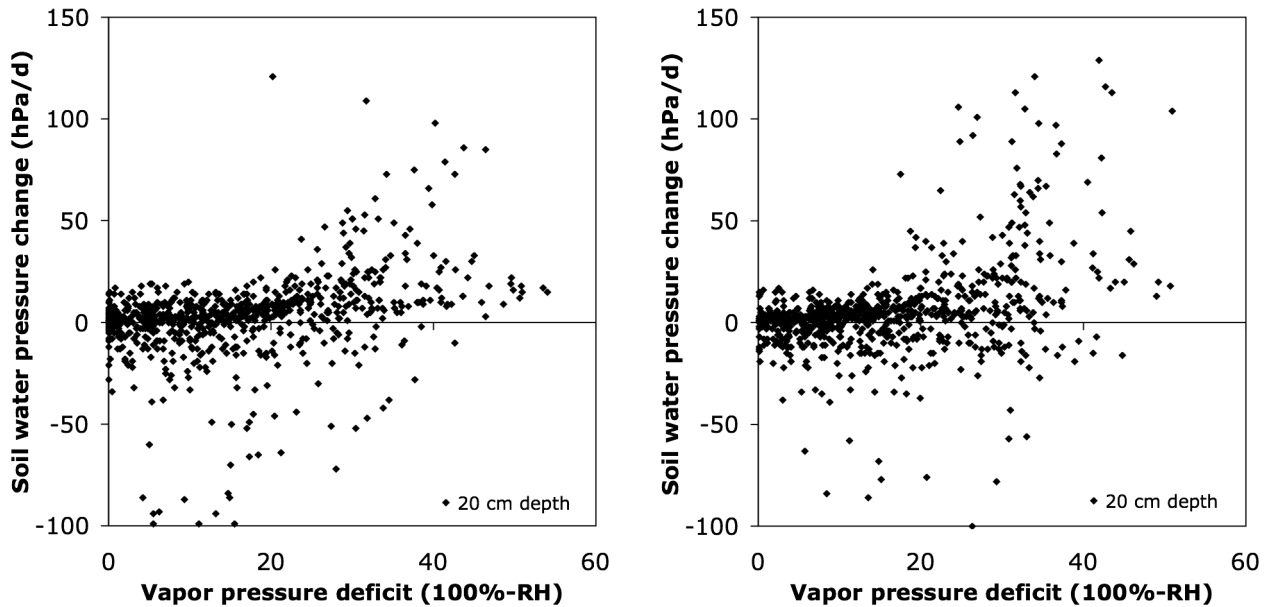
Fig. 59: *Daily soil water pressure change (value of the present day minus value of the previous day) plotted against vapor pressure deficit of the atmosphere for the Aetigkofen (sandy loam, grassland; left) and the Stüsslingen site (loam, grassland; right). There is a slight trend indicating that larger positive changes are occuring at higher vapor pressure deficits. Most of the daily positive changes seem to be small, though. Extreme values are not shown in the graph. Data: BMN.*

Since a high vapor pressure deficit of the atmosphere increases evaporation rates, soil water pressure values are expected to rise more if the relative humidity of the atmosphere is low. When plotting the daily soil water pressure change dependent of the vapor pressure deficit for the Aetigkofen and the Stüsslingen site, we can see that there is only a slight trend visible in the expected direction (see Fig. 59). Generally, the changes in the positive direction (drying) are smaller than the changes in the negative direction (wetting; data not completely shown in the graph). Most positive daily soil water pressure changes are small, around the range of ±20 hPa, and these also occur at high relative humidity. However, it seems that large daily soil water pressure changes of +50 hPa or more only occur at higher vapor pressure deficits, starting at about 20%. The very negative changes are again rather associated with lower vapor pressure deficits, most likely rainy days on which the soil water pressure dropped.

While including summer values with very high soil water pressures, a relationship with relative humidity can be made out, the question arises whether this can also be observed in wintertime when soil water pressure changes are lower in general. Fig. 60 shows the same plot, but just for wintertime values (October to March for the years available). When looking at all data together, a slight trend of higher values with higher vapor pressure deficit can be seen (data not completely shown in the graph). All negative values occur at a vapor pressure deficit of 40% or less for both sites. If we take only the positive changes into account, a relationship with vapor pressure deficit is, however, difficult to establish. In Aetigkofen, there is only one positive change that clearly exceeded 20 hPa. It occured in March 2012, when some warm days were observed in a row. It can be said that at higher vapor pressure deficits and therefore at lower relative humidity of the

atmosphere, larger soil water pressure changes into the positive direction are more likely to happen during wintertime. A strong relationship, however, fails to appear.
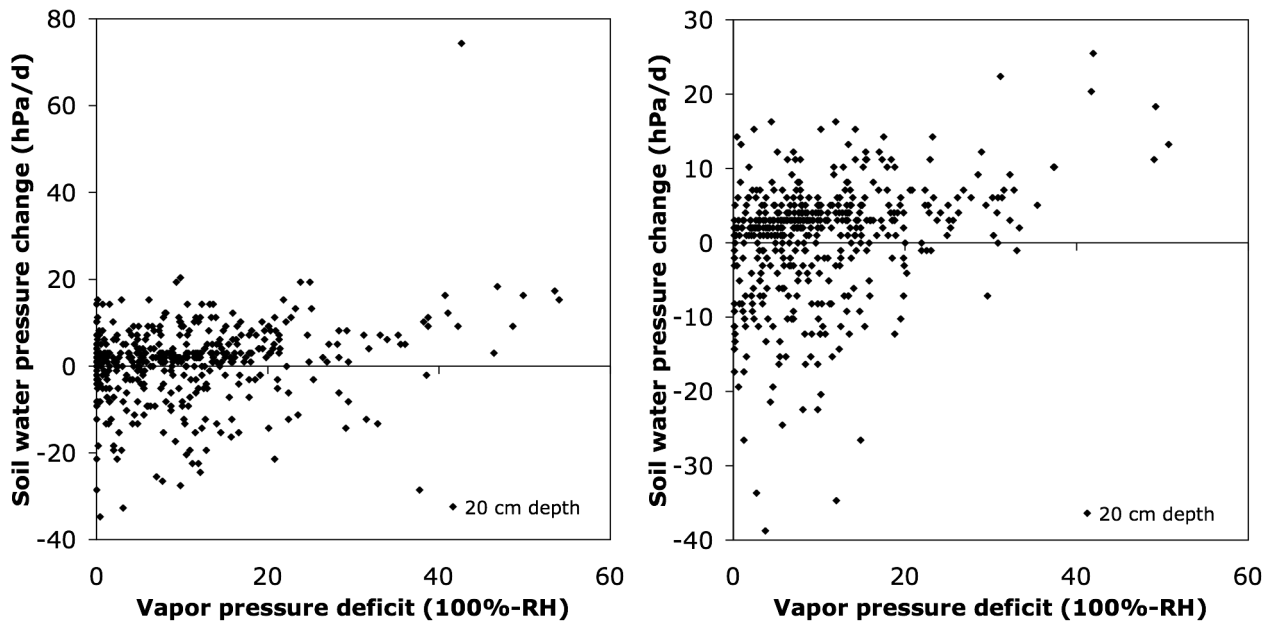
Fig. 60: *Daily soil water pressure change (value of the present day minus value of the previous day) during wintertime (October to March for the years available) plotted against vapor pressure deficit of the atmosphere for the Aetigkofen (sandy loam, grassland; left) and the Stüsslingen site (loam, grassland; right). Looking at all data, there is a trend of increasing values with higher vapor pressure deficit. Taking only positive changes into account, no real trend can be made out. Extreme values are not shown in the graph. Data: BMN.*

4.5   Sensor Comparison

Because there were some measurement problems with the tensiometers, the time period for the comparison was carefully chosen to be from the 10.1.2014 until the 21.1.2014. The data was averaged over six hours, hence, small fluctuations due to temperature changes or minor jumps of the TDR averaged out.

Fig. 61 shows that for both water content sensors and tensiometers the different sensors measure comparable values. All sensor types show similar reactions to the precipitation events. The additional tensiometer measurements, however, differ slightly from the data obtained by the T8 sensors of the BMN. Nevertheless, the difference between the two sensor types is only slightly bigger than the spatial variability recorded between the sensors. Furthermore, there is evidence that the measured values of the self-installed tensiometers would even be closer to the ones measured by the BMN sensors without the mentioned measurement problems.

The water content variation measured by the water content sensors could be explained by the drying of four soil samples, all taken inside the Stüsslingen station perimeter on December 12th, 2013 at a depth of 20 cm. The four water content values calculated with the help of the volume of the soil sample (see equation 18, Section 3.2.1) range from 0.335 to 0.414 (see Table 4 and red box in Fig. 61). They show a very similar range to the TDR and 10HS sensors at the same time, which lay between 0.337 and 0.4 in a depth of 20 cm.
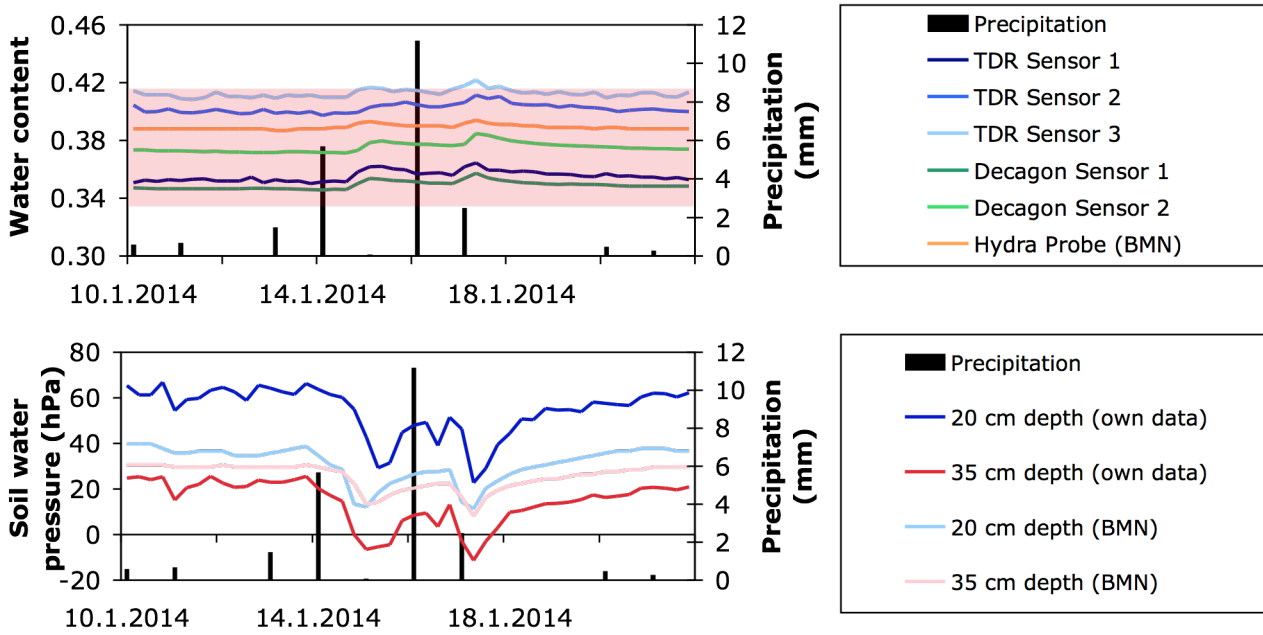
Fig. 61: *Comparison of the already installed sensors of the Bodenmessnetz (BMN) with own measurements (6-hour average) at the Stüsslingen site. The water content sensors (top; all in 20 cm depth) all show similar reactions to the precipitation events. Their wide range could be explained with the spatial variability (red box). The tensiometers (bottom; median value of three measurements) show similar trends, too. Their absolute values differ slightly, however. Data T8 and Hydra Probe: BMN.*

Table 4: *Variation of the soil water content inside the BMN station perimeter in Stüsslingen on December 12th, 2013. The calculated water content (column 4) shows a similar variation as the measurements of the TDR and 10HS sensors on the same day (between 0.337 and 0.4 in a depth of 20 cm).*

Soil sample weight (g)	Soil sample dry weight (g)	Weight loss during drying (g)	Volumetric water content (-)
271.8	233.9	37.9	0.386
266.3	230.4	35.9	0.366
270.2	229.6	40.6	0.414
280.0	247.1	32.9	0.335

It is remarkable that the water content sensors in Fig. 61 as well as over the whole measuring period (3 months) showed very little variation in their absolute measurement values. After a rise due to precipitation and thus water penetrating into the soil, the water content sinks again and remains then at a more or less constant level, similar to the soil water pressure.

Because Fig. 61 only displays median values of both the tensiometers of the BMN and the self-installed ones, Fig. 62 (left) shows a part of what is behind these curves. The raw data of the three additionally installed tensiometers in 20 cm depth is displayed from the 12th December, 2013 at 7 a.m. to the 15th December, 2013 at 6.15 a.m.. Before the rain starts, the three tensiometer measurements are comparable.

After the onset of rain on December 14th, the measured values of tensiometer 1 dropped quickly to zero while the other ones dropped only to a soil water pressure of about 15 hPa. These local effects of reaction to precipitation cannot be depicted when working with the median. Fig. 62 (right) shows that the measurements do not differ much when installed in a watered „Winzlerboden" soil in the lab where spatial homogeneity of the matric potential is assumed.
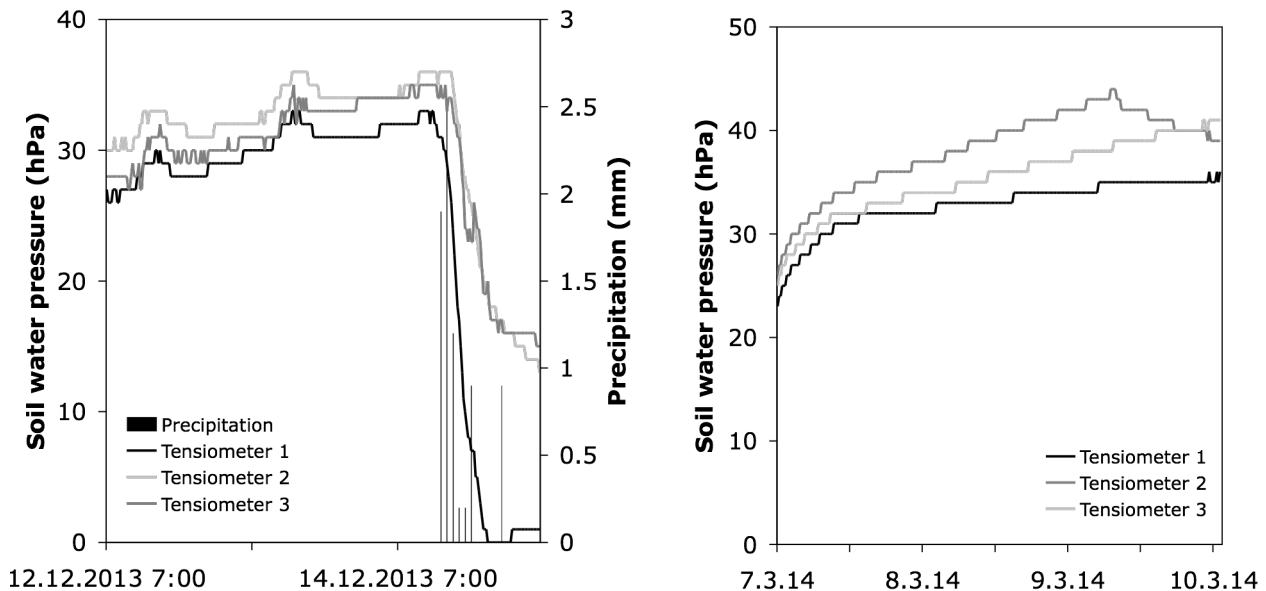
Fig. 62: *Left: Variation in soil water pressure measurements between the three self-installed tensiometers in 20 cm depth in the field. The raw data shows that the three measurements do not differ much during this time period until it starts to rain. Then, Tensiometer 1 reacts first and drops to zero, while the other two remain at about 15 hPa. Right: Variation in soil water pressure measurements between three of the tensiometers used in the field installed in a watered „Winzlerboden" soil in the lab. The raw confirms that the three sensors measure quite similarily. The slight drop of tensiometer two was due to water flowing out. Data precipitation: BMN.*

Since TDR and Degacon 10HS sensors have been installed in the same holes right next to each other, the measurements of these sensors, which differ considerably in the cost can be compared. In Fig. 63, the reaction of two pairs as well as the already installed Stevens Hydra Probe to the rather heavy precipitation events on February 13th, 2014 as well as in the night of Febuary 15th can be seen. Although the pairs installed closely to each other differ in the absolute values they measure, their reaction to precipitation and amplitude is very similar. The sensors at measuring point 3 (western hole) in 35 cm depth showed a much higher increase with precipitation than the two sensors at point 2 (middle hole) in 20 cm depth and the Stevens Hydra Probe, which is located closest to the middle hole. What can be seen very well in this graph is that the water content peaks shortly after the onset of precipitation and then decreases rapidly in a concave shape until, about two days after the event, the soil water content stabilises at its previous value.
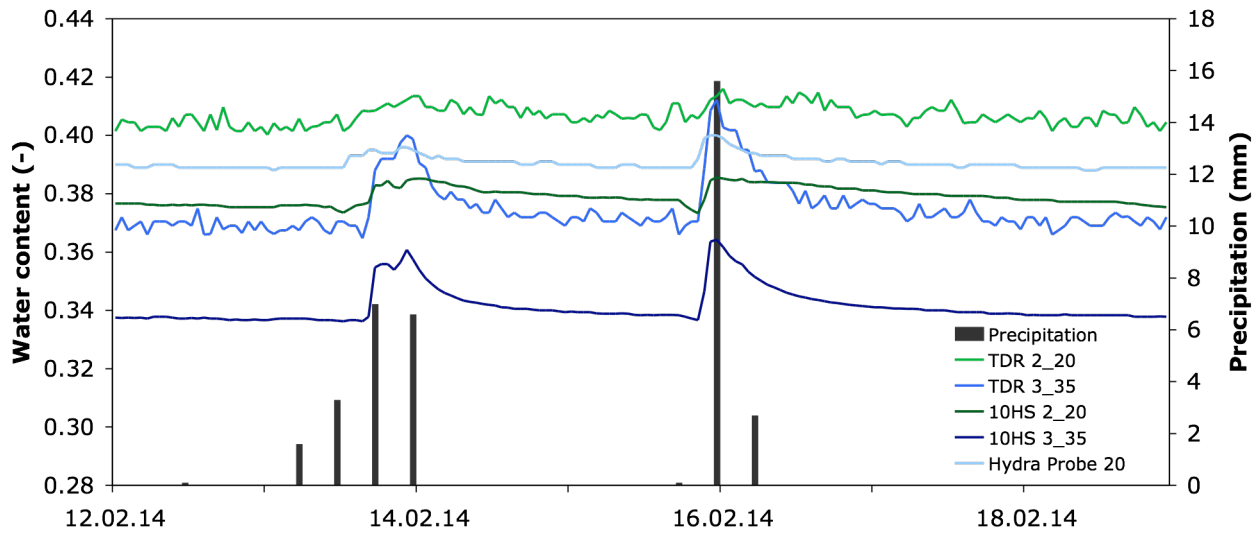
Fig. 63: *Reaction of five water content sensors to the precipitation events on February 13th and 15th/16th, 2014 (hourly values for water content, 6-hour-sum precipitation). Every measuring point (2 and 3) and depth (20 and 35 cm) is represented by two sensors, namely a TDR and a Decagon 10HS installed right next to each other. Both sensors at point 3 in 35 cm depth show a rather strong reaction while the ones installed at point 2 in 20 cm depth react shallower. The measurements of the TDR and 10HS as well as the Hydra Probe of the BMN are very similar both in response time and amplitude. Data precipitation and Hydra Probe: BMN.*

4.6   Water Balance Reconstruction

The calculation of the water fluxes occuring in a soil during wintertime (see Section 2.3 and 3.3.6) allowed a simple budget calculation involving precipitation data of the BMN site and evapotranspiration data calculated with the Primault (1962; 1981) formula of two MeteoSchweiz stations (Goesgen for Stüsslingen and Dulliken; Koppigen for Aetigkofen) to estimate the reliability of the recorded soil water pressure measurements in winter.

In Table 5, a summary of the used parameters can be found (obtained as mentioned under 3.3.6).

Table 5: *Parameters used for the flux calculation of the three soil types.*

Soil	Saturated water content θ_s (-)	Residual water content θ_r (-)	n (-)	α (1/cm)	Saturated hydraulic conductivity Ksat (cm/d)
Aetigkofen (sandy loam)	0.4143	0.0464	1.3237	0.0141	29.28
Dulliken (loam)	0.4017	0.0633	1.2919	0.0685	14.14
Stüsslingen (loam)	0.5038	0.0679	1.1819	0.0278	14.19

Fig. 64 (left) shows an example of the calculated daily flux for the Aetigkofen site in winter 2011/12. The data is only shown after December 29th, 2011 because evapotranspiration (ET) data from the Koppigen station (data: IDAWEB, MeteoSchweiz; calculated with the Primault formula (1962; 1981)) was newly available from then. It is clearly visible that the highest percolating fluxes occur after precipitation events. The high negative flux occuring after February 23th, 2012 was probably due to snowmelt. In winter, even during periods without precipitation, the soil water flux hardly turns positive because of low evapotranspiration (see e.g. period after January 12th, 2012). In

March, higher evapotranspiration (ET) values lead to stronger upward soil water fluxes. Between ET and soil water flux, a weak linear relationship can be made out (see Fig. 64; right, data not completely shown in the graph). Apparently, the strongest downward fluxes occur on days with little evapotranspiration. This relationship is obvious when looking at the precipitation: on days with a strong precipitation causing a negative soil water flux, usually a low evapotranspiration is measured. A big part of the strong positive fluxes also took place on days with a higher ET. Nevertheless, some of the positive fluxes of the same magnitude also happened when ET was low.
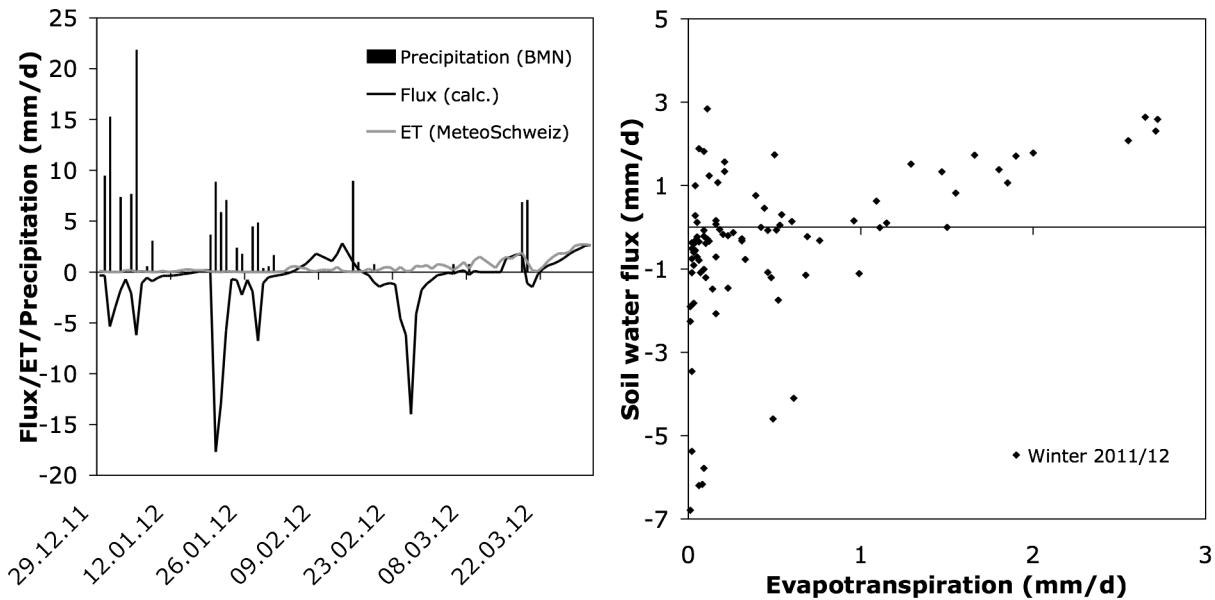
Fig. 64: *Daily calculated flux displayed with precipitation and evapotranspiration data for the Aetigkofen site in winter 2011/12 (left). The most negative fluxes usually occur after precipitation events. During December, January and February, evapotranspiration is very low and only little soil water flux takes place in an upward direction. In March, evapotranspiration values can be higher, thus followed by a larger upward flow inside the soil. The relationship between evapotranspiration and soil water flux shows a slight trend of higher evapotranspiration data leading to more positive soil water fluxes (right). Extreme values are not shown in the right graph. Data ET: IDAWEB, MeteoSchweiz; precipitation: BMN.*

The calculated fluxes have been summed up for the months October to March. All values thus obtained were negative, indicating a net water loss through percolation during these months for the soil layer between 20 and 35 cm depth. Secondly, the percolating water amounts expected with the water balance approach (see also Section 2.4) have been calculated by subtracting the ET sum from the precipitation (P) sum of the same months. These could thus be compared to the absolute percolation values obtained from the sum of the fluxes (see Fig. 65). When looking at the sandy loam in Aetigkofen, the values calculated seem to be in the right order of magnitude. For the winter 2011/12 (data from December 29th, 2011), the calculated and expected value almost match. For winter 2012/13 there is no data available for Aetigkofen due to a technical problem of the station. All values up to February 28th, 2014 have been included for the calculation of winter 2013/14. In Dulliken, the calculation also seems to be more or less in agreement with the excpected values. Nevertheless, in some years (e.g. winter 2011/12), the calculated values are clearly smaller than the expected ones. The same holds true for Stüsslingen, where the expected values are systematically underestimated by the calculation.
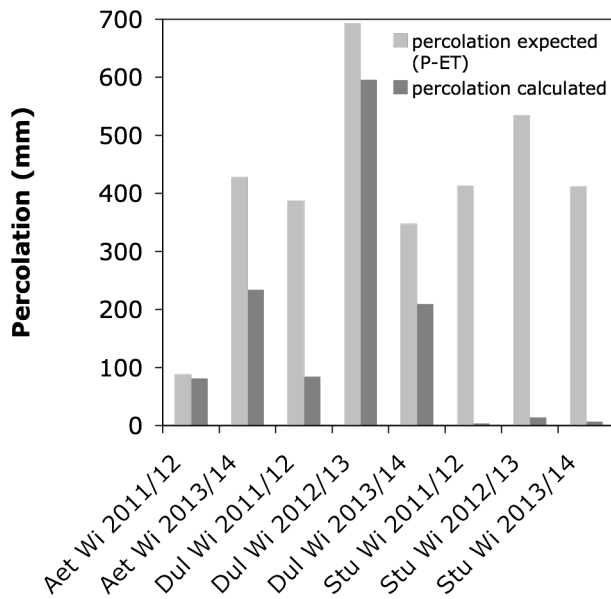
Fig. 65: *Comparison of the expected (winter precipitation sum – winter evapotranspiration sum) and the calculated (sum of all fluxes during wintertime, absolute value) percolation for the last three winters (Wi) of the three sites with close-by ET data available (Aet = Aetigkofen, Dul = Dulliken, Stu = Stüsslingen). The calculation tends to underestimate the values expected. Nevertheless, for Aetigkofen and Dulliken the results of the calculation are in the right magnitude. Data ET: IDAWEB, MeteoSchweiz; precipitation: BMN.*

4.7   Reconstruction of Situation with HYDRUS-1D

The appliance of the Inverse Solution in the HYDRUS-1D-Model to summer as well as winter soil water pressure data revealed quite divergent results for the van Genuchten parameters (see Table 6).

Table 6: *Van Genuchten parameter sets with the best fit to observed data of the Stüsslingen loam obtained by the Inverse Solution in comparison with the parameters fitted to lab data as in Section 3.3.6.*

Fit to...	Saturated water content θ_s (-)	Residual water content θ_r (-)	n (-)	α (1/cm)	Saturated hydraulic conductivity Ksat (cm/d)	R Square
observed soil water pressure summer (April to September 2012)	0.3602	0.0953	1.53	0.0022	0.4278	0.5571
observed soil water pressure winter (October 2012 to March 2013)	0.43	0.078	1.1891	0.0566	24.96	0.5358
lab data (details see Section 3.3.6)	0.5038	0.0679	1.1819	0.0278	14.19	-

The saturated water content for summer was predicted lower than for winter, and the parameter α related to the air entry value is larger by more than factor 10 in winter. Remarkable is also the difference in hydraulic conductivity, which was fitted very low in summer. As a comparison, the parameters obtained by curve fitting from the flux calculation are noted as well.

When plotting the observed and fitted values of the summer halfyear 2012, a reasonable fit can be made out (see Fig. 66). The time of the driest periods is represented very well, though this is not very astonishing since Fig. 66 shows the best fit of the simulated to the observed values, which were used as input data. Nevertheless, the top values of absolute soil water pressure are not as high for the simulated as for the observed data. It seems as if the simulated values are a compromise between a correct reproduction of the wet values close to saturation and the very dry peaks. To be able to reach such high absolute soil water pressure values as observed in summer, the fitted curve needs to react to drying very quickly, which leads to overestimation of soil water pressure before (April, beginning of May), in between (beginning of July) and after (September) the very dry periods. Furthermore, the observed values appear to be more robust against precipitation events than the simulated ones since not every event caused the soil water pressure to sink (see for example second half of June). Whereas the simulated values show the soil water pressure in 35 cm depth being almost always lower but very close to the values in 20 cm depth, the observed soil water pressure in 35 cm depth was able to clearly exceed the soil water pressure in 20 cm depth in August.
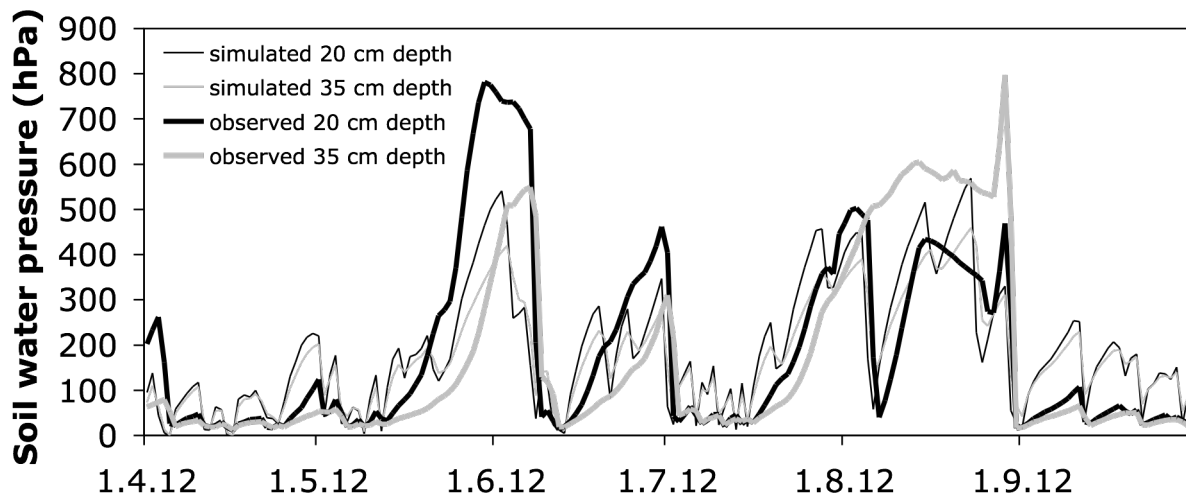
Fig. 66: *Simulated and observed soil water pressure values from April to September 2012 at the Stüsslingen site. The simulated values were obtained with the Inverse Solution in HYDRUS-1D, the shown solution is the best fit to the observed values. The ability to reach the dry values recorded in May/June and August seems to be dominant for the parameter set, since during short dry period the model overestimates the soil water pressure values. Data observed values: BMN.*

To be able to estimate the robustness of this best summer data fit, the same parameters as displayed in Table 6 were applied to the second summer with data available: April to September 2013 (see Fig. 67). The fit seems quite reliable, although it seems to suffer from the same problems as in 2012, for example the overestimation of soil water pressure in short periods without precipitation. Nevertheless, unlike in summer 2012, the very dry values in July and August could be reproduced with the same parameter set, but not the ones in June.
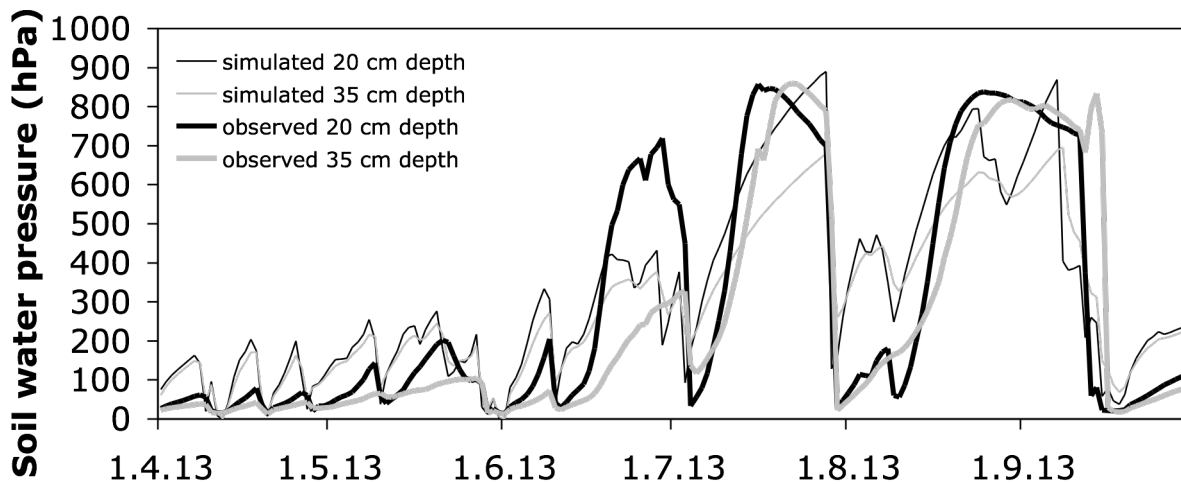
Fig. 67: *Simulated and observed soil water pressure values from April to September 2013 at the Stüsslingen site. The simulated values were obtained by applying the best fit parameters of summer 2012 to summer 2013. Though short dry periods especially in spring and beginning of autumn are still overestimated, the parameter set can apparently reproduce the top values recorded in July and August. Data observed values: BMN.*

This summer parameter set has then been applied to the daily precipitation and evapotranspiration data of the winter halfyear from October 2012 to March 2013 to see how it behaves in winter. The thus obtained simulated soil water pressure values in comparison to the measured data can be seen in Fig. 68. The parameters fit to summer data appear not to be suitable to estimate the soil water pressure in winter, because, as expected when looking at Fig. 66 and 67, the soil dries too quickly according to the model leading to an overestimation of the soil water pressure values. Nevertheless, the lower evapotranspiration in the winter halfyear seems to have an influence on the simulated values, because the maxima predicted in winter are only about half of the predicted maxima in summer.
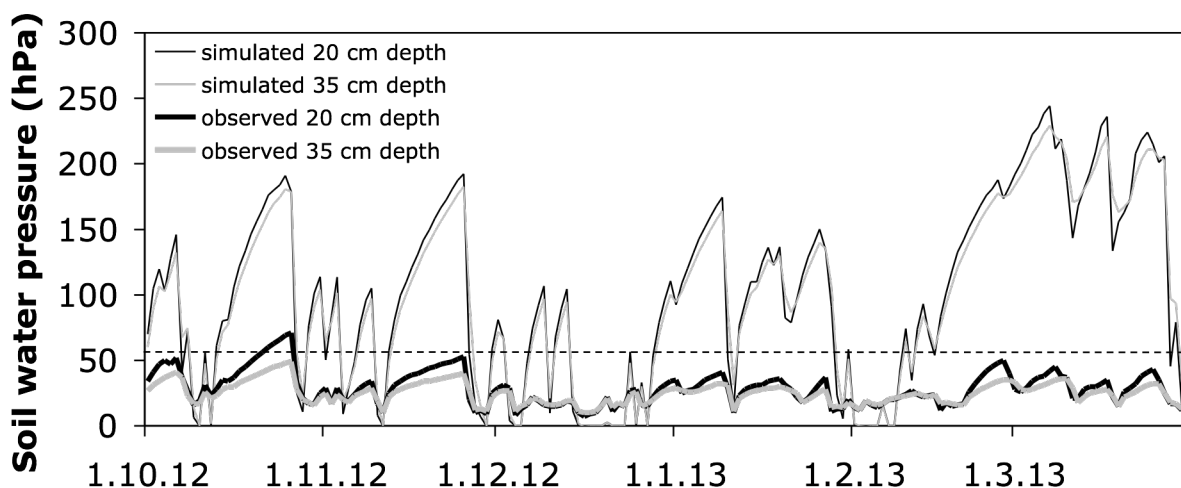
Fig. 68: *Simulated and observed soil water pressure values from October 2012 to March 2013 at the Stüsslingen site. The simulated values were obtained by applying the best fit parameters of summer 2012 to winter 2012/13. The parameter set systematically overestimates the drying process, leading to quite high soil water pressure measurements. The threshold at 60 hPa is shown with a dashed line. Data observed values: BMN.*

To see how a fitting parameter set for winter would look like, the same procedure has been repeated to fit the van Genuchten parameters to the period from October 2012 to March 2013. The parameters with the best fit can be found in Table 4. When we look at the simulated and observed values of that period (Fig. 69), a good agreement can be found in general. However, after rainfall the absolute soil water pressure prediction is generally lower than the observation. The measurements in October and November are usually higher than estimated from the simulation. This trend, however, turns into the opposite in March, when the predicted values tend to be higher than the observed ones.
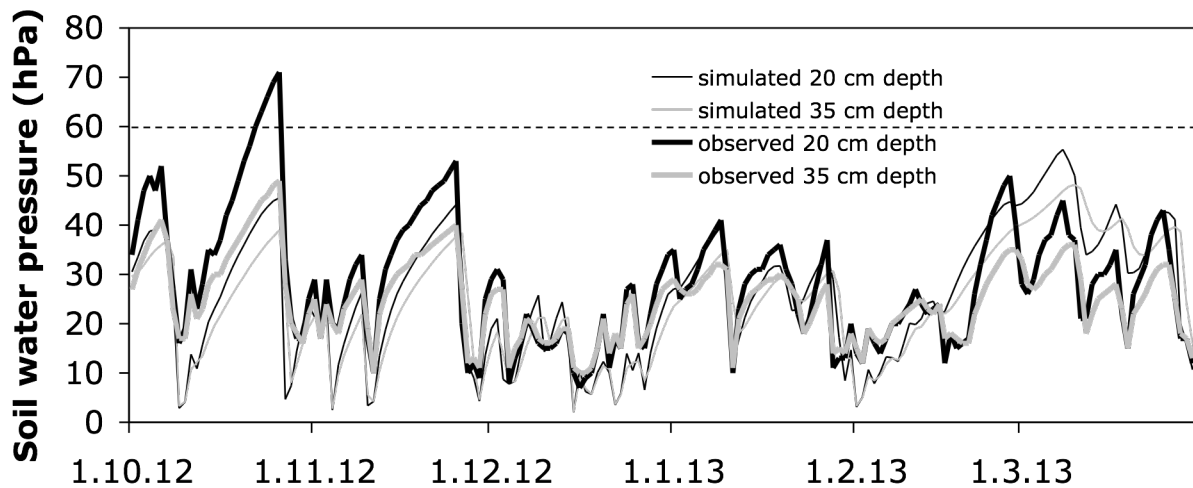
Fig. 69: *Simulated and observed soil water pressure values from October 2012 to March 2013 at the Stüsslingen site. The simulated values were obtained with the Inverse Solution in HYDRUS-1D, the shown solution is the best fit to the observed values. The prediction and the observed data match quite well with a tendency to overestimation of the model in autumn and underestimation in early spring. The threshold at 60 hPa is shown with a dashed line. Data observed values: BMN.*

As seen for the summer fit, the robustness of the obtained winter fit has been tested by applying the same parameter set to input precipitation and evapotranspiration data of two other winters (see Fig. 70). The fit is quite good, although the trend of the model underestimating the measured soil water pressure values can be observed throughout winter in both years, especially in autumn 2011. For February 2012, there is unfortunately no observed data available. In March 2012, the model's prediction of soil water pressure values is above the values measured in 35 cm depth, a trend similar to the one in March 2013. Nevertheless, in 2012 the absolute soil water pressure measured in 20 cm depth is clearly higher than the simulated values.

Finally, the best-fit winter parameter set has been used to predict soil water pressure in summer 2012 (see Fig. 71). This fit is probably the worst obtained so far, since soil water pressure measurements are definitely underestimated. The model is, using this parameter set, not able to reproduce the dry periods in summer. The highest absolute soil water pressure predicted by the model is around 106 hPa, whereas the measured values rise up to approximately 812 hPa. Nevertheless, there are periods in summer 2012 which are not badly represented by the model, such as April 2012 after the first drop of the soil water pressure. In September, the simulated and observed values also agree very well for both depths.
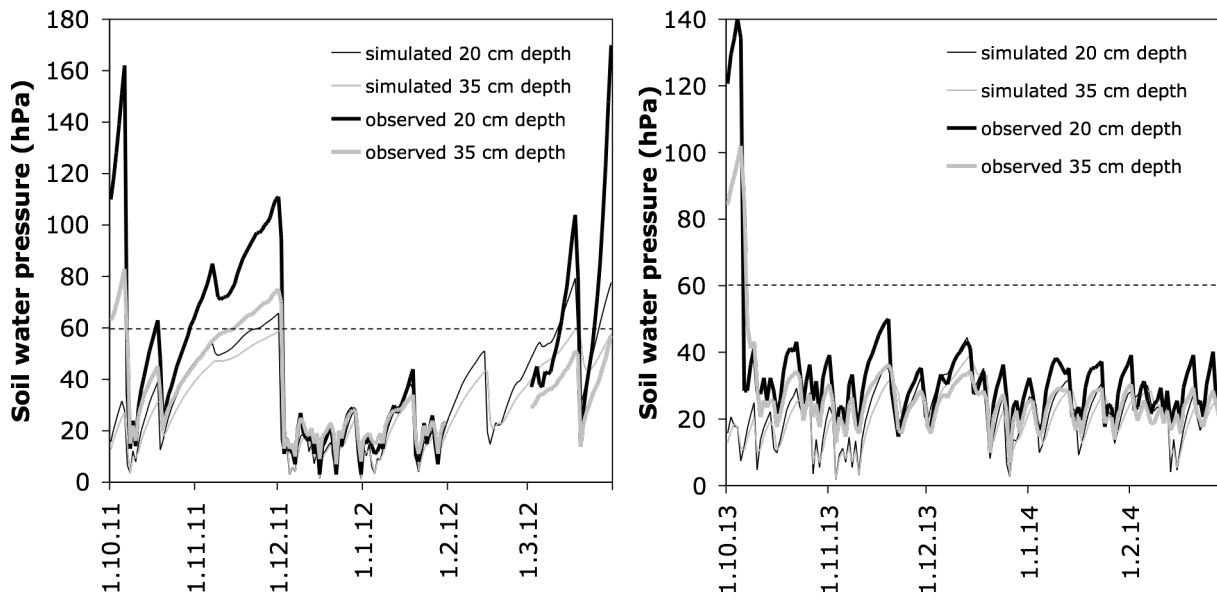
Fig. 70: *Simulated and observed soil water pressure values from October 2011 to March 2012 (left) and October 2013 to February 2014 (right) at the Stüsslingen site. The simulated values were obtained by applying the best fit parameters of winter 2012/13 to the year before and the year after. Although the values do match quite well, the apparent trend is an underestimation of the measured soil water pressure by the model. The threshold at 60 hPa is shown with a dashed line. Data observed values: BMN.*

The analysis with the help of HYDRUS-1D points out that there may be two different prevailing conditions with respect to water movement in the soil throughout the year: One is valid for the few very dry periods in summer when the soil water pressure must react very quickly to a drying process, the other one is valid for the rest of the year when the response of soil water pressure to dry atmospheric conditions (little precipitation, middle or high evapotranspiration) apparently is slower. An applicance of the parameter set fitting the first condition to winter settings results in a permanent overestimation of absolute soil water pressure. The exact opposite happens when the parameters of the second condition are applied to the very dry summer periods: The model predicts soil water pressure values that are way below what has been measured.
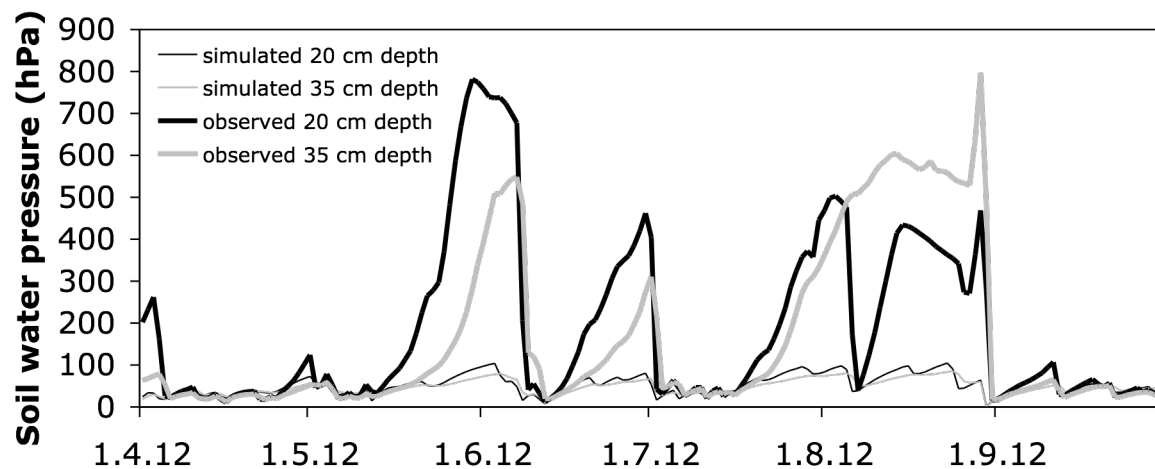

Fig. 71: *Simulated and observed soil water pressure values from April to September 2012 at the Stüsslingen site. The simulated values were obtained by applying the best fit parameters of winter 2012/13 to summer 2012. The model definitely underestimates the soil water pressure values; most clearly visible in the very dry periods. Data observed values: BMN.*

4.8 Penetration Resistance Measurements

The penetration resistance measurements show an increase with depth and, especially up to a depth of approximately 35 cm, a clearly distinguishable curve for every measurement day (see Fig. 72). However, after 35-40 cm depth, the position of a curve is somehow arbitrary due to large fluctuations and no clear trends between the measurement days can be made out. Since every curve displayed in Fig. 72 represents an average of various insertions, variations between the measurements on one day cannot be seen (see Discussion 5.7).
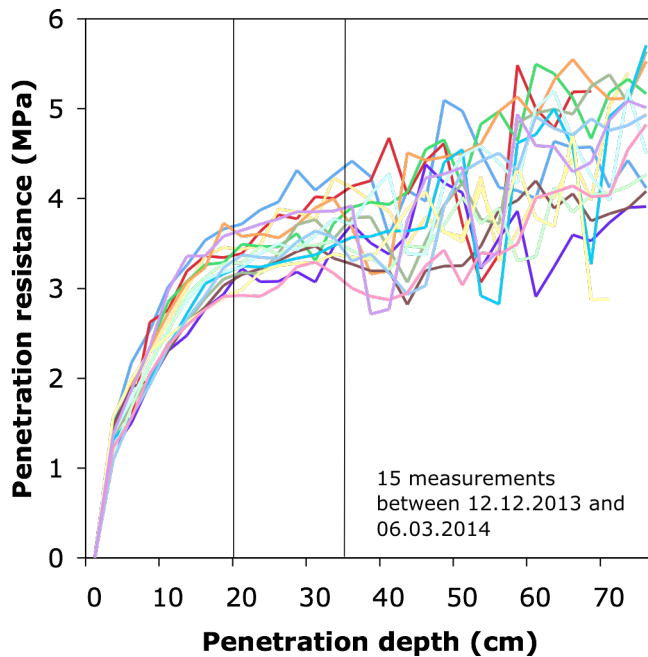
Fig. 72: *Penetration resistance of the uppermost 75 cm at the Stüsslingen site. Each curve represents the average of at least six cone penetrometer insertions performed on the same day within the station perimeter. Penetration resistance generally increases with depth, but large fluctuations can be made out after a depth of approximately 35 cm.*

When plotting the soil water pressure measurements of the Bodenmessnetz during the measurement against the penetration resistance at the respective depths, a linear relationship can be observed (see Fig. 73; left). Although the R square values depict only a slight linear dependency, a trend of increasing resistance with increasing absolute soil water pressure can be seen for both depths. The trend at 35 cm depth is weaker, though. A relationship between penetration resistance and water content can also be observed (see Fig. 73; right). The water content varied very little between all 15 measurement days, thus making a statement out of this small range is impossible.

The product of soil water pressure and effective saturation (equation 3, Section 2.1.2; θ_s = maximum water content measured during insertions (0.392), θ_r = minimum water content recorded during BMN datarow (0.27)) plotted against the penetration resistance in 20 cm depth (see Fig. 74; left) yields a very similar result to the one observed with soil water pressure in 20 cm depth. When looking at the field SWRC plotted for the soil water pressure and water content values recorded on measurement days, the expected pattern of lower water content at higher soil water pressure can be made out (see Fig. 74; right).

After the irrigation of a 1x1 m²-plot beside the station, the penetration resistance decreased over all depths when measured shortly after irrigation (average of 6 measurements, see Fig. 75). The water content in the uppermost 10 cm had by then risen from 0.402 to 0.423. However, the measured decrease in depths below 10 cm cannot be attributed to the irrigation because water does not percolate that quickly. It must thus be subject to random effects. 20 minutes later, the water content

had stabilised at 0.414, the largest pores had thus already drained. The penetration resistance measured at that time had decreased in the uppermost layers relatively to the one right after the irrigation, because they have been watered up to then. It then approaches the control measurement when going deeper into the soil.
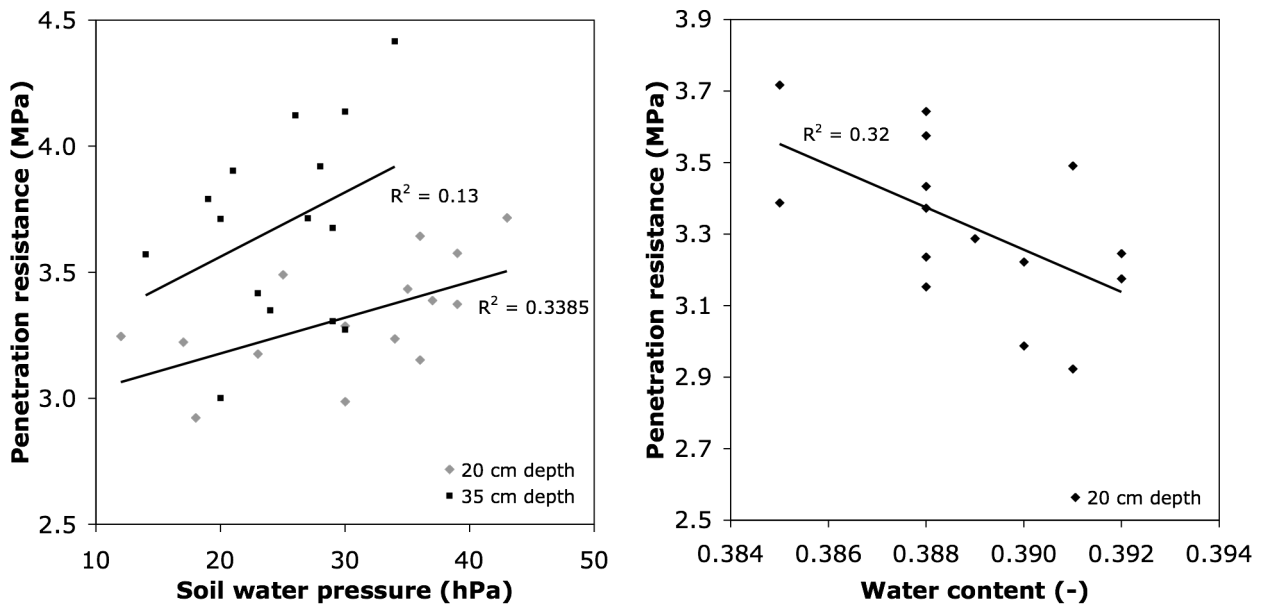
Fig. 73: *Relationship between penetration resistance and soil water pressure (left) respectively water content (right). Every dot stands for one measurement day (average). Although the relationship is weak, a linear trend can be seen for both variables showing an increase in penetration resistance with increasing soil water pressure and decreasing water content. Data soil water pressure/water content: BMN.*
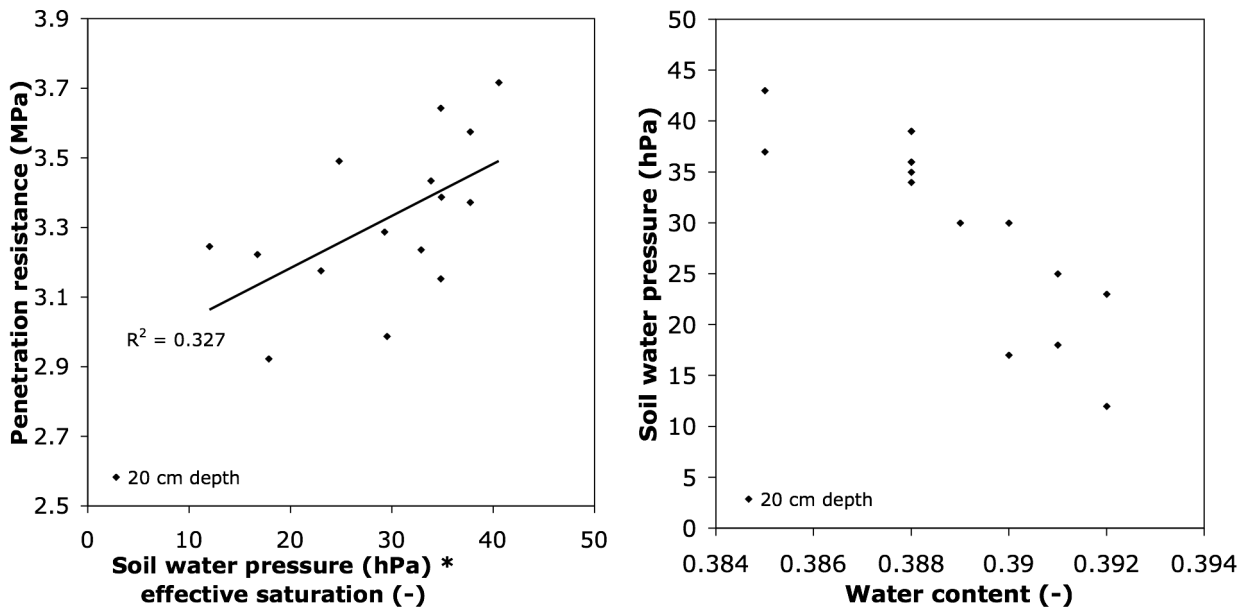
Fig. 74: *Left: Relationship between penetration resistance and the product of soil water pressure and effective saturation. The trend is very similar to the one observed for soil water pressure in 20 cm depth. Right: SWRC with data from the BMN on measurement days. Data soil water pressure/water content: BMN.*
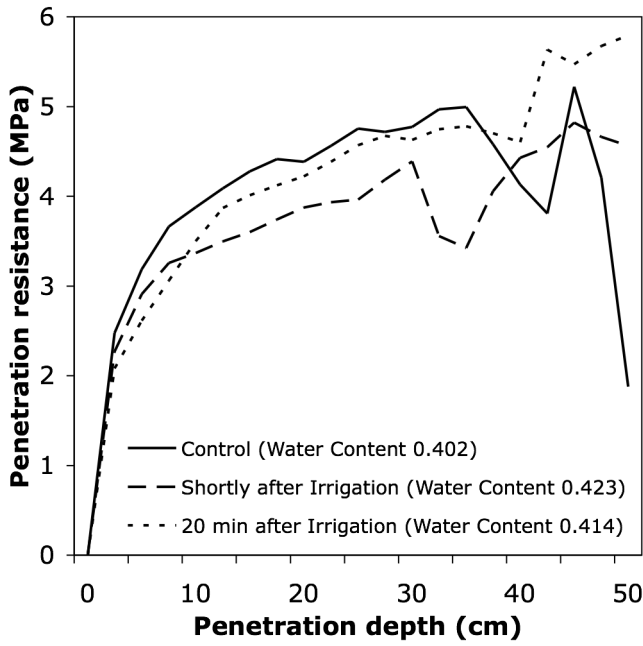
Fig. 75: *Penetration resistance with depth before (control) and after irrigation. The water content rose, making penetration resistance decrease in the uppermost 10 cm.*

5　Discussion

5.1　Soil Water Pressure Frequency Distribution

The results of the frequency distribution of soil water pressure measurements among Switzerland revealed that the low soil water pressure measurements observed in the Canton of Solothurn during wintertime are not unique, but appear to be the most common case in Switzerland.

However, the choice of the sites included in the analysis was somehow arbitrary, because the data availability was limited. The spatial distribution of the soil water pressure measurements analysed cannot be looked at as representative for whole Switzerland, because large areas, such as the western part of Switzerland including the Canton of Berne, almost the whole alpine area as well as most of eastern Switzerland do not have continuous soil water pressure measurements during winter. Not only is the spatial distribution restricted, but the timely dimension as well. Soil water pressure measurements of wintertime have not been available for a long time (as mentioned under Section 1.1.3), thus making the datarow with three winter's data rather short.

It was interesting to see that just in February, one of the months with the most very low soil water pressure measurements, very high soil water pressure values could be reached. All these dry recordings in February could be associated with the cold February 2012 (MeteoSchweiz, 2013). It is known that soil freezing causes soil water pressure to rise (Sutinen et al., 2007; Iwata et al., 2010), hence the soil probably froze at the sites with very high soil water pressure values.

The fact that only Breitenbach SO showed very high soil water pressure values in October indicates that local conditions are very important for the behaviour of a soil with respect to soil water pressure. Also, the difference in measurements for three soils with silty loam texture and a similar mean precipitation over the winter months (see Fig. 37; left) shows that texture cannot be considered as a single explanatory variable. Precipitation appears to play a role, as seen in Fig. 37 (right). However, since for the comparison the precipitation of Zurich has been used, it may not hold true for all Switzerland due to the high local variability of precipitation. It sticks out that a few soils - Rafz ZH, Waedenswil ZH and Erstfeld ZH, as mentioned before (details see Table C.1, Appendix C) - do reach higher soil water pressures also during winter. This may be due to higher hydraulic conductivity, since atmospheric conditions in winter are similar over the areas of Switzerland where the analysed sites are. The soil in Erstfeld lies on alluvial lands and may thus indeed have a high hydraulic conductivity (data: Canton UR).

5.2　Soil Water Retention Curves

5.2.1　Field SWRC

Some sites of the BMN did not provide reliable SWRC when plotted. Most of the time, the Hydra Probe measurements were the reason for their strange shape. The T8 do not seem to deliver unrealistic measurements, since the annual SWRC courses of all sites are quite similar. Although the SWRC in Fig. 38 look quite reliable for the four BMN sites presented, it has, as for the frequency analysis, to be considered that they have been plotted with a timely limited datarow available.

When dealing with daily mean values, as for the analyses seen under Section 4.2.1, we implicitly assume that the daily mean values represent the situation correctly and are not affected by the calculation of a mean. However, the mean could be influenced by for example delays due to different reaction times of soil water pressure and soil water content. Therefore, a SWRC has been plotted exemplarily with 15-minute values for February 2014 at the Etziken and Subingen sites (see Fig. 76) to see what the raw values recorded simultaneously (soil water pressure: spatial median of three measurements) display in comparison with the daily mean values.
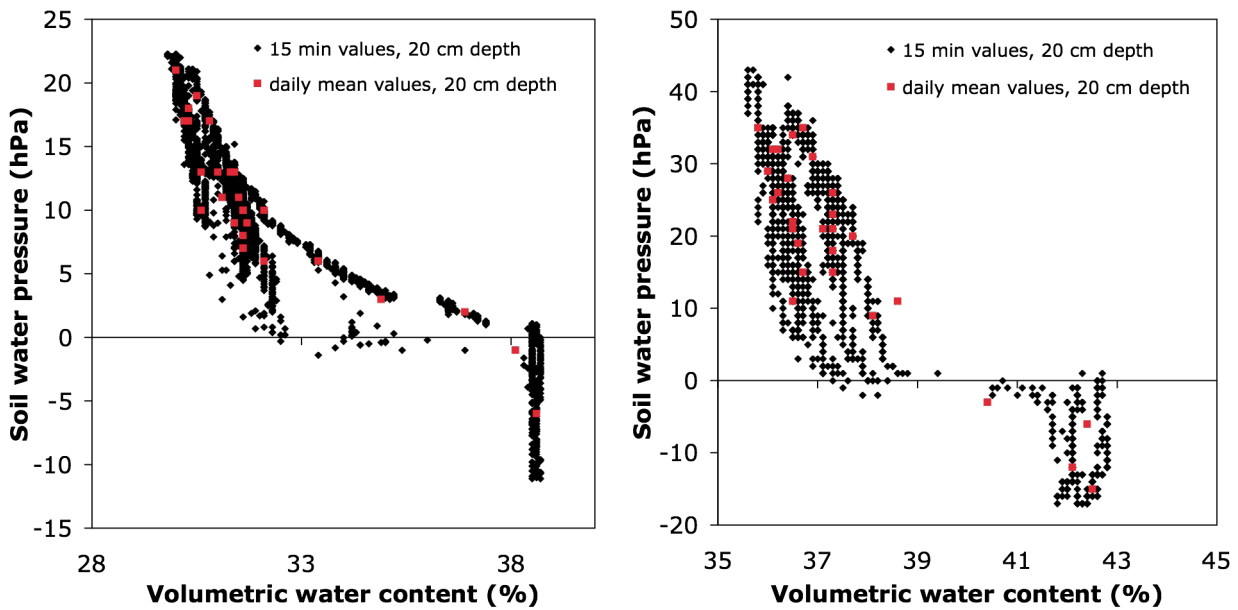
Fig. 76: *SWRC displayed with 15 minute values recorded simultaneously (spatial median of three measurements) in comparison to daily mean values for February 2014 at the Etziken (left) and Subingen (right) site. All daily mean values except for one at the Subingen site lie within the cloud of the 15 minute values, giving a good agreement. Values on the wetting curve (lower convex shape on the left) seem to be underrepresented by the daily mean. Data: BMN.*

For Etziken and Subingen in Feburary 2014, a good agreement between daily mean values and 15 minute raw data can be found. All daily mean values but one (at the Subingen site) lie within the 15 minute values displayed, thus representing their shape more or less. What stands out, though, is the underrepresentation of the values on the convex curve around 0 hPa soil water pressure by the daily means, clearly visible for example at Etziken (see Fig. 76; left). These values could be attributed to a wetting phase after a precipitation event. Since these wetting phenomena take place rather quickly (meaning on an hourly timescale) and the drying in contrast takes usually days, the wetting processes are not well represented by the daily averages. This effect has to be borne in mind when analysing hysteresis phenomena.
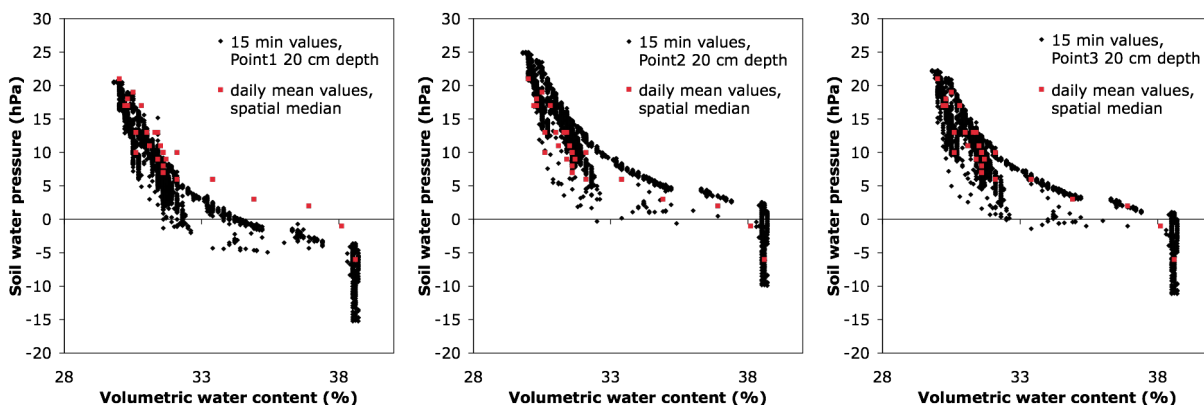
Fig. 77: *SWRC displayed with 15 minute values of every tensiometer (1, 2, 3 from left to right) in 20 cm depth in comparison to daily mean values calculated out of the median for February 2014 at the Etziken site. The shape of the SWRC of the single sensors are similar (note that there is only one water content sensor), although tensiometer 1 (left) appears measure lower soil water pressures. The median is mostly represented by tensiometer 3 (right), since its data points coincide very well with the daily mean values. Data: BMN.*

Not only is the data processed here affected by the mean calculation, but also by the generation of the median value. Fig. 76 only shows the median of three soil water pressure measurements recorded in 20 cm depth. Therefore, Fig. 77 exemplarily depicts the SWRC with 15 minute values for each of the three T8 in 20 cm depth in comparison to the daily mean values calculated with the help of the median in February 2014 at the Etziken site.

Although the tensiometer 1 (Fig. 77; left) has a tendency to measure lower values than the other two tensiometers, the shapes of the three SWRC in Fig. 77 are similar. This is not surprising with regard to the water content, because there is only one sensor installed close to the middle (tensiometer 2). Tensiometer 2 measures slightly higher soil water pressure values than tensiometer 3, making tensiometer 3 the median measurement most of the time. The daily mean values, which have been generated with the help of the spatial median, thus correspond best with the SWRC of tensiometer 3 (Fig. 77; right). Some spatial variability of the soil water pressure measurements can be observed, but the generated spatial median seems to be a suitable means to reduce the complexity of the data recorded.

The comparison of the BMN SWRC to SWRC obtained with other sensors (see Fig. 39) yielded quite similar curve shapes independent of the sensors used. Probably as important as the sensor influence were the different time rows used for the three sites, variing in seasons (just winter or both winter and summer) as well as in the years used for the analysis (usually October 2011 to February 2014, but November 1991 to October 1994 for the Agroscope data). The general shape can of course be compared, but the different conditions under which the data has been collected may play a role.

The results obtained when displaying the SWRC resolved for the seasons were quite astonishing, since a general pattern of higher water contents at a respective soil water pressure in spring and summer than in autumn could be made out. Because the pattern could repeatedly be observed at various sites, a dependence of the position of a data point on the SWRC on time could be supposed. The soils dried every summer in the datarows obtained up to now, so the drier autumn measurements at the same soil water pressure could be attributed to the different antecedent conditions. In spring and summer before the first rise of soil water pressure values into the dry range (>250 hPa), the soil was still wet from the winter. This may explain the larger water contents measured at a given soil water pressure during these seasons. The dependence of the SWRC on antecedent conditions leads us to the hysteresis phenomenon discussed in Section 2.1.4. Although other influences on this observation, for example measurement artifacts of different soil water pressure measurements after the refill of the tensiometers in summer or temperature, cannot be completely excluded, the repetition of the pattern described at every site examined leads to the suspect that this seasonal pattern is a result of hysteresis effects. A hint into the same direction is the fact that also when looking at data of smaller time scales, the data points in Fig. 76 show lower water content measurements at the same soil water pressure during a wetting period. Of course these February data are in a much lower soil water pressure range and the drying cannot be compared to the one of summer, but since the time scale is also smaller, the scales looked at may match again.

Assuming that these differences in water content at a given soil water pressure can be attributed to hysteresis, the width of the hysteresis loop observed here is wider (up to approx. 5 Vol. %) than the one observed for other soils by Smith (1933) observed to be around 3 Vol. %.

5.2.2   Lab SWRC

The lab SWRC obtained for the Stüsslingen and Aetigkofen sites in general show a similar curve for all six samples, but large variation between the water contents measured at the Stüsslingen site could be made out. Since, once again, all these samples had been collected inside the station

perimeter, these differences are assumed to represent the local variability (a high water content variability has been observed before: see Section 4.5).

Although the lab SWRC delivered results that seemed realistic at first glance, the results were somehow arbitrary with respect to the absolute values they delivered. This could already be seen when the samples were saturated and then weighted: weight differences up to 4.6 g (corresponding to 4.69 Vol. %) could be made out between two experiments with the same procedure. Differences could also be made out when comparing two different drying periods up to 500 hPa as seen in Fig. 42 for the two dots at 500 hPa: more than 2 g bigger a loss could be registered for one sample of the Aetigkofen sandy loam at the second measurement, although the system was left at equilibrium for a shorter time than the first time. It is remarkable, however, that these differences between the two measurements at 500 hPa could be recorded for the Aetigkofen sandy loam only, while the effects were much smaller for the Stüsslingen loam. Nevertheless, these observations show that the robustness of the values measured is not absolutely given.

These problems are probably due to the method chosen. One weakness was that the pF laboratory station was not always able to maintain the pressure entered, especially in the low range (of absolute pressures) the pressures displayed were often too high. Although the measurements were corrected for this effect by associating the weight recorded to the maximal subpressure seen, it is not clear whether the maximal subpressure seen as displayed on the apparatus corresponds to the maximal subpressure applied to the samples. It is also not clearly distinguishable whether this maximal value had just been recorded for a short time and the samples are thus not at equilibrium with it or if the pressure was exerted on them for a longer time. Solone et al. (2012) therefore recommend the use of hanging water columns instead of pressure plates in the wet range up to a soil water pressure of 100 hPa for the SWRC extraction. Most of the errors obtained with pressure plates measurements could be attributed to the contact between the samples and the membrane (Solone et al., 2012): backflow of water from the membrane into the samples (Richards and Ogata, 1961), no hydrostatic equilibrium between samples and apparatus (Campbell, 1988) and loss of hydraulic contact between sample and membrane (Campbell, 1988). The latter could be the reason for the different values obtained when draining the soil to 500 hPa for the Aetigkofen sandy loam. Maybe during the first period, hydraulic contact was lost, so even if the samples were left to equilibrate longer, they lost less water due to the missing contact.

Another important aspect of extracting a SWRC in general is the time needed to bring the samples into hydraulic equilibrium with the pressure at the membrane. The time required to reach equilibrium state is proportional to the square of the sample height (Klute, 1986b). Klute (1986b) thus recommends a height of 2-3 cm as a compromise, because smaller samples of about 1 cm height are not easy to handle. The samples used here with a height of 5 cm were thus quite high, leading to a long equilibration time. Solone et al. (2012) let their only 1 cm high samples equilibrate until no outflow could be measured during two days. This timescale would have been unrealistic for the purpose of this experiment. Nevertheless, it is clear that the large samples used here were probably not in equilibrium when the pressure was changed, because they were just left at one pressure level overnight, which appears to be too little when compared to other experiments. Solone et al. (2012) also performed three repetitions of their measurements, which was not done here either due to lack of time. The repetitions can account for arbitrary measurement errors that could also be observed here and would therefore definitely be helpful for a future experiment. At least three soil samples of every soil type were used, so that the spatial variability could be accounted for. While Solone et al. (2012) could find large measurement errors of the SWRC for fine-textured soils when measured with pressure plates, the analysis performed here should still be robust in the data range that is mostly looked at because the large differences were only recorded at pressures higher than 100 hPa.

A remarkable fraction of the total water loss during drainage occured between the measurement right after saturation and the one when no changes in weight at 0 hPa at the bottom of the sample

could be registered anymore. This fraction of pores must drain very quickly and can thus be attributed to the macropore fraction, of which the interaggregate pores drains at around 1 hPa (Carminati et al., 2008). According to the data obtained in the lab, these pores make out a larger fraction for the Stüsslingen loam (median 1.17; mean 1.57 Vol. %) than for the Aetigkofen sandy loam (median 0.87; mean 1.04 Vol. %) and may play an important role during the drainage process close to saturation (see also 5.4).

After this strong influence of the macropores at 0 hPa, there was not much change in water content to be measured up to a soil water pressure of 100 hPa. This was partly as to be expected from the field SWRC, especially for the Stüsslingen soil. The Aetigkofen sandy loam, however, may include some dubious measurements, because its water loss with rising soil water pressure should be bigger according to the field SWRC displayed in Fig. 38 (see also Fig. 45). Nevertheless, all three samples show a similar curve, making the measurements look reliable.

The comparison between the two lab SWRC (disturbed and undisturbed) discloses quite a big difference for both soils. The extraordinarily high water content at saturation of the disturbed SWRC could be attributed to the general observation that lab saturation tends to overvalue the more natural conditions (DIYS, 2009), because surely the undisturbed soil samples will be closer to the structure in the field and thus may represent it better. The other soil water pressure levels show a higher water content for the disturbed sample, too, but the difference gets smaller because for both soils, the disturbed SWRC has a smaller slope than the undisturbed one, meaning that more water flows out as soil water pressure rises. Especially for the Aetigkofen samples, the rise of the disturbed SWRC looks more realistic with what was to be expected from the field SWRC. The steeper slope of the undisturbed SWRC may be a consequence of lacking contact to the membrane or of too short equilibrium times at one soil water pressure level. A comparison between the two lab SWRC is, nevertheless, not that easy, because firstly, the disturbed SWRC is unlike the others just represented by one median measurement and secondly, there are a lot less soil water pressure levels available for the disturbed SWRC. The latter leads possibly to misleading interpretation, for example that the slope from 0 to 60 hPa is shallower, but in fact this might just be an effect of macropores in the 0 to 5 hPa range similar to what could be observed from the undisturbed SWRC. A better comparison can thus not be obtained with the limited resolution of the disturbed samples.

The method used for the wetting branch of the SWRC (hanging water column) was one of the first methods used for the extraction of a SWRC (Haines, 1930). The sample was in this experiment saturated, drained to 80 hPa and rewetted at the same place, namely on a ceramic plate densely sealed with an O-ring (see also Methods Section 3.2.3). This method is recommended for the extraction of macropore volumes by Matile and Buchter (2001), because the sample does not need to be moved. Although the samples are protected against evaporation, Matile and Buchter (2001) could observe a water loss of about 0.1 ml per day. It can be assumed that during the experiments done in this thesis, the samples also lost a small amount of water that way.

However, evaporation was not the biggest problem that was faced when trying to obtain a wetting curve. It was a real challenge to obtain a sample without air entering through the connection between it and the water reservoir for a week. Therefore, the result of only two soil samples is presented and the samples were not left to equilibrate for longer than a night, sometimes even shorter. It could thus be that the measurements were made when the soil still was not at equilibrium. Furthermore, the water taken up by the soil was not measured by weighting but by the outflow of a syringe, which operated as water reservoir. It could thus just be read with an accuracy of about 0.5 ml. Nevertheless, the results for the two samples are somewhat as expected from theory. Their discussion with respect to field measurements can be found in the next Section (5.2.3).

5.2.3   Comparison Lab/Field SWRC

The comparison between the undisturbed SWRC and the field SWRC, as seen in Fig. 44 inclusive hysteresis loop as measured in the lab shows that the undisturbed SWRC lie slightly closer to field observations than the disturbed ones (see Fig. 44 and 45).

For the Stüsslingen loam, the shape of the undisturbed SWRC is quite similar to field data with respect to the slope of the curve. The absolute water content, however, is not well represented by the Stu3 sample, because it already appeared to be the one with the highest water content at saturation in Fig. 42. The Stu1 sample, in contrast, fits the drainage curve observed in the field very well. The hysteresis loop of the Stüsslingen sample has almost the same width as the one observed in the field. It is, nevertheless, not clear if all the range of water content measurements at a certain soil water pressure in the field can be explained with hysteresis. In addition, the lab wetting curve has only been started at 40 hPa after a drainage to 80 hPa and thus cannot be expected to represent the whole amplitude up to 120 hPa.

For the Aetigkofen sandy loam, neither the shape nor the amplitude of the data points with respect to their water content can be reproduced with the lab measurements. The change in water content with rising soil water pressure is, as mentioned before, too small. Therefore, the wetting curve, which was started at the absolute value of 80 hPa of the drying curve, cannot be as far left as to explain the whole scatter of the field data. The discrepancies between field and lab SWRC are thus attributed to possible measurement problems of the undisturbed SWRC, as mentioned before.

As expected from the discussion of Klute (1986b), the saturated water content of every soil measured with repacked samples is by far overestimated with respect to the field values when looking at the lab data in Fig. 45. The water content measured in the lab at the respective soil water pressures of 60, 100, 300 and 1000 hPa is almost always too high, as well. If the measured values in the field are assumed to be correct, a lab analysis with disturbed samples is not able to reproduce a reliable SWRC as measured in the field.

5.3   *Temperature and Relative Humidity Dependence of Soil Water Pressure*

In Fig. 46 and 47, the statement is clearly that higher soil water pressure measurements in the dry range (>250 hPa) could only be measured at higher air and soil temperatures than usually occuring in winter. This could lead to the conclusion that the maximum soil water pressure reachable is considerably influenced by temperature, or even that at low temperatures no high soil water pressure measurements can be reached. The question is now whether temperature itsself is the limiting factor or if the soil water pressure measurements are low because of other influences that were accompanied by low temperatures. Other influences can be (as mentioned under 4.3 before) water content, relative humidity, radiation and precipitation. At first, the influence of only temperature on soil water pressure measurements will be discussed, before the topic is extended to measurements obtained under the influence of other factors as well.

5.3.1   Temperature as Isolated Factor

When looking at the equation of capillary rise (Flühler and Roth, 2004), it becomes clear that the surface tension of water as well as its density are temperature dependent and thus lead to an expected change in soil water pressure with changing temperature. The effect of temperature on soil water pressure has been looked at in two cases: case 1 including surface tension and density of water and case 2 including only surface tension as a temperature dependent parameter (calculation see Section 3.3.4). The results from 0 to 25°C are shown in Table 7.

Table 7: *Influence of i) surface tension and density of water and ii) surface tension on soil water pressure measurements with changing temperature. The values indicate the factors the soil water pressure measurement must be multiplied with starting at 0°C.*

Temperature dependent parameters included	Factor at 0°C	Factor at 5°C	Factor at 10°C	Factor at 15°C	Factor at 20°C	Factor at 25°C
surface tension and density of water	1	1.0092	1.0190	1.0307	1.0423	1.0543
surface tension of water	1	0.9908	0.9815	0.9709	0.9610	0.9511

For case 1 where density as well as surface tension is considered, the absolute soil water pressure is expected to rise for a constant water content with rising temperature, though the effect is small (+ 5% from 0 to 25°C). The opposite should be the case when looking only at the surface tension: the absolute soil water pressure for a constant water content is expected to fall with rising temperature. This effect has already been reported by Richards and Gardner (1936) as well as by Philip and de Vries (1957). Here, too, the effect is very small (not even -5% from 0 to 25°C).

Several studies, such as Philip and de Vries (1957), Nimmo and Miller (1986) and Klute (1986b) reported that a temperature rise is followed by a reduction of the water content at a given pressure head, what could also be observed to be a tendency at the Subingen site (see Fig. 49). This observation in combination with the above calculations leads to the expectation that a soil appears drier according to the measurements with rising temperature for case 1 (including surface tension and density) for both components of the SWRC, whereas for case 2, the dominant component cannot be made out since the soil water pressure change goes into the direction of a wetter soil, while the water content goes into the opposite direction.

When isolating other factors and just looking at temperature, a rise of soil water pressure measurements with increasing temperature could be observed both in the lab (T8, soil temperature) and in the field (self-installed tensiometer, air temperature) as seen in Fig. 55 and 56.

The soil water pressure rise of the T8 as tested in the lab is larger than expected when looking at surface tension of water only, because it has been observed to rise with +0.21 hPa/°C while soil water pressure would be expected to decrease at higher temperatures. This rise is not consistent with results that have been reported by Nimmo and Miller (1986) and Hopmans and Dane (1986), who found that soil water pressure decreased with increasing temperature at given water content. Nevertheless, the observed decline of soil water pressure observed by the same studies is larger than could be explained with just the surface tension. Experiments by Gardner (1955), Haridasan and Jensen (1972), Wilkinson and Klute (1962), Novak (1975) and Nimmo (1983) yielded a decrease in soil water pressure of 2 to 10 times the one expected by calculation. The rise observed here with the T8 tensiometer in the lab thus seems at least consistent with the finding that the difference cannot be explained with the surface tension only. Even when considering the density and the surface tension of water, the expected rise would be about 0.06 hPa/°C (calculated with the help of Table 7), making the observed rise almost 4 times larger.

The T8 measurements over time in Fig. 55 have shown to rise as soon as the temperature starts to drop, but then drop even further than the value recorded before. This effect of the first rise can be attributed to a temperature correction, which the T8 does automatically for the electronic components, so the calibration of the pressure sensor (information by the manufacturer, UMS; see also Durner and Or, 2005). While this correction on short-term timescale seems to overcorrect the values measured, it does not prove very useful on a longer timescale either, because apparently soil water pressure measurements of the T8 do depend on the temperature, and even more and in the opposite direction than classically could be expected from the physical effects. During the experiment performed in the climate chamber, the water content measured with the HydroSense declined from 16 to 14 Vol. % and rose again to 16 % when the soil was rewarmed to ambient

temperature. A temperature dependence of the water content measurement with the HydroSense can thus be suspected, which is not surprising (see Section 5.4).

When looking at the reaction of the self-installed tensiometer with air temperature, an increase of 1.19 hPa/°C can be made out (see Fig. 56). The rise is, as for the T8, larger than expected when considering density and surface tension, but this time by a factor of 20. The self-installed tensiometer thus seem to be even more sensitive to air temperature changes than the T8, which is not surprising because they have a large water column above-ground which expands when exposed to temperature changes (Durner and Or, 2005). The T8 in contrast has a very small water column, making it, as all advanced tensiometers, quite robust against water density changes with temperature (Sisson et al., 2002).

Also, the thermal expansion of air may lead to this measurement effect observed (Nimmo and Miller, 1986). Due to the limited time period included in the analysis, the air temperature measurements range only from 0 to 7°C, which made a statement for other temperature ranges impossible. Also, the changes cannot exclusively be attributed to changes in air temperature, they may also be a consequence of radiation changes on the shaft of the tensiometer (although it was protected with a shield as the other tensiometers).

Although some reaction of the tensiometers with temperature could be observed, the change is not big enough for the temperature to be responsible for high soil water pressure in summer only, or said differently temperature change cannot be the only reason for observing low soil water pressure measurements in winter. Even the change of the T8 of 0.21 hPa/°C observed from 0 to 12°C could only account for a rise of 5.25 hPa at a quite extreme temperature change from 0 to 25°C. However, the measurements obtained with the self-installed tensiometers could produce a bigger measurement error of up to 29.75 hPa if temperature changes from 0 to 25°C. But since the question is related to the values measured at the BMN, the T8 is the relevant sensor to consider.

For the temperature dependent SWRC obtained in a climate chamber at about 2-3°C, a decrease in water content of typically about 1 to 1.5 Vol. % at the same soil water pressure with respect to the SWRC obtained at ambient temperature (approximately 21°C) could be made out. This observation is at odds with the findings by Hopmans and Dane (1986), who found that the water content should be larger at lower temperature, as mentioned before. The effect observed by them was approximately 0.5 Vol. % at a 10°C temperature change. As already mentioned, the samples weighted less at full saturation before starting the drainage at 2°C than before starting drainage at 21°C. This difference has been accounted for by choosing the effective saturation as x-axis instead of the water content, where the saturated water content was chosen to be the respective one at full saturation. Nevertheless, it could be observed that the samples lost slightly more water at lower temperatures, which was not as expected from other studies (Hopmans and Dane, 1986; Nimmo and Miller, 1986). Although the temperatures chosen by Hopmans and Dane (1986) were all above 20°C and ranged up to 44.5°C, a dependency on the outcome of the temperature range is excluded since Nimmo and Miller (1986) observed the same trend down to a temperature of 4°C.

It is therefore not clear how these differences came about, and whether they can be attributed to temperature change or not. They could also be caused by the randomness of the SWRC measurements, because for each temperature only one measurement has been made. A repetition would be helpful to estimate the reliability of these results.

5.3.2   Temperature and Other Factors Influencing Soil Water Pressure

When looking at Fig. 48 showing the SWRC displayed with variing soil temperatures, no clear influences of temperature on the relationship between water content and soil water pressure could be identified except for the fact that most soil water pressure measurements above 60 hPa occur at soil temperatures above 8°C, which could already be seen in Fig. 46 and 47. The difference between the two sites with regard to minimum temperature recorded for soil water pressure above 60 hPa

could be due to the fact that the Etziken site is situated in a forest and therefore has a different temperature regime than the grassland site in Subingen. The fact that no clear trend with temperature can be seen in the wet range supports the claim that the relationship between soil water pressure and soil water content depends on time and thus on prevalent conditions rather than on temperature (see also 5.2.1) than on temperature. The hint that temperature may not play a crucial role influencing the field SWRC could be confirmed by Fig. 49, 50, 51 and 52, of which none shows a clear relationship between water content and temperature or soil water pressure and temperature respectively. Summarising, it appears that the relationship between soil water pressure and water content is not significantly influenced by temperature in either direction when looking at soil water pressure measurements that were recorded under „natural conditions" and thus subject to many factors influencing it, not just temperature.

The influence of air temperature on soil water pressure measurements could be observed in Fig. 54 and 56. As mentioned under Results 4.3, huge fluctuations of soil water pressure could be observed before the protection shield was improved. These fluctuations may be due to the combined effect of temperature on the calibration of the pressure transducer, on the expansion of the tensiometer shaft and the ceramic cup as well as the expansion of water (Durner and Or, 2005). Also, rapid air temperature fluctuations may lead to large air pressure changes at the pressure transducer, leading to wrong soil water pressure measurements because they are always related to the air pressure (Butters and Cardon, 1998). Although the tensiometers were filled with deareated water, a 1 cm air bubble had to be left on top because the water must not touch the pressure transducer, as also recommended by Durner and Or (2005). This air bubble may be responsible for soil water fluctuations as well since air is much more sensitive to temperature expansion than water is (UMS, 2008). All these effects together were probably responsible for the huge fluctuations up to ± 80 hPa especially observed at the tensiometers installed in 35 cm depth. At these tensiometers, a typical pattern of declining soil water pressure when the sun came out (around 9 to 10 a.m.), then a sharp rise around noon into quite high soil water pressure measurements declining during the afternoon until reaching plausible values again in the evening around 6 p.m. could be observed. Exactly the same shape of soil water pressure measurements has been reported by Buchter et al. (1999), who worked with a similar self-constructed tensiometer as was used in this thesis. They could attribute the fluctuations to the material with CAB being more robust to changes in temperature than PVC. Although Buchter et al. (1999) claimed changes in air temperature and radiation to be causing the observed fluctuations, which also seems to be causing them here due to the daily fluctuation pattern coinciding with air temperature, the exact mechanism remains unknown. An influence of the material rather than the pressure transducer, however, seems plausible because in Fig. 53, the changes of the shorter tensiometers of 47 cm length installed in 20 cm depth suffered less from fluctuations than the 70 cm long tensiometer shafts installed in 35 cm depth that had a larger part above-ground. After the improvement of the radiation shield, the values recorded seemed acceptable. Buchter et al. (1999) also conclude that a protection against radiation and temperature changes is crucial when working with PVC shafts. Since the T8 also has a filling pipe above-ground where air bubbles can form, they have been protected against radiation at the BMN since the beginning, too (UMS, 2008). For the T8, this protection seems reliable, because in Fig. 53, almost no changes of the raw soil water pressure measurements by the T8 could be made out.

When looking at Fig. 46 and 47, the clear cut between only low recorded soil water pressure measurements and suddenly higher ones at a certain air respectively soil temperature catches one's eye. It leaves speculation to the thought that a factor is activated at a certain temperature and may cause the soil water pressure to rise. Since plants are known to start growing at certain temperatures (Defila, 1991; Primault, 1972) and both sites of which the temperature dependency has been displayed, Stüsslingen and Subingen, are located on grassland, it may be that plant or root growth plays a key role in the rise of soil water pressure. Plants extract water from the soil, thus letting the
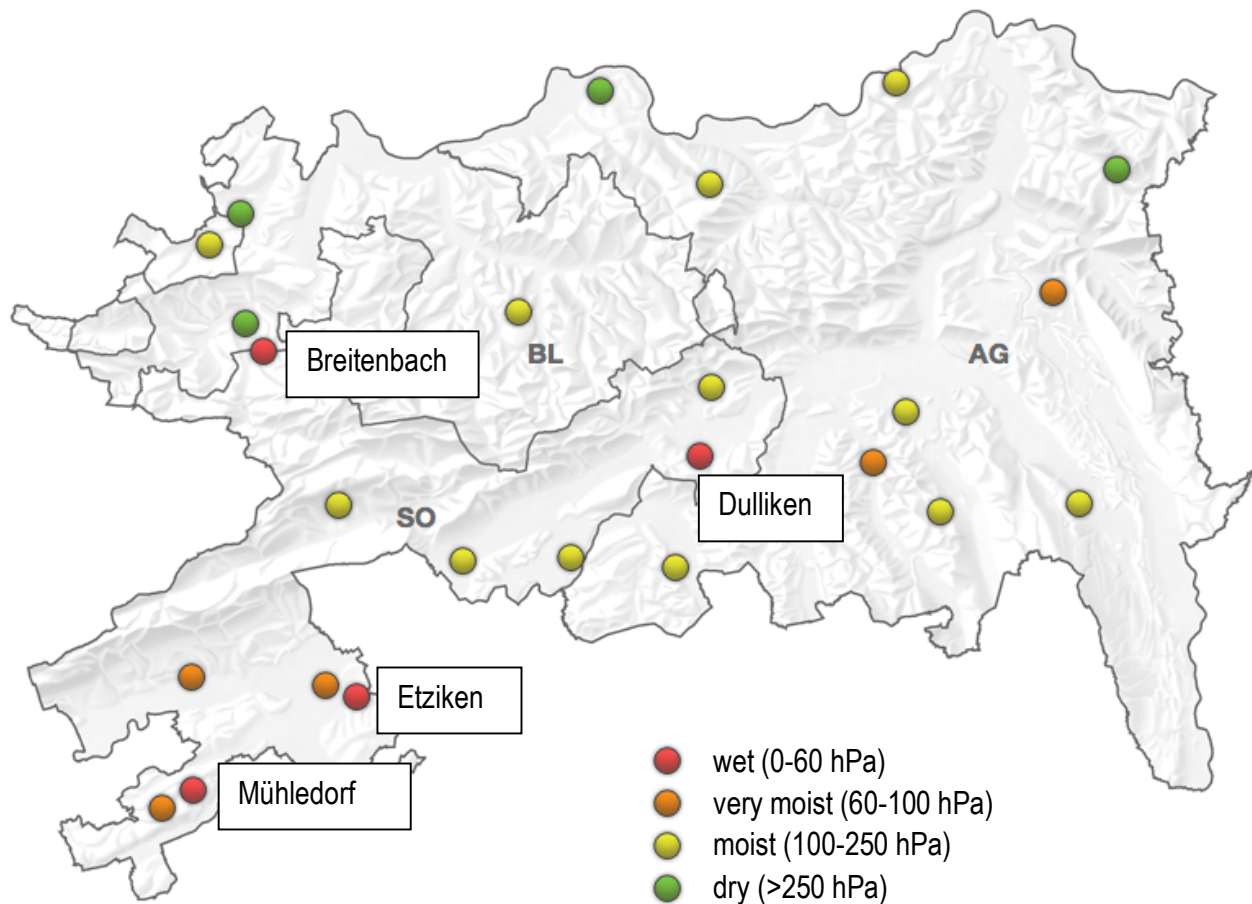
Fig. 78: *Soil water pressure measurements of the BMN sites on April 21st, 2014, 10.30 a.m., grouped into the four categories (see Table 1). A few sites already reached the dry range while most of the measurements are in the moist category. All four sites with a red dot (soil water pressure measurement below 60 hPa) are located in a forest (labelled). Data: BMN.*

soil water content sink and soil water pressure rise. During an experiment performed in Austria, Lammeranner and Obriejetan (2011) found that *Salix purpurea* (purple willow) had a big influence on soil water balance already shortly after its plantation, while grass-herb vegetation only had an effect in the upper soil layers and at the end of the growing season. An additional hint that plants may have an influence on soil water pressure is that in April 2014 during a longer period with only little precipitation, the soil water pressure measurements of the grassland sites seemed to rise faster than the ones of the forest sites of the BMN (see Fig. 78). However, the exact mechanisms of the influence of plants on soil water pressure cannot be discussed with the results presented here, because no information on root growth and plant activity has been collected.

If there is no suction from the atmosphere or, as discussed before, by plants, a saturated soil can only drain by gravitational water and thus only to approximately 60 hPa according to theory (Scheffer and Schachtschabel, 2002). Relative humidity influencing the amount of water the atmosphere or the plant can suck out of a soil is therefore one of the key drivers of soil water pressure measurements over the seasons. Although a relationship between soil water pressure measurements and relative humidity can be seen in Fig. 58, the ongoing discussion shows that soil water pressure measurements cannot be explained by only taking temperature or relative humidity into account (at least not on a daily basis), even though these two factors are expected to correlate, too.

Soil water pressure measurements are significantly influenced by the antecedent conditions, obviously more than just by temperature or relative humidity on a daily scale. To exclude these at least partly and only look at the change in soil water pressure, Fig. 59 and 60 have been plotted in Section 4.4. As already mentioned, small rises of soil water pressure can even be observed on days with a high relative humidity. These may be caused by gravitational drainage, which occurs independent of atmospheric conditions because it is rather influenced by the hydraulic conductivity. When looking only at positive soil water pressure changes, a relationship between relative humidity and soil water pressure change would be expected: The drier the atmosphere, the larger the change in soil water pressure per day. However, this relationship appears to be surprisingly weak at the Aetigkofen and the Stüsslingen site. Fig. 79 (left) shows the same plot for soil temperature at the Stüsslingen site: the warmer the soil, the higher the soil water pressure change per day if only looking at positive changes. A similar curve could be observed for air temperature (not shown here). Since both relative humidity and temperature seem to have an influence not necessarily on the absolute value, but on the soil water pressure change per day, the relationship between the latter and evapotranspiration (being influenced by both temperature and relative humidity as well as water availability) is displayed in Fig. 79 (right).
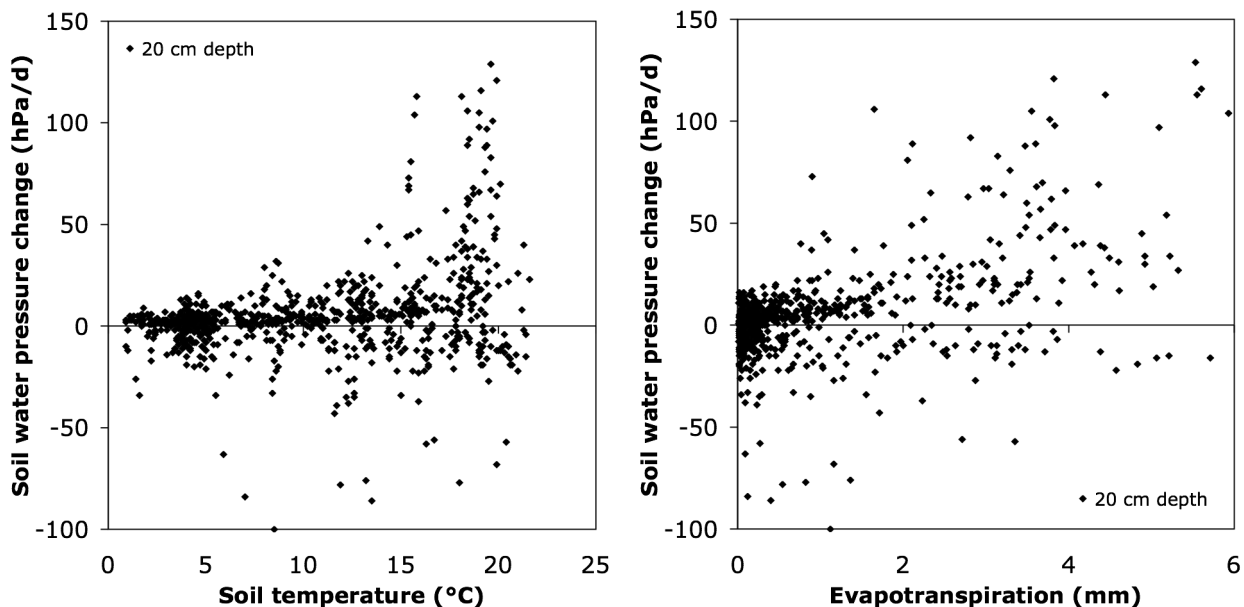
Fig. 79: *Daily soil water pressure change (value of the present day minus value of the previous day) plotted against soil temperature (left) and evapotranspiration calculated with the Primault formula (right) at the Stüsslingen site. Both graphs show a trend of higher soil water pressure changes with higher temperature and higher evapotranspiration when looking only at the positive values. Extreme values are not shown in the graph. Data: BMN and IDAWEB, MeteoSchweiz (ET).*

The evapotranspiration data used in this thesis is from nearby MeteoSchweiz stations (for Fig. 79: Goesgen, 2 km from Stüsslingen) and has been calculated with the empirical Primault (1962; 1981) formula. The values can thus only be taken as approximation, because they have not been measured right at the station (see also 5.5). Even though the relationship between daily soil water pressure change and evapotranspiration (ET) is smaller than expected when looking at the ones relating it to temperature and relative humidity, it can be clearly seen in Fig. 79 that at lower ET values a lower change in soil water pressure is to be expected. The soil water fluxes also seem to correlate best with ET (see 5.5). Since ET values are very low in winter (see Fig. 80; the values lie clearly below 1 mm from October to March for the agricultural land in the Swiss Plateau), this factor involving a combination of temperature, relative humidity and radiation may be considered to limit soil water pressure rise in winter.

The correlation with ET values can be supported when going back to the frequency distribution plots (Fig. 36). The observed pattern of very dry soils being still possible in October, but not in other months unless the soil freezes corresponds quite well to the typical evapotranspiration measured on agricultural land in the Swiss plateau by Menzel et al. (1999, see Fig. 80). In October and March, evapotranspiration is highest of the winter semester according to the orange curve of the Swiss Plateau in Fig. 80. Although the very high values of October were measured at a single site in Breitenbach, October values generally are higher than those of the rest of the months. One reason why March values are not that high could be the influence of the quite wet spring in 2013 (MeteoSchweiz, 2014) on the cumulative frequency. Since the evapotranspiration of agricultural lands in winter months is almost zero (Spreafico and Weingartner, 2005; see also Fig. 80), it somehow makes sense that the observed soil water pressure does hardly exceed field capacity from November to February because only gravitational water may drain.
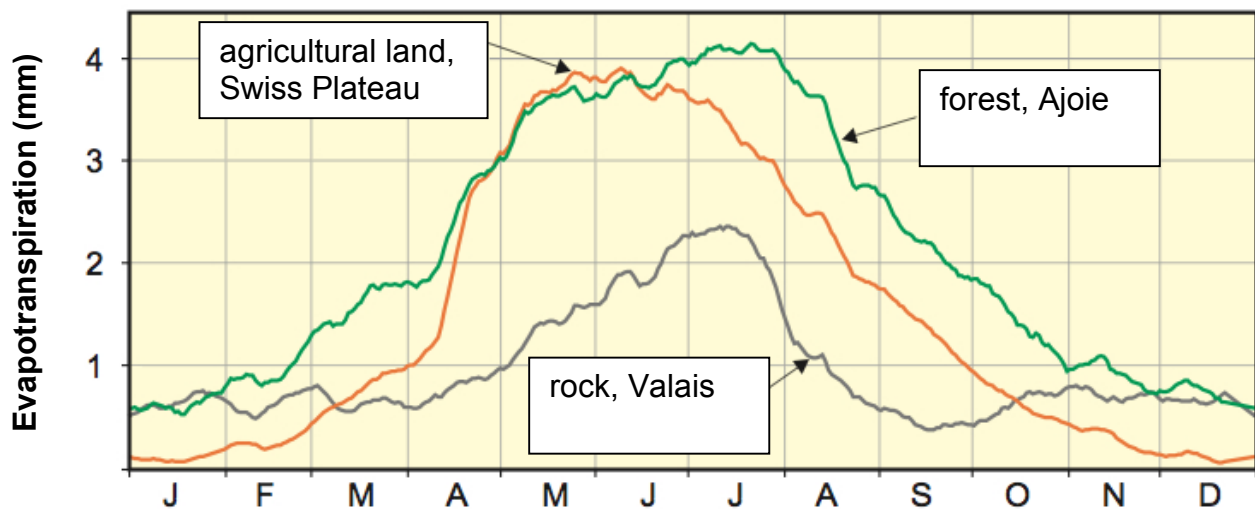
Fig. 80: *Examples of daily mean evapotranspiration values for different surfaces and regions in Switzerland (modified after Spreafico and Weingartner, 2005; data: Menzel et al., 1999).*

5.4   Sensor Comparison

5.4.1   Tensiometer Measurements

As seen in Fig. 62, the soil water pressure measurements do not differ much from each other when looking at three of the self-installed tensiometers, assuming spatial homogeneity of the matric potential. With time, the variance increased, which could be due to unequal distribution of evaporation effects, for example through solar radiation during the experiment. Nevertheless, because the variation has proven to be small in the lab, discrepancies between tensiometer measurements in the field are believed to represent the spatial variability of soil water pressure. To account for this spatial effects, which can be quite large, the recommendation to obtain reliable soil water pressure measurements is to install at least three, better five tensiometers in every depth at a site and then take the median of their readings as representative value (Matile et al., 2011). The number of tensiometers installed at the BMN as well as my self-installed tensiometers thus corresponds to the minimum number suggested (Webster, 1965). Of course, more sensors would have given a more complete picture, but the effort as well as the cost is higher.

It has already been mentioned under Section 3.1.2.2 that some measurement problems among all tensiometers could be observed after the lysimeter had been installed. Most of the problems could be attributed to pressure transducer number 8 (installed at the tensiometer in 35 cm depth in the lysimeter), which frequently measured a positive pressure or a number out of range. This measurement error then caused the measurements of the other pressure transducers to jump. This means that the reactions of the self-installed tensiometers in Fig. 61 are reliable, but not necessarily

their absolute values. Rosenkranz et al. (2013) found in their field study where they compared the measurements of various soil water pressure sensors (among these the T8 tensiometer) also that large differences of the absolute values between the sensors can be made out, although their reaction to precipitation is very similar.

Although the absolute values measured by the self-installed tensiometers cannot be taken for granted, there is no reason to doubt the reliability of the T8 measurements considering the range of soil water pressure in winter. The T8 and the self-installed tensiometers show about the same absolute drop in values with respect to precipiation and rise at about the same speed again (see Fig. 61), which means that they must lie in the same range, even if the absolute values are unknown.
The T8 was in the study already mentioned by Rosenkranz et al. (2013) shown to be the sensor with the smallest deviation from the median of all soil water pressure measurements, which again supports the observation of the T8 delivering reliable values. Also, it was used as a reference sensor in the study of Gimper (2010).

5.4.2   Water Content Sensors

When looking at Fig. 61, a large deviation in absolute measurement values between the water content sensors can be made out, although their reaction to precipitation are similar. The same effect with deviations of about the same magnitude as observed here (up to 10 Vol. % between the different sensors) was found in other comparing studies (Rosenkranz et al., 2013; Gimper, 2010) and an even bigger one of differences up to 40 Vol. % in 15 cm depth by Mittelbach et al. (2012). As mentioned under 4.5, the difference in water contents measured with the sensors could be explained with the local variation of the water content of dried soil samples. The variation displayed by the sensors thus seems to correspond with the high spatial variability. This claim is supported by the comparison of the measured values at points 2 and 3 in Fig. 63 showing different reactions to precipitation. Since at both locations the water content has been measured with at least two different sensors and they respectively show the same curve, the diverging rise of the water content is very likely to be due to local variability, here between the middle and western hole.
Both precipitation events displayed in Fig. 63 were of almost the same size (summed up 18.5 mm for 13.2. and 18.4 mm for 15./16.2.), which is also displayed by the similar reaction of the water content sensors. Since a water amount of 18.5 l/m^2 fell onto the study site in Stüsslingen, the water content is expected to rise about 0.0185 when looking at the volume of 1 m^3. This corresponds roughly to the rise measured by the water content sensors, being around + 0.02 or even a bit more for point 3_35, around + 0.01 for the Hydra Probe and around + 0.01 to 0.015 for point 2_20. A delay of the reaction in 35 cm could not be made out on an hourly timescale as in Fig. 63 nor when looking at the raw data with a 15-minutes resolution.

Although the two water content sensor types (10HS and TDR) were installed right next to each other in every hole, they show a difference in water content measurements up to 3 Vol. % (see Fig. 63). This difference may well be attributed to spatial variability if a larger pore has been hit during the installation. Likely is also a deviation due to limited accuracy of the sensors: The Hydra Probe and 10HS sensors have an accuracy of ± 0.03 m^3/m^3 (see boxes in Section 2.2.1.3), which corresponds to 3 Vol. % and thus would be able to explain the observed differences. The TDR using the Topp equation have been reported to measure with a standard estimate error of 0.013 equal to 1.3 Vol. % (Topp et al., 1980), thus slightly less than expected for the other sensors. However, Evett and Parkin (2005) assign it an accuracy of 2 Vol. %, Hook and Livingston (1995) one of 2.3 to 3.4 Vol. %. TDR measurements with the Topp (Topp et al., 1980) have also been reported to be less accurate if there are many clay minerals and a high cation exchange capacity or long cable lengths because then the measurement frequency sinks to values lower than the insensitive 1 GHz (Kelleners et al., 2005; Evett et al., 2005). Since the Stüsslingen loam has quite a high clay content of about 22.1 % (see Table 2), this might play a role here. While FDR sensors have been reported to

be sensitive to temperature (Seyfried and Grant, 2007), TDR measurements are also sensitive to temperature due to the reduction in dielectric permittivity as well as the release of bound water with increasing temperature counteracting the first effect (Or and Wraith, 1999). However, the effects observed by the studies mentioned are expected to be small in the range of the temperatures measured during this experiment and are therefore not further considered.

Apart from the lower accuracy, no disadvantage of lower cost sensors such as the Stevens Hydra Probe or the 10HS sensors with respect to exactness of the measurements could be made out in this study. The same conclusion has also been drawn by Rosenkranz et al. (2013), who found that TDR probes did not perform better than the 10HS when comparing measured water content and water content of dried soil samples. These results are both at odds with the findings by Walker et al. (2004) and Mittelbach et al. (2012) who found that the TDR performed best when compared to other water content sensors. However, Walker et al. (2004) did not include any of the sensors used here in their study. Mittelbach et al. (2012) compared amongst others the 10HS to a TDR TRIME-IT/EZ probe. They concluded that the 10HS sensor did not manage to capture extremely wet as well as extremely dry conditions in the uppermost soil layers (to 15 cm depth) and that its underestimation of the water content with respect to the TDR measurements increased with increasing water content. However, the water contents measured during the study of Mittelbach et al. (2012) ranged up to more than 70 Vol. %, which is an almost unrealistically high value. None of these observations regarding the 10HS sensors could be confirmed in this study, but dry conditions were never reached. Also, most of the critics at the 10HS sensor were only related to an installation down to 15 cm depth, and the 10HS in this study have been installed deeper. Gimper (2010) recommends a site-specific calibration of the 10HS because he found its performance regarding reaction time as well as its absolute measurement displacement of about 10 to 14 Vol. % compared to a PICO64-TDR insufficient. Such large differences could not be observed in this thesis.

What is interesting to see when looking at Fig. 63 is that the water content rises shorty after the onset of a precipitation event, then declines in a concave shape and finally reaches the water content level observed before the event after about two days again. From then on, the water content hardly changes. For soil water tension, a similar pattern could be made out, but since its reaction seems to be more sensitive in general, it still could be observed to rise slightly even two days after a precipitation event (see Fig. 61). The obviously rather quick penetration of water into the soil could be favoured by a high saturated conductivity. The saturated conductivity of the Stüsslingen loam measured in the laboratory (see Section 3.2.2) revealed with 78.35 cm/d a significantly higher value than predicted with the semi-empirical approach of the Rosetta database (Schaap et al., 2001). For a standard loam texture, Rosetta predicts a Ksat value of 24.96 cm/d while the specific Stüsslingen texture with its higher clay content is predicted as 14.14 cm/d. Although Ksat has only been measured for one soil sample and the obtained value is somehow subject to random measurement effects as well as a not representative sample, the trend of Ksat being larger than expected due to the texture is clearly visible. This indicates that macropores formed by soil aggregation (also called interaggregate pores, Carminati et al., 2008) play an important role for the drainage close to saturation. The relatively large interaggregate pores provide pathways for the rapid infiltration of rain water (Beven and Germann, 1982). However, since they drain already at approximately 1 hPa, their influence can only be observed close to saturation and thus during intense water inputs (Carminati et al., 2008). In fact, macropores probably were saturated during these two precipitation events looked at in Fig. 63, because soil water pressure in 20 cm depth reached a minimum of 0 hPa during both events. The next step of drainage is when the aggregate-aggregate contacts dry between 15 and 43 hPa (Carminati et al., 2008). These processes all still occur below the 60 hPa threshold and thus are relevant for winter, too. It has been hypothesized by Carminati et al. (2008) that in aggregated top-soils, the flow may be controlled by aggregate-aggregate contacts. If water flows into large macropores, a non-equilibrium flow-state may be reached where the flow rate increases

considerably, but the absolute soil water pressure decreases only slightly (Jarvis, 2007). For macropore flow, Darcy's law may thus not be suitable because its assumptions are not always met: macropore flow mainly occurs under gravity influence where turbulent flows may be initiated (Jarvis, 2007). It was shown by Flury et al. (1994) that during their experiment with Brilliant Blue FCF at various locations in Switzerland, bypass flow was the rule rather than the exception in most soils. These effects are thus to be expected for heavy precipitation events at the Stüsslingen site and the rather quick drainage process may be associated with macropore flow.

Both soil water pressure and soil water content appear to react fairly quickly to precipitation and then stabilise again by reaching the previously recorded value within about two days. From then on, changes in the measurements observed during dry periods in winter are very slow. This observation is interesting, because traditionally field capacity is defined to be the amount of water present in a soil 2-3 days after the last precipitation event (Scheffer and Schachtschabel, 2002) and thus may be associated with the stabilised values observed here. However, even if conditions are stable, the soil water pressure recorded simultaneously at the BMN sensors is about 35 hPa in 20 cm depth and thus lower than most of the definitions for field capacity (Cavazza et al., 2007; Richards and Weaver, 1944, Scheffer and Schachtschabel, 2002). However, White (1997) found field capacity to be around 50 hPa, which would be fairly close to the conditions observed here. Twarakavi et al. (2009) reported in their study that matric potentials are not suitable to describe the state of field capacity. Instead, they consider the time-based approach to be more robust, what could be an indicator for field capacity being lower than traditionally expected with respect to soil water pressure values for the data observed during this study.

5.5   Water Balance Reconstruction

Although a weak trend between the fluxes and evapotranspiration in winter 2011/12 at the Aetigkofen site could be established when looking at Fig. 64 (right), some high upward fluxes also seemed to take place at low ET. These measurements could be attributed to the cold February 2012 (MeteoSchweiz, 2013), when upward fluxes could have been due to a penetrating freezing front. Although there is a trend visible between relative humidity and daily water flux (see Fig. 81; left), evapotranspiration as seen in Fig. 64 (right) seems to have the best correlation with water fluxes, what also has been found for daily change in soil water pressure (Section 5.3.2). The similarity of the trend between relative humidity and evapotranspiration is not astonishing, because they are expected to correlate quite high between themselves. What is rather surprising is that there is no trend visible for soil water flux with respect to air temperature, (see Fig. 81; right) because a relationship between air temperature and change in soil water pressure measurements could be established (see Fig. 79). There are quite high positive fluxes possible even at very low temperatures, which can be attributed to the upward flow due to a freezing front as discussed above. All negative values of more than 2 mm/d have been observed at positive air temperatures when a precipitation event took place.

The calculated versus expected percolation displayed in Fig. 65 does not seem to match for all sites. In Stüsslingen, calculated percolation is definitely less than expected. The reason for this observation is most probably the difficult estimation of Ksat, which is a very dominant parameter in the flux calculation. The data shown in Fig. 65 points out that the Ksat used in the analysis is probably too small for the Stüsslingen loam. The measured hydraulic conductivity of the Stüsslingen loam with the constant head method (see Section 3.2.2) gave a Ksat of 78.35 cm/d, again indicating that the Ksat of 14.19 cm/d used in the analysis as predicted by the Rosetta database may be too small. The same effect could be expected for Dulliken, where a very similar Ksat (14.14 cm/d) has been used. Another reason for the very small fluxes calculated in Stüsslingen may be the large difference between θ_s used for the calculation (0.5038) and the water content

observed in the field (mostly between 0.38 and 0.4). This leads to a small K_r, because the hydraulic conductivity rapidly decreases as a soil distances from saturation.
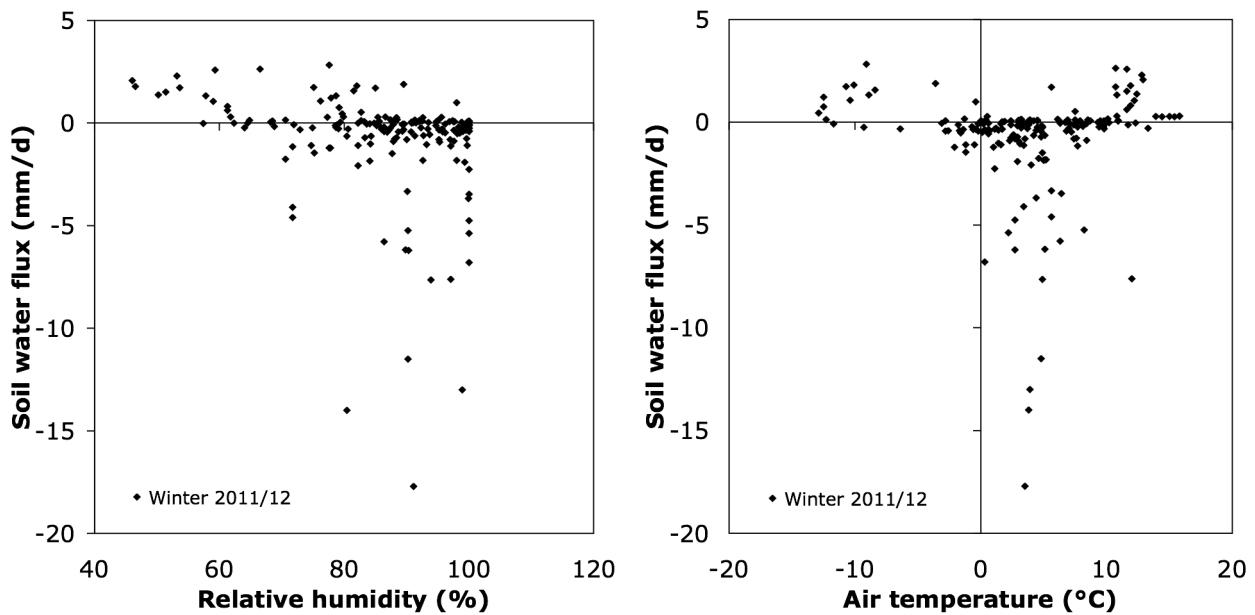
Fig. 81: *Daily calculated flux displayed dependent of relative humidity (left) and air temperature (right) for the Aetigkofen site during winter 2011/12. While for relative humidity a weak relationship can be made out, no trend can be seen for air temperature. Data: BMN.*

Of course, the two other parameters α and n are also associated with uncertainties. Since n is related to the pore-size distribution, it is usually rather large (around 4-10) for sandy texture and smaller for finer textures (e.g. 1.17 for clay; van Genuchten, 1980). The n values fitted in this study are rather small, namely between 1.1819 for the Stüsslingen loam and 1.3237 for the Aetigkofen sandy loam. Relatively, this is in agreement with the findings of van Genuchten (1980), because Aetigkofen has the coarsest texture of the three soils. Nevertheless, the values found here are lower than expected, corresponding more to the ones found for a clay soil by van Genuchten (1980). The values for loam (as Dulliken and Stüsslingen are) postulated by van Genuchten (1980) are around 2 to 2.5 and thus larger than observed here. The parameter α is the reciprocal of the air entry value and therefore large if the air entry value is small. Some of the values fitted in this study are larger than the ones found by van Genuchten (1980). The approximate range seems to be in agreement with the values published by van Genuchten (1980). It is interesting that for the Stüsslingen loam, the fitted α of 0.027 cm^{-1} lies very close to the one observed for a loam by van Genuchten (1980) being 0.02, but the one for Dulliken with the same texure is with 0.685 cm^{-1} more than three times larger. The reason for this deviation is unknown. Since the lab SWRC has shown a slightly bimodal structure due to the influence of macropores in the wet range, the van Genuchten parameters may not be able to perfectly reproduce the real shape of the SWRC as observed in the field and lab.

There surely are errors in the calculation, because evapotranspiration (ET) has a high spatial variability and the values of the Goesgen and the Koppigen station of MeteoSchweiz, although quite close to the respective sites (Goesgen is at 2 km from Stüsslingen and 2.5 km from Dulliken, Koppigen at 7 km from Aetigkofen), cannot be taken as absolutely true. Additionally, the ET is calculated with the Primault (1962; 1981) formula, an empirical approach which has shown to perform weakest of several methods when comparing the calculated to measured values (Calanca et al., 2011). Furthermore, the ET values used in the analyses are surely not representative for the Dulliken site, because it is located in a forest and a different ET is expected due to a different

energy budget and radiation. In Dulliken, the flux calculation revealed negative values and thus percolation in a depth of 20 to 35 cm almost during the whole winter. Positive values were hardly calculated. This supports the suspicion that ET values in a forest are lower during wintertime, thus making an upward transport of water in the soil rare in the season mentioned.

Also, the measured precipitation has been assumed to fully infiltrate the soil. Interception has thus been neglected respectively presumed to be zero at all sites (see also Section 2.4). For grassland, the interception is probably not that large a part, whereas for the forest in Dulliken, this assumption may be quite different from reality, because a part of the precipitation is retained by the trees. Nevertheless, the differences in winter are expected to be smaller than the ones in summer when deciduous trees carry leaves.

Although there are some differences between the expected and the calculated percolation values, the results obtained for the fluxes do make sense. The indicated net percolation of water in winter is consistent with the findings of Borer (1982), but statements can only be made for the depth between 20 and 35 cm because there are no other measurements available. The overall goal of this analysis to prove the consistency of the soil water pressure measurements could be accomplished since the measurements appear to provide results in the right order of magnitude when compared with precipitation and ET data.

5.6   Reconstruction of Situation with HYDRUS-1D

When looking at Table 6 and the different parameter sets, it is not surprising that the outcomes are very different for summer and winter and that neither the summer fit applied on winter nor the winter fit applied on summer provides reasonable predictions. It is interesting that, although the data has been fitted to the observed values, the highest R Square obtained is 0.5571, which still is not a very good prediction. Nevertheless, the applicance of the winter parameter set to other winters led to a good estimation of the soil water pressure observed. However, as already discussed for the flow reconstruction, there might be errors associated with the ET data since it was not obtained at the same place as the soil water pressure and precipitation measurements. Also, the graphs may be irritating, because the data points represented by the observed values are daily mean values and the ones displaying the simulation are values predicted at a certain time and are thus not averaged. The observed differences in soil water pressure measurements after precipitation events for the winter fit in Fig. 69 may be due to this effect, because actually predicted values will be lower than observed daily means.

When looking for example at Fig. 67 showing the summer fit obtained for 2012 applied to data of 2013, it seems as if there was a trigger that suddenly causes very dry values in summer season, whereas the measurements before were rather low. This effect cannot be reproduced by the simulation, leading to an overestimation of the soil water pressure in spring and a tendency to underestimate them in midsummer. For winter data, no such trigger is released and the fit thus looks better because only little systematic over- and underestimation can be made out.

Also, the fits are somehow arbitrary with respect to interpretation of the van Genuchten parameters obtained. There is for example no reason why the saturated water content should be 7 % lower in summer than in winter. Furthermore, the significant difference in saturated hydraulic conductivity stands out. It is very low in summer and thus a slow penetration of wetting fronts after precipitation events could be expected. However, this effect cannot be seen in the graphs on a daily timescale. It is interesting that the model is able to reproduce the very high soil water pressure measurements in summer in spite of the mentioned low Ksat.

There appear to be several maxima for R Square that can be reached with very different parameter sets. Sometimes a parameter could not be fitted, but it could as soon as boundary values were

entered. For the winter fit for example, all parameters could be fitted if reasonable boundary values were chosen, but the fit was very poor with only an R Square of 0.31027. Furthermore, often the lowest saturated water content value entered at the boundary was shown to deliver the best fit, and it lowered if the boundary conditions were lowered, too. Ksat then increased from 10.618 cm/d to 93.77 cm/d as the saturated water content changed from 0.4 to 0.37 (according to the entered boundaries), while n stayed almost the same and α doubled its value. In addition, the set with the highest R Square for the winter fit includes three parameters which all are exactly as predicted for a standard loamy texture by Rosetta (Schaap et al., 2001). They all were adapted manually, but with every trial a lower R Square was obtained. This leads to the conclusion that if the other values are left unchanged according to the best fit obtained before, the fit cannot get better than with the standard loam texture unless the fitted values are changed as well. These observations made clear that the parameter set with the best fit depends a lot on the initial values (here: standard loam) and on the boundary conditions entered and the parameters obtained thus do not necessarily have a physical meaning for the soil, but are rather empirically obtained by fitting. We therefore cannot really interpret for example the difference in Ksat between summer and winter, but we can make a graphical comparison between the observed and fitted values.
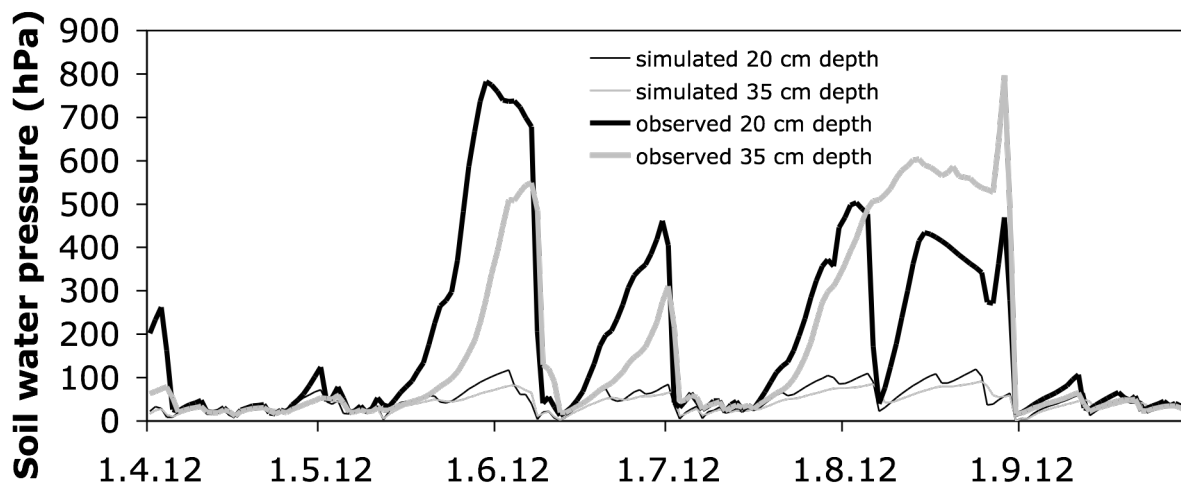
Fig. 82: *Simulated and observed soil water pressure values from April to September 2012 at the Stüsslingen site. The simulated values were obtained by applying the van Genuchten parameter set used for the flux analysis (fitted to lab data) on summer 2012. The observed soil water pressure measurements are underestimated during the dry periods, but the simulation predicts the wetter times quite well. Data observed values: BMN.*

The main message that can be read out of the graphs obtained with HYDRUS-1D is that there is apparently a difference between the very dry summer values and the low soil water pressure measurements close to saturation in winter, which cannot both be reproduced by classical soil physics. If the summer fit is applied to winter data, the simulated values are permanently too high, whereas the opposite is the case if the winter fit is applied during summer season. As discussed above, even in summer there appears to be somehow a cut between lower and high soil water pressure values, which cannot be represented by the summer fit either. Winter conditions, however, could be reproduced quite well with the best fit to data of the years 2012/2013 as shown in Fig. 70. The observed soil water pressure measurements in winter do thus not seem to be at odds with classical soil physics theory.

As a last analysis with HYDRUS-1D, the van Genuchten parameter set used for flux calculation, which has been obtained by fitting the van Genuchten equation to lab data and not with the help of the Hydrus Inverse Solution, has been applied to the summer 2012 period. The parameters used can

be seen in Table 6, and it is clear that the two parameter sets differ quite a bit. The comparison with observed values (see Fig. 82) reveals that the obtained soil water pressure values cannot describe the drier periods, because the maximum of the predicted values reaches only about 120 hPa. The wetter periods in April and September seem to be represented quite well in the simulation. This observation makes sense when looking at the van Genuchten parameter set obtained by fitting, which seems to be closer to the winter than to the summer fit. The comparison shows that the curve-fitted parameters to lab data are not that far from the ones obtained when fitting the parameters to observed field values, although the lab data itsself does not at all correspond to the values observed in the field (see Section 4.2.3). The parameter set used for the flux analysis thus seems to serve its purpose for the winter period.

5.7   *Penetration Resistance*

The penetration resistance measured with at least six insertions every day as performed for all graphs under Section 4.8 is not that simple a variable when looking closer at it. The variation between the single insertions on one day is quite high. Fig 83 therefore exemplarily depicts the situation on February 28th, showing that variations between the measurements may vary almost in the same magnitude as the averages seen in Fig. 72 under Results (Section 4.8). These differences may be attributed to a high local variability of the penetration resistance, especially when a stone is streaked. Nevertheless, the averages are assumed to straighten out these effects and to deliver an acceptable picture of the average penetration resistance under the prevalent conditions up to a depth of 40 cm. Would this assumption not be fulfilled, no relationship between penetration resistance and soil water pressure or water content could be observed.

The large fluctuations in depths below 40 cm can be assigned to streaking of stones as well as less measurements that reached that deep and thus stronger influence of single insertions on the average. The measurements in this depth must thus be looked at with care. Already in 35 cm depth, the measurements of the average curve may suffer from this effect because the relation between the soil water pressure and the penetration resistance is weaker than in 20 cm depth, as seen in Fig. 73 (left). The relationship between the product of soil water pressure and effective saturation as displayed in Fig. 74 (left) seems to suffer from the already mentioned effect that the water content at the measurement times varied very little. The soil water pressure is thus almost multiplied with a constant, leading to a similar picture as for the relationship with only soil water pressure.

In agricultural studies, a value of 2 MPa is considered to be the limit between an uncompacted and a compacted soil (Tormena et al., 1998; Silva et al., 2008; Lima et al., 2012). For non-tilled soils, this limit has been extended to 3.5 MPa (Tormena et al., 2007; Tuzzin de Moraes et al., 2014). These values have been reported for Brazil, where a higher temperature and a lot more precipitation as well as different soil types are to be expected. Nevertheless, they correspond very well to the values reported by the BGS (2004) for Switzerland, which state that for agricultural soils, the penetration resistance should not exceed 2 MPa and is considered critical if above 3.5 MPa. When comparing these values to the measurements in this study (Fig. 72), it appears that already in a depth of 35 cm, many measurements are above 3.5 MPa, although the Stüsslingen loam has a natural structure and no signs of compaction could be observed. This difference could be due to the fact that the penetration according to the BGS (2004) is measured with a different device (the PANDA sensor) and at a soil water pressure of 150 to 550 hPa, which has never been reached in this study. However, since penetration resistance decreases closer to saturation, it is expected to be even higher at higher soil water pressure measurements. Therefore, the stones in the soil increasing the penetration resistance as well as possible differences between the sensors are more likely to explain the discrepancy.

Although the single insertions of one day vary almost as much as the average between all measurement days, the range of measurement values observed obviously does make sense when compared to other studies.
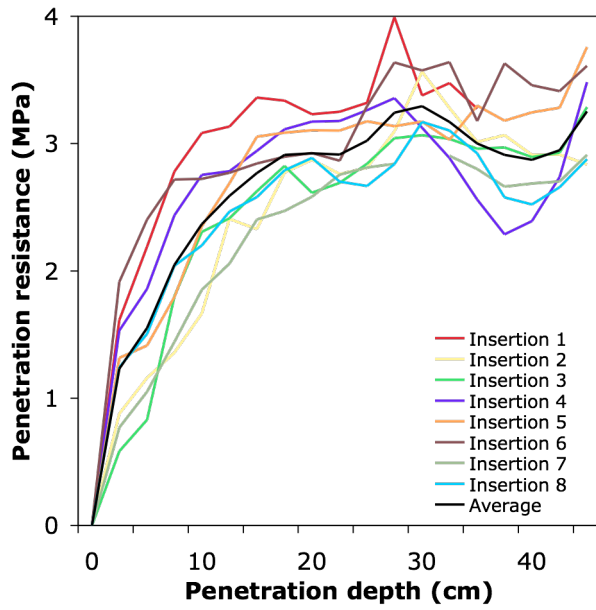
Fig. 83: *Penetration resistance on February 28th, 2014 at the Stüsslingen site. Each curve represents one insertion executed within the site perimeter. The large fluctuations may be due to large spatial variability.*

6   Conclusion and Outlook

With respect to the first research question, we can conclude that the low absolute soil water pressure measurements observed at Swiss sites are the rule rather than the exception. 90% of the daily mean soil water pressure measurements of the sites analysed lie below the critical threshold at 60 hPa. Only few sites show higher values, which is assumed to be due to their higher hydraulic conductivity.

By operating additional sensors at the Stüsslingen site, measurements were obtained to compare with the sensors already installed. Although there were some measurement problems with the self-installed tensiometers, large sensor-specific artifacts of the BMN sensors could be excluded.
Both soil water pressure and water content show a very high spatial variability inside the station perimeter. While the water content of a single sensor varied only little, the reaction of all sensors after a precipitation event was rather similar.

As observed by Buchter et al. (1999), short-term variations in temperature and radiation can cause errors in soil water pressure measurements that are larger than the range of the measured values. This effect could be observed with the self-installed tensiometers. A good protection shield thus has proven mandatory to reduce these fluctuations.
Although some tensiometers obviously do react with air temperature, as could be observed with a self-installed tensiometer in a lysimeter in the field (+1.19 hPa/°C), the values measured at the BMN so far have proven not to be significantly influenced by temperature in various analyses. The T8 as advanced tensiometer also seems fairly robust regarding temperature change, because it showed a smaller reaction than the self-installed tensiometer in the field (+0.21 hPa/°C) when tested in a climate chamber from 2 to 12°C. Nevertheless, the change observed when isolating temperature as only influencing factor points into the opposite direction than expected from the change in soil water pressure when including temperature dependence of the surface tension. The experiments here could thus not confirm the results obtained by Hopmans and Dane (1986) and Nimmo and Miller (1986), neither with respect to soil water pressure change with temperature as mentioned before, nor for the change in water content with temperature. The latter was expected to rise at lower temperatures, but has shown to decline at 2°C when compared to the measurements obtained at 21°C. It is, however, unclear whether this shift can be fully attributed to temperature change.
Even though higher soil water pressure measurements are to be expected at higher temperatures according to the experiments performed, the effect is not of a magnitude that could explain the cause of low soil water pressure measurements in winter.

Because large measurement errors of the T8 tensiometer could thus be excluded, the fourth research question aimed at explaining the cause of the low soil water pressure measurements recorded.
The influence of the saturated hydraulic conductivity on drainage could not be fully proven, because it has only been measured for the Stüsslingen loam. The constant head experiment yielded a Ksat of 78.35 cm/d, a value significantly higher than would be expected according to the texture (14.19 cm/d, Rosetta database by Schaap et al., 2001). All water content sensors at the Stüsslingen site showed a rapid drainage after rainfall and reached their original value about 2 days after the end of the event. The analysis of the fluxes, mostly showing large downward fluxes after rainfall, further supports the suspicion that the hydraulic conductivity is not the limiting factor for further drainage in winter.
The atmospheric variables recorded at the BMN sites (relative humidity and temperature) failed to predict the daily positive changes in soil water pressure. Evapotranspiration data from nearby MeteoSchweiz stations, though, correlated at least slightly with the daily positive soil water pressure changes as well as with the positive fluxes. The strong seasonality of evapotranspiration is in agreement with the low soil water pressure measurements in winter, because it does not exceed 1

mm/d from October to March (Menzel et al., 1999). Also, the analysis carried out with HYDRUS-1D revealed that conditions are different between summer and winter and cannot, although evapotranspiration was used as input data, be simply reproduced with classical soil physics. Since evapotranspiration is a rather complex parameter influenced by many factors, it can be concluded that soil water pressure measurements cannot be explained with single variables such as temperature or relative humidity. According to the data analyses in this thesis, the low soil water pressure measurements in winter are therefore believed to be caused by atmospheric conditions rather than by limited hydraulic conductivity.

Several data visualisations, such as the lab SWRC for undisturbed soil samples and the progress of water content measurements after a precipitation event, indicate the presence of macropores, which have a large influence on drainage within the first few hPa. It is especially startling that, about two days after a rainfall event, both water content and soil water pressure seem to stabilise more or less at a certain value – a hint that the largest pores have drained by then. The relatively large Ksat measured for the Stüsslingen loam shows a strong aggregation of the soil and thus interaggregate pores must exist as well. Nevertheless, the spatial variability of the Stüsslingen soil appears to be very large when looking at the SWRC retrieved for three samples in the lab as well as the water content of dried samples.

Also, the phenomenon of hysteresis is, although often used as a (rather convenient) explanation for variing water content at given soil water pressure, very plausible to occur in the data series of the BMN. For the four sites with a reasonable SWRC shape, the same pattern could be made out more or less clearly among several years. It shows a higher water content at a given soil water pressure in spring and early summer, when the soils dry for the first time, than in autumn. This hysteresis loop could also be reproduced in the lab up to 80 hPa. The width of the measurements could not explain the whole variability observed in the field, but at least a part of it. It still remains unclear, however, to what portion the field SWRC scatter can be explained with hysteresis effects.

Both water content and soil water pressure measurements at the Stüsslingen site showed a very high spatial variability in the field. This observation could be confirmed in the lab with the drying of soil samples for absolute water content determination as well as with the measurement of the SWRC for three soil samples, which all yielded quite differing results. Spatial heterogeneity thus seems to be a characteristic of the mentioned soil, making the description of its soil water state with one single soil water pressure value almost impossible. For the Aetigkofen sandy loam, the differences of the SWRC between the three soil samples appeared to be much smaller, letting the suspicion arise that the spatial variability is unique for every measurement site.

The regularly performed penetrometer measurements showed quite a variation in penetration resistance (about 2.9 to 3.7 MPa in 20 cm depth), even though both soil water pressure (12 to 43 hPa in 20 cm depth) and water content (0.385 to 0.392 in 20 cm depth) covered only a rather narrow range below the first threshold at 60 hPa. A weak positive relationship (increase in soil water pressure leads to increase in penetration resistance) could be established between soil water pressure and penetration resistance. As expected, the opposite trend (increase in water content leads to decrease in penetration resistance) could be observed for water content and penetration resistance. Nevertheless, it is impossible to make a clear statement about this relationship, because the range of measured water content values during the insertions is very small (0.007, not even 1 Vol. %). Similar to the water content and to soil water pressure, the local variation of the penetration resistance has shown to be very large.

As an overall conclusion, it can be stated that the T8 measurements seem to provide reliable measurements, which represent the prevailing conditions in winter. The explanation of these low absolute soil water pressure measurements is, however, not that easy, because the spatial variability

and complexity of soil physical parameters is very large and can thus not simply be reproduced in the lab.

Relevant for the Soil Protection authorities of the Cantons is thus that both tensiometers and water content sensors of similar type record trustful data. The T8 appeared to be even more robust against temperature changes than the other tensiometer type installed. The Stevens Hydra Probe at the Stüsslingen site showed, although its absolute values varied very little during the observation period, a course similar to other sensors. Since the spatial variability has shown to be very high inside the Stüsslingen site perimeter, it is plausible that the Hydra Probe measurements represent the local conditions.

Both soil water pressure and water content measurements at the BMN sites indicate persistent wet soil conditions in winter. The observation of pedological experts in the field that the soil appears drier than indicated by the measurements could thus not be confirmed with either soil water state parameter measured. This means for the implementation that, for most soils, no passing over is possible from November to March, except for remarkable dry periods in November or March or under frozen conditions. Nevertheless, a wide range of penetration resistance, being a proxy for soil stability, has been recorded even below the critical threshold of 60 hPa. The relevant question for the application of the measurements in practice, namely whether another parameter exists to estimate soil stability in winter, could not be answered in this study and could thus be of interest for further research.

There is evidence established in this thesis that a stable status similar to field capacity may be reached at a lower pressure head than, as traditionally defined, at 60 hPa in winter. It remains unclear what consequences this would have with respect to the threshold choice. The 60 hPa threshold was never surpassed during the field experiment. It would therefore be of interest to investigate the dynamics of penetration resistance all year round in a further study, so that the choice of critical thresholds can be further evaluated.

The focus in this thesis lay on the exclusion of sensor specific measurement artifacts as well as temperature effects. The question concerning the causes of these low absolute soil water pressure measurements could thus not be fully answered with the results presented here. To prove the suspicion that evapotranspiration best explains the soil water pressure measurements, recordings of it directly at a BMN site could provide additional insights. The role of plants with respect to soil water pressure dynamics could also be looked at more in detail. Furthermore, the hydraulic conductivity could be measured in the field to get a better idea of this parameter. In general, a focus on field studies would be advisable, since the analyses in the lab were not always able to reproduce the conditions and the variability observed in the field.

References

Alakukku, L. (1996): Persistence of soil compaction due to high axle load traffic II. Long-term effects on properties of fine-textured and organic soils. Soil and Tillage Research 37: 223-238.

Al Majou, H., Bruand, A. and Duval, O. (2008): Use of in situ volumetric water content at field capacity to improve prediction of soil water retention properties. Canadian Journal of Soil Science 88(4): 533-541.

American Society of Agricultural and Biological Engineers (ASABE) (2004): ASAE S313.3 FEB04 Soil Cone Penetrometer. ASABE, St. Joseph MI: 1-3.

Arvidsson, J. and Håkansson, I. (1996): Do effects of soil compaction persist after ploughing? Results from 21 long-term field experiments in Sweden. Soil and Tillage Research 39: 175-197.

Arvidsson, J. (2001): Subsoil compaction caused by heavy sugarbeet harvesters in southern Sweden I. Soil physical properties and crop yields in six field experiments. Soil and Tillage Research 60: 67-78.

Bundesamt für Energiewirtschaft (BFE) (1997): Richtlinien zum Schutze des Bodens beim Bau unterirdisch verlegter Rohrleitungen. Bodenschutzrichtlinien vom 1. Januar 1997: 1-28.

Bundesamt für Umwelt (BAFU, then still Bundesamt für Umwelt, Wald und Landschaft BUWAL) (2001): Bodenschutz beim Bauen. Leitfaden Umwelt 10: 1-85.

Bundesamt für Umwelt (BAFU) und Bundesamt für Landwirtschaft (BLW) (2013): Bodenschutz in der Landwirtschaft. Ein Modul der Vollzugshilfe Umweltschutz in der Landwirtschaft. Reihe Umwelt-Vollzug: 1-61.

Berisso, F. E., Schjønning, P., Keller, T., Lamandé, M., Simojoki, A., Iversen, B. V., Alakukku, L. and Forkman, J. (2013): Gas transport and subsoil pore characteristics: Anisotropy and long-term effects of compaction. Geoderma 195-196: 184-191.

Beven, K. J. and Germann, P. F. (1982): Macropores and water flow in soils. Water Resources Research 18: 1311-1325.

Beven, K. J. (2012) Rainfall-runoff modelling: The primer. Second Edition, John Wiley and Sons, Ltd.

Bianchi, W. B. (1962): Measuring soil moisture tension changes. Agricultural Engineering 43: 393-399.

Bishop, A. W. (1954): The use of pore water coefficients in practice. Geotechnique 4: 148-152.

Bishop, A. W. (1959): The principle of effective stress. Teknisk Ukeblad 106: 859-863.

Bodenkundliche Gesellschaft Schweiz (BGS) and Eidgenössische Forschungsanstalt für Agrarökologie und Landbau, Reckenholz (FAL) (2002): Klassifikation der Böden der Schweiz; Bodenprofiluntersuchungen, Klassifikationssystem, Definitionen der Begriffe, Anwendungsbeispiele. Second Edition: 1-87.

Bodenkundliche Gesellschaft Schweiz (BGS) (2004): Vorschläge für Richt- und Prüfwerte zur Definition von Bodenschadverdichtungen. In: BGS-Dokument Nr. 13: Definition und Erfassung von Bodenschadverdichtungen, Zollikofen.

Borer, F. (1982): Zum Wasserhaushalt einer dominierenden Douglasie in einem Waldbestand. Mitteilungen der eidgenössischen Anstalt für das forstliche Versuchswesen 50: 3-162.

Bradford, J. M. (1986): Penetrability. In: Klute A. (ed.): Methods of Soil Analysis, Part 1. Agronomy Monograph 9, ASA, Madison WI: 463-478.

Bristow, K. L., Kluitenberg, G. J. and Horton, R. (1994): Measurement of soil thermal properties with a dual-probe heat-pulse technique. Soil Science Society of America Journal 58: 1288-1294.

Brooks, R. and Corey, A. (1964): Hydraulic properties of porous media. Hydrology Papers, Colorado State University, Fort Collins 3: 1-27.

Buchter, B., Hinz, C., Wydler, H. and Flühler, H. (1999): Evaluation of temperature and bypass flow sensitivity of tensiometers in a field soil. Geoderma 87: 281-291.

Buchter, B. and Häusler, S. (2009): Arbeitshilfe zur Erfassung und Beurteilung von Bodenschadverdichtungen. Kantonale Bodenschutzfachstellen: 1-12.

Buckingham, E. (1907): Studies on the movement of soil moisture. Bulletin 38, U.S. Department of Agriculture, Government Printing Office, Bulletin 25, Washington D.C.

Butters, G. L. and Cardon, G. E. (1998): Temperature effects on air-pocket tensiometers. Soil Science 163: 677-685.

Calanca, P., Smith, P., Holzkämper, A. and Ammann, Ch. (2011): Die Referenzverdunstung und ihre Anwendung in der Agrarmeteorologie. Agrarforschung Schweiz 2: 176-183.

Campbell, G. S. (1988): Soil water potential measurement: an overview. Irrigation Science 9: 265-273.

Campbell, G. S., Calissendorff, C. and Williams, J. H. (1991): Probe for measuring soil specific heat using a heat-pulse method. Soil Science Society of America 55: 291-293.

Campbell, G. S. and Shiozawa, S. (1992): Prediction of hydraulic properties of soils using particle-size distribution and bulk density data. In: Van Genuchten, M. T., Leij, F. J. and Lund, L. J. (eds.): Indirect Methods for Estimating the Hydraulic Properties of Unsaturated Soils. University of California, Riverside: 317-328.

Campbell Scientific (2010): HydroSense soil water measurement system: Instruction manual. Revision 7/10: 1-24.

Carminati, A., Kaestner, A., Lehmann, P. and Flühler, H. (2008): Unsaturated water flow across soil aggregate contacts. Advances in Water Resources 31: 1221-1232.

Cavazza, L., Patruno, A. and Cirillo, E. (2007): Field capacity in soils with a yearly oscillating water table. Biosystems Engineering 98: 364-370.

CESBIO, Cabot, F. and Kerr, Y. (2011): Space in images: Soil moisture, November 2010 and 2011. European Space Agency (ESA): http://www.esa.int/spaceinimages/Images/2011/12/Soil_moisture_November_2010_and_2011 (visited: 10.3.2014).

Dane, J. H. and Hopmans, J. W. (2002): Pressure plate extractor. In: Dane, J. H. and Topp., G. C. (eds.): Methods of Soil Analysis. Part 4, Physical Methods. SSSA, Madison WI: 688-690.

Darcy, H. (1856): Les Fontaines Publiques de la Ville de Dijon. Victor Dalmont, Paris.

Decagon Devices, Inc. (2010): 10HS soil moisture sensor: Operator's manual. Version 3: 1-20.

Defila, C. (1991): Pflanzenphänologie der Schweiz, Dissertation an der Universität Zürich. Veröffentlichungen der Schweizerischen Meteorologischen Anstalt 50: 1-235.

Dexter, A. R. and Richard, G. (2009): The saturated hydraulic conductivity of soils with n-modal pore size distributions. Geoderma 154: 76-85.

Do it your soil (DIYS) (2009): Bestimmung der Desorptionskurve. Modul 1, Sequenz 2, https://moodle-app2.let.ethz.ch/course/info.php?id=51 (visited: 24.2.2014).

Dorigo, W. A., Wagner, W., Hohensinn, R., Hahn, S., Paulik, C., Xaver, A., Gruber, A., Drusch, M., Mecklenburg, S., van Oevelen, P., Robock, A. and Jackson, T. (2011): The International Soil Moisture Network: a data hosting facility for global in situ soil moisture measurements. Hydrology and Earth System Sciences 15: 1675-1698.

Durner, W. and Or, D. (2005): Soil water potential measurement. In: Anderson, M. G. (ed.): Encyclopedia of Hydrological Sciences. John Wiley and Sons, Ltd.

Eijkelkamp Agrisearch Equipment (2013): 07 Sample ring kits: Operating instructions. M1.07.E, October 2013: 1-12.

E.S.I. Environmental Sensors Inc. (2010): Moisture Point high resolution moisture profiling. Brochure Version 2010: 1-4.

Etana, A. and Håkansson, I. (1994): Swedish experiments on the persistence of subsoil compaction caused by vehicles with high axle load. Soil and Tillage Research 29: 167-172.

European Space Agency (ESA) (2013): SMOS scientific objectives. http://www.esa.int/Our_Activities/Observing_the_Earth/The_Living_Planet_Programme/Earth_Explorers/SMOS/Objectives (visited: 20.2.2014).

Evett, S. R. and Parkin, G. W. (2005): Advances in soil water content sensing: The continuing maturation of technology and theory. Vadose Zone Journal 4: 986-991.

Evett, S. R. Tolk, J. A. and Howell, T. A. (2005): Time domain reflectometry laboratory calibration in travel time, bulk electrical conductivity, and effective frequency. Vadose Zone Journal 4: 1020-1029.

Feng, M. and Fredlund, D. G. (1999): Hysteretic influence associated with thermal conductivity sensor measurements. In: Proceedings from Theory to the Practice of Unsaturated Soil

Mechanics in Association with the 52nd Canadian Geotechnical Conference and the Unsaturated Soil Group, Regina, Sask., 23.-24. October 1999: 14-20.

Flühler, H. and Roth, K. (unpublished Lecture Notes, 2004): Physik der ungesättigten Zone. Version 2004.1.

Flury, M, Flühler, H., Jury, W. A. and Leuenberger, J. (1994): Susceptibility of soils to preferential flow of water: A field study. Water Resources Research 30: 1945-1954.

Food and Agricultural Organization of the United Nations (FAO) (2006): Guidelines for soil description. Fourth Edition: 1-98.

Gallipoli, D., Gens, A., Sharma, R. and Vaunat, J. (2003): An elasto-plastic model for unsaturated soil incorporating the effects of suction and degree of saturation on mechanical behaviour. Geotechnique 53: 123-135.

Gardner, W., Israelsen, O. W., Edlefsen, N. E. and Clyde, D. (1922): The capillary potential function and its relation to irrigation practice. Physical Review 20: 196.

Gardner, R. (1955): Relation of temperature to moisture tension of soil. Soil Science 79: 257-265.

Geischeder, R. and Demmel, M. (2006): Landtechnische Möglichkeiten zur Vermeidung von schädigenden Bodenbelastungen im Ackerbau. Schriftenreihe Bayrische Landesanstalt für Landwirtschaft (LfL) 21: 75-88.

Gimper, S. (2010): Evaluierung bestehender Messsensoren zur Ermittlung des Matrixpotenzials in Böden. Diploma thesis at the University of Applied Sciences in Jena: 1-76.

Goutal, N., Renault, P. and Ranger, J. (2013): Forwarder traffic impacted over at least four years soil air composition of two forest soils in northeast France. Geoderma 193: 29-40.

Haines, W. B. (1930): The hysteresis effect in capillary properties and the modes of moisture distribution associated therewith. Journal of Agricultural Science 20: 96-105.

Håkansson, I. (2005): Machinery-induced compaction of arable soils. Incidence – consequences – counter-measures. Reports of the Division of Soil Management 109, Department of Soil Sciences, Swedish University of Agricultural Sciences, Uppsala: 1-158.

Haridasan, M. and Jensen, R. D. (1972): Effect of temperature on pressure head-water content relationship and conductivity of two soils. Soil Science Society of America Proceedings 36: 703-708.

Hartge, K. H. (1978): Einführung in die Bodenphysik. Ferdinand Enke Verlag, Stuttgart.

Hartge, K. H. and Horn, R. (1989): Die physikalische Untersuchung von Böden. Ferdinand Enke Verlag, Stuttgart, Second Edition.

Hook, W. R. and Livingston, N. J. (1995): Errors on converting time domain reflectometry measurements of propagation velocity to estimates of soil water content. Soil Science Society of America Journal 59: 35-41.

Hopmans, J. W. and Dane, J. H. (1986): Temperature dependence of soil hydraulic properties. Soil Science Society of America Journal 50: 562-567.

Hopmans, J. W., Šimunek, J., Romano, N. and Durner, W. (2002): Inverse Methods. In: Dane, J. H. and Topp, G. C. (eds.): Methods of Soil Analysis. Part 4, Physical Methods. SSSA, Madison WI: 963-1008.

Horn, R. and Fleige, H. (2003): A method for assessing the impact of load on mechanical stability and on physical properties of soils. Soil and Tillage Research 73: 89-99.

ICT International Pty Ltd (2012): CP40II Cone Penetrometer Operation Manual. DocRef Ver1.0: 1-25.

IMKO Mikromodultechnik GmbH (2006): Allgemeine Anforderungen an Kapazitive-, Mikrowellen- und TDR-Sensoren zur präzisen Materialfeuchtemessung. http://www.imko.de/images/stories/Anforderungen%20an%20Materialfeuchtesensoren_web.pdf (visited: 24.2.2014).

IPCC (2013): Summary for policymakers. In: Stocker, T. F., Qin, D., Plattner, G.-K., Tignor, M., Allen, S. K., Boschung, J., Nauels, A., Xia, Y., Bex, V. and Midgley, P. M. (eds.): Climate Change 2013: The Physical Basis. Contribution of Working Group 1 to the Fifth Assessment Report of the Intergovernmental Panel on Climate Change. Cambridge University Press, Cambridge, United Kingdom and New York, NY, USA.

Iwata, Y., Hirota, H., Hayashi, M., Suzuki, S. and Hasegawa, S. (2010): Effects of frozen soil and snow cover on cold-season soil water dynamics in Tokachi, Japan. Hydrological Processes 24: 1755-1765.

Jackson, R. D. (1972): On the calculation of hydraulic conductivity. Soil Science Society of America Proceedings 36: 380-382.

Jarvis, N. J. (2007): A review of non-equilibrium water flow and solute transport in soil macropores: principles, controlling factors and consequences for water quality. European Journal of Soil Science 58: 523-546.

Johnson, A. I. (1962): Methods of measuring soil moisture in the field. Geological Survey Water Supply paper 1619-U.

Kelleners, T. J., Robinson, D. A., Shouse, P. J., Ayars, J. E. and Skaggs, T. H. (2005): Frequency dependence of the complex permittivity and its impact on dielectric sensor calibration in soils. Soil Science Society of America Journal 69: 67-76.

Kerr, Y. H., Waldteufel, P., Wigneron, J.-P., Martinuzzi, J.-M., Font, J. and Berger, M. (2001): Soil moisture retrieval from space: The soil moisture and ocean salinity (SMOS) mission. IEEE Transactions on Geoscience and Remote Sensing 39: 1729-1735.

Klausner, Y. (1991): Fundamentals of continuum mechanics of soils. Springer-Verlag, New York.

Klute, A. (1986a): Hydraulic conductivity and diffusivity: Laboratory methods. In: Klute A. (ed.): Methods of Soil Analysis, Part 1. Agronomy Monograph 9, ASA, Madison WI: 687-734.

Klute, A. (1986b): Water retention: Laboratory methods. In: Klute A. (ed.): Methods of Soil Analysis, Part 1. Agronomy Monograph 9, ASA, Madison WI: 635-662.

Khalili, N. and Khabbaz, M. H. (1998): A unique relationship for χ for the determination of the shear strength of unsaturated soils. Geotechnique 48 (5): 681-687.

Kizito, F., Campbell, C. S., Campbell, G. S., Cobos, D. R., Teare, B. L., Carter, B. and Hopmans, J. W. (2008): Frequency, electrical conductivity and temperature analysis of a low-cost capacitance soil moisture sensor. Journal of Hydrology 352: 367-378.

Kosugi, K. (1996): Lognormal distribution model for unsaturated soil hydraulic properties. Water Resources Research 32 (9): 2697–2703.

Lammeranner, W. and Obriejetan, M. (2011): Untersuchungen zum Bodenwasserhaushalt und zur Durchwurzelung unter einem Gehölzbestand (Salix purpurea L.) im Vergleich zu einer Gräser-Kräuter-Narbe. Band zur 1. Tagung der Österreichischen Gesellschaft für Wurzelforschung: 75-80.

Lassen, P., Jørgensen, M. S., Stettler, M., Lamandé, M., Keller, T., Lilja, H., Alakukku, L., Pedersen, J., Hansen, T. K., Nielsen, J. A. and Schjønning, P. (2012): Terranimo® - a web based tool for evaluating soil compaction: Model design and user interface. In: Proceedings of the NJF seminar 448, 6-8 March 2012, Helsinki: 83-86.

Lima, C. L. R., Miola, E. C. C., Timm, L. C., Pauletto, E. A. and Silva, A. P. (2012): Soil compressibility and least limiting water range of a constructed soil under cover crops after coal mining in Southern Brazil. Soil and Tillage Research 124: 190-195.

Livingston, B. E. (1908): A method for controlling plant moisture. Plant World 11: 39-40.

Livingston, B. E. (1918): Porous clay cones for the auto-irrigation of potted plants. Plant World 21: 202-208.

Lu, N., Godt, J. W. and Wu, T. (2010): A closed-form equation for effective stress in unsaturated soil. Water Resources Research 46: W05515, doi: 10.1029/2009WR008646.

Lüscher, P., Frutig, F., Sciacca, S., Spjevak, S. & Thees, O. (2010). Physikalischer Bodenschutz im Wald – Bodenschutz beim Einsatz von Forstmaschinen. Merkblatt für die Praxis 45: 1-12.

Marthaler, H. P., Vogelsanger, W., Richard, F. and Wierenga, P. J. (1983): A pressure transducer for field tensiometers. Soil Science Society of America Journal 24: 624-627.

Matile, L. and Buchter, B. (2001): Grobporenbestimmung – Verfahrensoptimierung für den Vollzug. Bericht und Laboranleitung, Fachstelle Bodenschutz Kanton Zürich.

Matile, L., Berger, R. and Krebs, R. (2011): Tensiometermessung beim Bodenschutz auf der Baustelle. ZHAW Wädenswil.

Menzel, L., Lang, H. and Rohmann, M. (1999): Mittlere jährliche aktuelle Verdunstungshöhen 1973–1992. In: Bundesamt für Wasser und Geologie (BWG): Hydrologischer Atlas der Schweiz, Tafel 4.1, Bern.

MeteoSchweiz (2013): Klimabulletin Jahr 2012. Zürich.

MeteoSchweiz (2014): Klimabulletin Jahr 2013. Zürich.

Mittelbach, H., Lehner, I. and Seneviratne, S. I. (2012): Comparison of four soil moisture sensor types under field conditions in Switzerland. Journal of Hydrology 430-431: 39-49.

Mohanty, B. P., Kanwar, R. S. and Everts, C. J. (1994): Comparison of saturated hydraulic conductivity measurement methods for a glacial-till soil. Soil Science Society of America Journal 58: 672-677.

Moitzi, G. and Boxberger, J. (2007): Vermeidung von Bodenschadverdichtungen beim Einsatz von schweren Landmaschinen – eine aktuelle Herausforderung. Ländlicher Raum: Online-Fachzeitschrift des Bundesministeriums für Land- und Forstwirtschaft, Umwelt und Wasserwirtschaft: 1-27.

Mualem, Y. (1974): A conceptual model of hysteresis. Water Resources Research 10: 514-520.

Mualem, Y. (1976): A new model for predicting the hydraulic conductivity of unsaturated porous media. Water Resources Research 12 (3): 513-522.

Mualem, Y. (1984): Prediction of the soil boundary wetting curve. Journal of Soil Science 137: 379-390.

Nimmo, J. R. (1983): The temperature dependence of soil-moisture characteristics. Ph.D. thesis, University of Wisconsin-Madison.

Nimmo, J. R. and Miller, E. E. (1986): The temperature dependence of isothermal moisture vs potential characteristics of soils. Soil Science Society of America Journal 50: 1105-1113.

Novak, V. (1975): Non-isothermal flow of water in unsaturated soils. Journal of Hydrological Sciences (Polish Academy of Science) 2: 37-51.

Odegard, C. (2000): Reflectometry techniques aid IC failure analysis. EDN network: http://www.edn.com/electronics-news/4378350/Reflectometry-Techniques-Aid-IC-Failure-Analysis (visited: 17.2.2014).

Organe consultatif sur les changements climatiques (OcCC) (2002): Das Klima ändert – auch in der Schweiz. Die wichtigsten Ergebnisse des dritten Wissenstandsberichts des IPCC aus Sicht der Schweiz. Bern.

Or, D. and Wraith, J. N. (1999): Temperature effects on soil bulk dielectric permittivity measured by time domain reflectometry: A physical model. Water Resources Research 35: 371-383.

Or, D., Tuller, M. and Wraith, J. N. (2013): Vadose Zone Hydrology/Environmental Soil Physics (lecture notes, not published).

Pham, H. Q., Fredlund, D. G. and Barbour, S. L. (2005): A study of hysteresis models for soil-water characteristic curves. Canadian Geotechnical Journal 42: 1548-1568.

Philip, J. R. and de Vries, D. A. (1957): Moisture movement in porous materials under temperature gradients. Transactions American Geophysical Union 38: 222-232.

Primault, B. (1962): Du calcul de l'évapotranspiration. Archiv für Meteorologie, Geophysik und Bioklimatologie Series B 12: 124-150.

Primault, B. (1972): Etude méso-climatique du Canton de Vaud. Office cantonal vaudoise de l'urbanisme, Lausanne: Cahiers de l'amenagement régional 14: 1-186.

Primault, B. (1981): Extension de la validité de la formule suisse de calcul de l'évapotranspiration. Bericht der Schweizerischen Meteorologischen Anstalt (Meteo-Schweiz) 103: 1-8.

Reece, C. F. (1996): Evaluation of a line heat dissipation sensor for measuring soil matric potential. Soil Science Society of America Journal 60: 1022-1028.

Richards, L. A. (1928): The usefulness of capillary potential to soil moisture and plant investigators. Journal of Agricultural Research (Cambridge) 37: 719-742.

Richards, L. A. (1931): Capillary conduction of liquids through porous mediums. Physics 1: 318-333.

Richards, L. A. and Gardner, W. (1936): Tensiometers for measuring the capillary tension of soil water. Journal of the American Society of Agronomy 28 (5): 352-358.

Richards, L. A. and Weaver, L. R. (1944): Moisture retention by some irrigated soils as related to soil moisture tension. Journal of Agricultural Research 69: 215-235.

Richards, L. A. (1948): Porous plate apparatus for measuring moisture retention and transmission by soils. Soil Science 66: 105-110.

Richards, L. A. and Ogata, G. (1961): Psychometric measurements of soil samples equilibrated on pressure membranes. Soil Science Society of America Journal 25: 456-459.

Richards, L. A. (1965): Physical condition of water in soil. In: Black, C. A. (ed.): Methods of Soil Analysis, Part 1. Agronomy Monograph 9, ASA, Madison WI: 128-152.

Richard, F. and Lüscher, P. (1983): Physikalische Eigenschaften von Böden der Schweiz, Nummer 11: Winzlerboden. In: Bosshard, W. (ed.): Lokalformen, Volume 3.

Rosenkranz, H., Durner, W., He, W., Knoblauch, C. and Meurer, K. H. E. (2013): Ringversuch zum Praxisvergleich von 13 Sensortypen zur Wassergehalts- und Wasserspannungsbestimmung in Böden. Bericht über die 15. Lysimetertagung, 15.-17.4.2013, HBFLA Raumberg-Gumpenstein: 93-102.

Roth, K., Schulin, R., Flühler, H. and Attinger, W. (1990): Calibration of time domain reflectometry for water content measurement using a composite dielectric approach. Water Resources Research 26: 2267-2273.

Sachs, W. and Meyn, V. (1995): Pressure and temperature dependence of the surface tension in the system natural gas/water; principles of investigation and the first precise experimental data for

pure methane/water at 25°C up to 46.8MPa. Colloids and Surfaces: A, Physiochemical and Engineering Aspects 94: 291-301.

Scanlon, B. R., Andraski, B. J. and Bilskie, J. (2002): Miscellaneous methods for measuring matric or water potential. In: Dane, J. H. and Topp, G. C. (eds.): Methods of Soil Analysis. Part 4, Physical Methods. SSSA, Madison WI: 643-670.

Schaap, M. G., Leji, F. J. and van Genuchten, M. Th. (2001): Rosetta: A computer programm for estimating soil hydraulic parameters with hierarchical pedotransfer functions. Journal of Hydrology 251: 163-176.

Schädler, B. and Weingartner, R. (2002): Komponenten des natürlichen Wasserhaushaltes 1961-1990. In: Bundesamt für Wasser und Geologie (BWG): Hydrologischer Atlas der Schweiz, Tafel 6.3, Bern.

Scheffer, F. and Schachtschabel, P. (2002): Lehrbuch der Bodenkunde. Springer-Verlag, Berlin Heidelberg.

Seneviratne, S. I., Corti, T., Davin, E. L., Hirschi, M., Jaeger, E. B., Lehner, I., Orlowsky, B. and Teuling, A. J. (2010): Investigating soil moisture-climate interactions in a changing climate: a review. Earth-Science Reviews 99: 125-161.

Seyfried, M. S., Grant, L. E., Du, E. and Humes, K. (2005): Dielectric Loss and Calibration of the Hydra Probe Soil Water Sensor. Vadose Zone Journal 4: 1070-1079.

Seyfried, M. S. and Grant, L. E. (2007): Temperature effects on soil dielectric properties measured at 50 MHz. Vadose Zone Journal 6: 759-765.

Silva, A. P., Tormena, C. A., Fidalski, J. and Imnhoff, S. (2008): Funções de pedotransferência para as curvas de retenção de água e de resistência do solo à penetração. Revista Brasileira de Ciencias do Solo 32: 1-10.

Šimunek, J., Šejna, M., Saito, H., Sakai, M. and van Genuchten, M. Th. (2013): The HYDRUS- 1D Software Package for Simulating the Movement of Water, Heat, and Multiple Solutes in Variably Saturated Media, Version 4.17, HYDRUS Software Series 3, Department of Environmental Sciences, University of California Riverside, Riverside, California, USA.

Sisson, J. B., Gee, G. W., Hubbell, J. M., Bratton, W. L., Ritter, J. C., Ward, A. L. and Caldwell, T. G. (2002): Advances in tensiometry for long-term monitoring of soil water pressures. Vadose Zone Journal 1: 310-315.

Smith, W. O. (1933): The final distribution of retained liquid in an ideal uniform soil. Physics 4: 425-438.

Solone, R., Bittelli, M., Tomei, F. and Morari, F. (2012): Errors in water retention curves determined with pressure plates: Effects on the soil water balance. Journal of Hydrology 470-471: 65-74.

Spreafico, M. and Weingartner, R. (2005): Hydrologie der Schweiz: Ausgewählte Aspekte und Resultate. Kap. 4, Verdunstung. Berichte des BWG, Serie Wasser, Nr. 7, Bern.

Starr, J. L. and Paltineanu, I. C. (2002): Capacitance devices. In: Methods of Soil Analysis, Part 4. Agronomy Monograph 9, ASA, Madison WI: 463-474, 534-545.

Steele-Dunne, S. C., Rutten, M. M., Krzeminska, D. M., Hausner, M., Tyler, S. W., Selker, J., Bogaard, T. A. and van de Giesen, N. C. (2010): Feasibility of soil moisture estimation using passive distributed temperature sensing. Water Resources Research 46: W03534, doi:10.1029/2009WR008272.

Stettler, M., Keller, T., Schjønning, P., Lamandé, M., Lassen, P., Pedersen, J. and Weisskopf, P. (2012): Terranimo® - a web-based tool for evaluating soil compaction: Machinery-induced stresses versus soil strength. In: Proceedings of the NJF seminar 448, 6-8 March 2012, Helsinki: 87-90.

Stevens Water Monitoring System, Inc. (2007): The Hydra Probe soil sensor. Version July 2007: 1-63.

Sutinen, R., Pekka, H. and Ari, V. (2007): Effect of mild winter events on soil water content beneath snowpack. Cold Regions Science and Technology 51: 56-67.

Tandeske, D. (1991): Pressure sensors: Selection and application. Marcel Dekker, New York.

Taylor, H. M., Roberson, G. M. and Parker Jr., J. R. (1966): Soil strength-root penetration relations to medium to coarse-textured soil materials. Soil Science, Baltimore 102: 18-22.

Tektronix, Inc. (2000): 1502C Metallic Time-Domain Reflectometer, User's Manual.

Terzaghi, K. (1943): Theoretical soil mechanics. John Wiley and Sons, New York.

Topp, G. C., Davis, J. L. and Annan, A. P. (1980): Electromagnetic determination of soil water content: Measurement in coaxial transmission lines. Water Resources Research 16: 574-582.

Topp, G. C. and Ferré, T. P. A. (2005): Measuring of soil water content. In: Anderson, M. G. (ed.): Encyclopedia of Hydrological Sciences. John Wiley and Sons, Ltd.

Tormena, C. A., Silva, A. P. and Libardi, P. L. (1998): Caracterização do intervalo hídrico ótimo de um Latossolo Vermelho Roxo sob plantio direto. Revista Brasileira de Ciencia do Solo 22: 573-581.

Tormena, C. A., Araujo, M. A., Fidalski, J. and Costa, J. M. (2007): Variação temporal do intervalo hídrico ótimo de um Latossolo Vermelho distroférrico sob sistemas de plantio direto. Revista Brasileira de Ciencia do Solo 31: 211-219.

Tuzzin de Moraes, M. Debiasi, H., Carlesso, R., Franchini, J. C. and Rodrigues da Silva, V. (2014): Critical limits of soil penetration resistance in a Rhodic Eutrudox. Revista Brasileira de Ciencia do Solo 38: 288-298.

Twarakavi, N. K. C., Sakai, M. and Šimunek, J. (2009): An objective analysis of the dynamic nature of field capacity. Water Resources Research 45: W10410, doi:10.1029/2009WR007944.

UMS GmbH (2001): trime-EZ / -IT, TDR-Sonden zur Messung von Wassergehalt und Leitwert. Datasheet, Version 01.2001.

UMS GmbH (2004): ThetaProbe soil moisture sensor, type ML2x: User manual. Version 1.21: 1-22.

UMS GmbH (2005): TensioLink USB Konverter. Version August 2005: 1-12.

UMS GmbH (2008): T8 long-term monitoring tensiometer: User manual. Revision 2012: 1-56.

USG, SR 814.01 (2010): Bundesgesetz vom 7. Oktober 1983 über den Umweltschutz (Umweltschutzgesetz, USG).

Vachaud, G. and Thony, J. (1971): Hysteresis during infiltration and redistribution in a soil column at different initial water contents. Water Resources Research 7: 111-120.

Van der Ploeg, R. R., Ehlers, W. and Horn, R. (2006): Schwerlast auf dem Acker. Spektrum der Wissenschaft August 2006: 80-88.

Van Genuchten, M. Th. (1980): A closed-form equation for predicting the hydraulic conductivity of unsaturated soils. Soil Science Society of America 44: 892-898.

VBBo, SR 814.12 (2012): Verordnung über Belastungen des Bodens (VBBo) vom 1. Juli 1998.

Walker, J. P., Willgoose, G. R. and Kalma, J. D. (2004): In situ measurement of soil moisture: A comparison of techniques. Journal of Hydrology 293: 85-99.

Watson, K. K. (1967): A recording field tensiometer with rapid response characteristics. Water Resources Research 5: 33-39.

Webster, R. (1965): The measurement of soil water tension in the field. The New Phytologist, 65 (2): 249-258.

Weast, R. C. (1969): CRC Handbook of Chemistry and Physics. Fiftieth Edition by The Chemical Rubber Co.

Weiler, M. and Naef, F. (2003): An experimental tracer study of the role of macropores in infiltration in grassland soils. Hydrological Processes 17: 477-493.

Weisskopf, P., Reiser, R., Rek, J. and Oberholzer, H. R. (2010): Effect of different compaction impacts and varying subsequent management practices on soil structure, air regime and microbiological parameters. Soil and Tillage Research 111: 65-74.

White, R. E. (1997): Principles and Practice of Soil Science. The Soil as a Natural Resource. Third Edition, Blackwell, Carlton, Australia.

Wilkinson, G. E. and Klute, A. (1962): The temperature effect on the equilibrium energy status of water held by porous media. Soil Science Society of America Proceedings 26: 326-329.

Appendix A

Program file for the datalogger CR1000 used for the sensor comparison in Stüsslingen:

```
'CR1000
'Created by Short Cut (2.8)

'Declare Variables and Units
Dim LCount
Public BattV
Public FullBR(8)
Public Tensio(8)

Units BattV=Volts
Units FullBR=mV/V
Units Tensio=bar

Public JULDAY, JD1, JD2, JD3,
Public LaL(6)
Public LaL2(6)
Public ToppVWC(6)
Public MuxChan
Dim I
Dim TIME(9)
Alias TIME(1)=YEAR
Alias TIME(2)=MONTH
Alias TIME(3)=DAI
Alias TIME(4)=HOUR
Alias TIME(5)=MINUTES
Alias TIME(6)=SECONDS
Alias TIME(7)=mSECONDS
Alias TIME(8)=DAY_OF_WEEK
Alias TIME(9)=DAY_OF_YEAR

'Declare Constants
'Topp Equation Dielectric Constants
Const a0= -0.053
Const a1= 0.0292
Const a2= -0.00055
Const a3= 0.0000043

'Define Data Tables
DataTable(Data_Tensio,True,-1)
        DataInterval(0,15,Min,10)
        Sample(8,FullBR(1),FP2)
        Sample(8,Tensio(1),FP2)
EndTable

DataTable(Batt,True,-1)
        DataInterval(0,1440,Min,10)
        Minimum(1,BattV,FP2,False,False)
EndTable

DataTable(Data_TDR,1,-1) 'TDR100 VWC Measurements
DataInterval (0,15,Min,10)
```

```
Sample(6,LaL(),IEEE4)
Sample(6,ToppVWC(),FP2)
Sample(9,Time,FP2)
Sample(1,JULDAY,IEEE4)
EndTable

'Main Program
BeginProg

  SDMSpeed(50) 'Fix TDR100 to CR1K communication timing
 Scan(5,Sec,0,0) 'Scan instructions every 5 seconds

  If TimeIntoInterval(0,15,Min) Then

  SW12 (1) 'Turn on 12V power to TDR100 and SDMX50
  'Wire TDR100 & SDMX50 12V power leads to CR1000 SW12 Terminal

              'Default Datalogger Battery Voltage measurement BattV
              Battery(BattV)
              'Turn AM416 Multiplexer On
              PortSet(5,1)
              For LCount=1 To 9
                    'Switch to next AM416 Multiplexer channel
                    PulsePort(4,10000)
                    'Generic Full Bridge measurements FullBR() on the AM416 Multiplexer:
                    BrFull(FullBR(LCount),1,mV25,1,1,1,2500,True,True,0,_50Hz,1,0)
              Next LCount

              Tensio(1)=-0.1187*FullBR(1)+0.0712
              Tensio(2)=-0.1217*FullBR(2)+0.0927
              Tensio(3)=-0.1204*FullBR(3)+0.0747
              Tensio(4)=-0.118*FullBR(4)+0.0685
              Tensio(5)=-0.118*FullBR(5)+0.0738
              Tensio(6)=-0.1212*FullBR(6)+0.0886
              Tensio(7)=-0.1184*FullBR(7)+0.0782
              Tensio(8)=-0.1161*FullBR(8)+0.055

              'Turn AM416 Multiplexer Off
              PortSet(5,0)
              CallTable(Data_Tensio)
              CallTable(Batt)


              ' Program TDR

  'Measure La/L on SDMX50 channel no1 though channel no8 & convert to VWC using Topp Eq.
              TDR100 (LaL(1),0,0,1001,4,1.0,251,9.6,2.5,.18,0.06,1,0)
              TDR100 (LaL(2),0,0,2001,4,1.0,251,9.6,2.5,.18,0.06,1,0)
              TDR100 (LaL(3),0,0,3001,4,1.0,251,9.6,2.5,.18,0.06,1,0)
              TDR100 (LaL(4),0,0,4001,4,1.0,251,9.6,2.5,.18,0.06,1,0)
              TDR100 (LaL(5),0,0,5001,4,1.0,251,9.6,2.5,.18,0.06,1,0)
              TDR100 (LaL(6),0,0,6001,4,1.0,251,9.6,2.5,.18,0.06,1,0)

              For I=1 To 6
    LaL2(I) = LaL(I)^2 'Apparent Dielectric Constant K = (La/L)^2
    Next I
```

```
'Topp Conversion from Dielectric Constant to Volumetric Water Content (VWC)
For I=1 To 6
  ToppVWC(I)=a0+a1*LaL2(I)+a2*LaL2(I)^2+a3*LaL2(I)^3
  Next I
  RealTime(TIME)
  JD1=DAY_OF_YEAR-1
  JD2=HOUR/24
  JD3=MINUTES/1440
  JULDAY=JD1+JD2+JD3

          'Call Data Tables and Store Data

          CallTable(Data_TDR)

  SW12(0) 'Switched 12V Low
  EndIf
  PortsConfig (&B00000111,&B00000000)'configure SDM ports C1, C2, C3 as inputs
  NextScan

EndProg
```

Appendix B

Field Journal Stüsslingen

Date: 4.12.2013   **Time:** 11.00-14.45
Weather: foggy, later sun came out, cold
Precipitation: none   **Air temperature:** -2.2 - + 1.2°C
Soil water pressure 20 cm: 30 hPa   **Soil water pressure 35 cm:** 25 hPa
Stevens Hydra Probe measurement: 0.388
Work: Installation of all sensors, solar panel and measuring devices

Date: 9.12.2013   **Time:** 9.00-9.30
Weather: sunny, cold
Precipitation: none   **Air temperature:** -4 - -2.2°C
Soil water pressure 20 cm: 37 hPa   **Soil water pressure 35 cm:** 31 hPa
Stevens Hydra Probe measurement: 0.386
Work: First download of data, visual check of station

Date: 12.12.2013   **Time:** 10.00-13.30
Weather: foggy, cold
Precipitation: none   **Air temperature:** -5.4 - -4°C
Soil water pressure 20 cm: 43 hPa   **Soil water pressure 35 cm:** 34 hPa
Stevens Hydra Probe measurement: 0.385
Work: Download of data, visual check of station, improve radiation shield on tensiometers, first cone penetrometer measurements (file 114-119), take of 5 undestroyed soil samples

Date: 19.12.2013   **Time:** 10.00-11.30
Weather: rainy (rain just started -> some reaction of suction in 20 cm depth)
Precipitation: during stay ca. 20 mm   **Air temperature:** -2.2 - + 1.2°C
Soil water pressure 20 cm: 37 hPa   **Soil water pressure 35 cm:** 30 hPa
Stevens Hydra Probe measurement: 0.385
Work: Download of data, visual check of station, installation of lysimeter, cone penetrometer measurements (file 120-125)

Date: 23.12.2013   **Time:** 16.30-17.15
Weather: sunny, rather warm
Precipitation: none   **Air temperature:** 8.2 – 7.3°C
Soil water pressure 20 cm: 35 hPa   **Soil water pressure 35 cm:** 26 hPa
Stevens Hydra Probe measurement: 0.388
Work: Download of data, visual check of station, filling of tensiometer 8 (lysimeter 35 cm), cone penetrometer measurements (file 126-134)

Date: 27.12.2013   **Time:** 13.30-14.30
Weather: some clouds, windy
Precipitation: none   **Air temperature:** 3.1 – 4°C
Soil water pressure 20 cm: 25 hPa   **Soil water pressure 35 cm:** 21 hPa
Stevens Hydra Probe measurement: 0.391
Work: Download of data, visual check of station, replacement and filling of tensiometer 8 (lysimeter 35 cm), cone penetrometer measurements (file 135-140)

Date: 04.01.2014   **Time:** 11.30-12.15
Weather: cloudy, rainy
Precipitation: during stay ca. 2 mm   **Air temperature:** 5.1°C
Soil water pressure 20 cm: 17 hPa (rapidly sinking due to rainfall: from 24 hPa at 10:30 a.m. to 7 hPa at 1:00 p.m.)   **Soil water pressure 35 cm:** 20 hPa
Stevens Hydra Probe measurement: 0.390
Work: Download of data, visual check of station, cone penetrometer measurements (file 141-149)

Date: 09.01.2014   **Time:** 09.30-11.00
Weather: some clouds
Precipitation: none   **Air temperature:** 3.5-6.2°C
Soil water pressure 20 cm: 39 hPa   **Soil water pressure 35 cm:** 29 hPa
Stevens Hydra Probe measurement: 0.388
Work: fix programm, download of 10HS-data, visual check of station, drying of pressure transducer at tensiometer 8, cone penetrometer measurements (file 150-156), take of 3 undestroyed soil samples

Date: 11.01.2014   **Time:** 16.00-16.45
Weather: cloudy
Precipitation: none   **Air temperature:** 5.6°C
Soil water pressure 20 cm: 36 hPa   **Soil water pressure 35 cm:** 30 hPa
Stevens Hydra Probe measurement: 0.388
Work: download of data, visual check of station, drying of pressure transducer at tensiometer 8, cone penetrometer measurements (file 157-162)

Date: 17.01.2014   **Time:** 14.30-16.00
Weather: friendly, rather warm
Precipitation: none   **Air temperature:** 6.5°C
Soil water pressure 20 cm: 23 hPa   **Soil water pressure 35 cm:** 19 hPa
Stevens Hydra Probe measurement: 0.391
Work: download of data, visual check of station, drying of pressure transducer at all tensiometers, replacement of pressure transducers 7 and 8, cone penetrometer measurements (file 163-170)

Date: 20.01.2014   **Time:** 8.30-9.00
Weather: cloudy
Precipitation: none   **Air temperature:** 1.9°C
Soil water pressure 20 cm: 36 hPa   **Soil water pressure 35 cm:** 28 hPa
Stevens Hydra Probe measurement: 0.389
Work: download of data, visual check of station

Date: 21.01.2014   **Time:** 15.30-16.00
Weather: cloudy
Precipitation: none   **Air temperature:** 3.0°C
Soil water pressure 20 cm: 39 hPa   **Soil water pressure 35 cm:** 29 hPa
Stevens Hydra Probe measurement: 0.388
Work: removal of pressure transducer 8 out of tensiometer 8

Date: 24.01.2014   **Time:** 13.30-15.00
Weather: friendly
Precipitation: none   **Air temperature:** 3.9°C
Soil water pressure 20 cm: 12 hPa   **Soil water pressure 35 cm:** 14 hPa

Stevens Hydra Probe measurement: 0.392
Work: download of data, visual check of station, change of program (_newbound), cone penetrometer measurements (file 171-181)

Date: 27.01.2014   **Time:** 8.00-8.45
Weather: cloudy, changing
Precipitation: none   **Air temperature:** 2.9°C
Soil water pressure 20 cm: 8 hPa   **Soil water pressure 35 cm:** 8 hPa
Stevens Hydra Probe measurement: 0.392
Work: download of data, visual check of station, refill and reinstallation of pressure transducer 8 in tensiometer 8

Date: 29.01.2014   **Time:** 16.30-17.30
Weather: friendly
Precipitation: none   **Air temperature:** 1.6°C
Soil water pressure 20 cm: 34 hPa   **Soil water pressure 35 cm:** 27 hPa
Stevens Hydra Probe measurement: 0.388
Work: download of data, visual check of station, cone penetrometer measurements (file 182-193)

Date: 04.02.2014   **Time:** 8.00-8.45
Weather: cloudy
Precipitation: none   **Air temperature:** 1.6°C
Soil water pressure 20 cm: 30 hPa   **Soil water pressure 35 cm:** 23 hPa
Stevens Hydra Probe measurement: 0.389
Work: download of data, visual check of station, refill of tensiometer 1_20, 2_20 and L_20, cone penetrometer measurements (file 194-199)

Date: 15.02.2014   **Time:** 9.30-10.15
Weather: changing
Precipitation: none   **Air temperature:** 3.2-4°C
Soil water pressure 20 cm: 30 hPa   **Soil water pressure 35 cm:** 24 hPa
Stevens Hydra Probe measurement: 0.39
Work: download of data, visual check of station, refill of tensiometer L_20, cone penetrometer measurements (file 200-210)

Date: 20.02.2014   **Time:** 13.00-13.45
Weather: sunny
Precipitation: none   **Air temperature:** 7.9-10.7°C
Soil water pressure 20 cm: 39 hPa   **Soil water pressure 35 cm:** 29 hPa
Stevens Hydra Probe measurement: 0.388
Work: download of data, visual check of station, refill of tensiometer L_20, cone penetrometer measurements (file 210-217)

Date: 28.02.2014   **Time:** 8.00-9.00
Weather: cloudy, windy
Precipitation: little in the beginning (0.2 mm/h)   **Air temperature:** 3.1-3.9°C
Soil water pressure 20 cm: 18 hPa   **Soil water pressure 35 cm:** 20 hPa
Stevens Hydra Probe measurement: 0.391
Work: download of data, visual check of station, refill of tensiometers 1_35 and L_20, cone penetrometer measurements (file 218-228)

Date: 03.03.2014   **Time:** 17.15-18.00
Weather: friendly
Precipitation: none   **Air temperature:** 5.3-4.8°C
Soil water pressure 20 cm: 32 hPa   **Soil water pressure 35 cm:** 26 hPa
Stevens Hydra Probe measurement: 0.389
Work: removal of tensio L_20, installation of T8 instead

Date: 04.03.2014   **Time:** 10.00-10.30
Weather: cloudy
Precipitation: none   **Air temperature:** 2.5°C
Soil water pressure 20 cm: 35 hPa   **Soil water pressure 35 cm:** 27 hPa
Stevens Hydra Probe measurement: 0.388
Work: change of accumulator in logging computer

Date: 06.03.2014   **Time:** 10.15-12.30
Weather: sunny, some wind
Precipitation: none   **Air temperature:** 4.9-8.3°C
Soil water pressure 20 cm: 36 hPa   **Soil water pressure 35 cm:** 28 hPa
Stevens Hydra Probe measurement: 0.388
Work: change of accumulator in logging computer, removal of the installation inclusive all additional sensors, last cone penetrometer measurements (file 230-235), additional cone penetrometer experiment with wetting (control: file 236-241, first after wetting 241-246, second ca. 20 min. later 247-253).

Field Journal Aetigkofen

Date: 09.01.2014   **Time:** 13.30-14.30
Weather: some clouds
Precipitation: none   **Air temperature:** 7.8°C
Soil water pressure 20 cm: 29 hPa   **Soil water pressure 35 cm:** 20 hPa
Stevens Hydra Probe measurement: 0.387
Work: take of 4 undestroyed soil samples

Appendix C

Table C.1: *Soil water pressure and soil water content data worked with for the frequency analysis.*

Institution	Site	Texture	Soil water pressure sensor type (depth cm)	Soil water content sensor type (depth cm)	Data row since
Agroscope	Reckenholz	loam	Septum Tensiometer (10, 20, 35, 55)	Moisture Point vertical probes (0-105 cm in 15 cm intervals) (E.S.I. 2010)	07.2004 until 07.2008
Canton of AG	Boswil	loam	T8 (20, 35)	-	05.2013
	Fislisbach	(sandy) loam	T8 (20, 35)	-	05.2013
	Gränichen-Liebegg	sandy loam	T8 (20, 35)	-	04.2013
	Leutwil	loam	T8 (20, 35)	-	04.2013
	Mettauertal	silty clay loam	T8 (20, 35)	-	05.2013
	Möhlin	silt loam	T8 (20, 35)	-	04.2013
	Schafisheim	sandy loam	T8 (20, 35)	-	05.2013
	Schneisingen	loam	T8 (20, 35)	-	04.2013
	Schupfart	clay	T8 (20, 35)	-	11.2012
	Strengelbach	loam	T8 (20, 35)	-	09.2013
Canton of BL	Brislach	loam	T8 (20, 35)	-	11.2012
	Therwil	loam	T8 (20, 35)	-	11.2012
	Zunzgen	clay/silty clay	T8 (20, 35)	Stevens Hydra Probe (20)	10.2011
Canton of LU	Sursee	loam	T8 (20, 35, 60)	-	
	Urswil 1	loam	T8 (20, 35, 60)	-	04.2011
	Urswil 2	loam	T8 (20, 35, 60)	-	
Canton of SO	Aetigkofen	sandy loam	T8 (20, 35)	Stevens Hydra Probe (20)	10.2011
	Bellach	sandy clay loam	T8 (20, 35)	Stevens Hydra Probe (20)	10.2011
	Breitenbach	sandy loam	T8 (20, 35)	Stevens Hydra Probe (20)	10.2011
	Dulliken	loam	T8 (20, 35)	Stevens Hydra Probe (20)	10.2011
	Etziken	sandy loam	T8 (20, 35)	Stevens Hydra Probe (20)	10.2011
	Hofstetten-Flüh	silt loam	T8 (20, 35)	Stevens Hydra Probe (20)	10.2011
	Kestenholz	clay loam	T8 (20, 35)	Stevens Hydra Probe (20)	10.2011
	Matzendorf	clay loam	T8 (20, 35)	Stevens Hydra Probe (20)	10.2011
	Stüsslingen	loam	T8 (20, 35)	Stevens Hydra Probe (20)	10.2011
	Subingen	sandy loam	T8 (20, 35)	Stevens Hydra	10.2011

				Probe (20)	
Canton of TG	Arenenberg	loam	T8 (20, 35)	Stevens Hydra Probe (20)	04.2013
Canton of UR	Erstfeld	silt loam	T8 (20, 35, 60)	trime-EZ (35, 60)	03.2008
Canton of ZH	Rafz	not known	T8 (20, 40, 70)	-	10.2011
	Reckenholz	sandy loam	T8 (20, 40, 70)	Theta Probe ML2x (20, 40, 70)	10.2011
	Wädenswil	loam	T8 (20, 40, 70)	-	10.2011

Annex

Personal declaration: I hereby declare that the submitted thesis is the result of my own, independent, work. All external sources are explicitly acknowledged in the thesis.

Trimbach; April 30th, 2014

Lea Reusser